THE UNIVERSITY OF MICHIGAN

INDUSTRY PROGRAM OF THE COLLEGE OF ENGINEERING

THE EFFECTS OF TEMPERATURE AND HYDROSTATIC PRESSURE
ON INTERFACIAL TENSIONS IN THE SYSTEM
SOLID NICKEL-LIQUID LEAD

Charles A. Stickels

Doctoral Committee:

        Professor Edward E. Hucke, Chairman
        Professor Wilbur C. Bigelow
        Professor Samuel K. Clark
        Professor Maurice J. Sinnott
        Professor Lawrence H. Van Vlack

ACKNOWLEDGMENTS

It is a pleasure for the author to acknowledge the assistance of many individuals and organizations during the course of this investigation.

Professor Edward E. Hucke stimulated interest in the role of interfacial tensions in determining microstructures, and his advice was invaluable on many occasions. The interest and co-operation of the rest of the doctoral committee is also gratefully acknowledged. Dr. David V. Ragone, who served on the doctoral committee for more than a year, was a frequent source of counsel.

The Universal-Cyclops Corporation, the University of Michigan Research Institute and the Muchnic Foundation provided fellowships for the author during his graduate study. The International Nickel Company supplied some of the materials used in this work and performed a chemical analysis on one alloy.

Preparation of the dissertation was expedited by Janet Maloney, who did the typing, and the Industry Program of the College of Engineering, who prepared the figures and published the thesis in its final form.

Finally, special thanks are due to Mr. Robert W. Dunlap for a critical reading of many sections of the dissertation during its formative stages, and to the author's wife, Patricia F. Stickels, for her continued moral and financial support.

TABLE OF CONTENTS

LIST OF TABLES

LIST OF FIGURES

ABSTRACT

A study was made of the effect of temperature and hydrostatic pressure on ratios of interfacial tensions in the binary system nickel-lead at temperatures above the melting point of lead. Ratios of interfacial tensions were obtained by measurement of the dihedral angle made by the intersection of two nickel/lead interfaces with a nickel/nickel grain boundary.

At zero pressure, the dihedral angle decreases from 52° to 32° as the temperature is increased from 371°C to 816°C. At 371°C, the dihedral angle decreases from 52° to 39° as hydrostatic pressures up to 50,000 psi are applied. At 593°C, the dihedral angle decreases from 41° to 32° with increasing hydrostatic pressure up to 52,600 psi.

The assumption is made, that, in the temperature and pressure range studied, the interfacial tensions in this system vary linearly with changes in temperature or pressure. It is shown that the experimental data is consistent with this assumption. Using this assumption, pressure and temperature coefficients are calculated for each interface. The values obtained for these coefficients are all positive.

It is assumed that the Gibbs Adsorption Equation may be applied to solid/liquid and solid/solid interfaces to obtain expressions for the pressure and temperature coefficients of interfacial tension. Applying the expressions derived to the temperature and pressure coefficients of interfacial tension permits calculation of the excess entropy and the excess concentration of nickel at the nickel/lead interface. Although similar calculations cannot be carried out for the nickel/nickel grain boundary, it is shown that in all likelihood, lead segregates strongly at these boundaries.

Several specimens of leaded nickel were subjected to uniaxial tension and compression at 371°C. Significant changes in the dihedral angle were measured as a function of stress. It is felt, however, that the conditions which allow interpretation of the dihedral angle as a ratio of interfacial tensions are not satisfied under these conditions of loading. It is concluded that the changes observed in the dihedral angle in these experiments need not have been due to changes in interfacial tensions.

CHAPTER I

INTRODUCTION

The grain structures of well-annealed, single-phase polycrystalline metals have been shown to bear a striking resemblance to the structure of soap bubbles in a froth. This similarity arises because metal grain boundaries and soap films both possess a certain free energy associated with their interfaces. When certain conditions are satisfied, the most stable configuration of the boundaries in both cases is the one which minimizes the total interfacial free energy.

The grain structures of well-annealed, multi-phase alloys are determined by the same condition. No soap froth analogy can be made here, however, because the interfaces between like and unlike phases in the alloy possess different energies.

This fact has some interesting consequences. In a single phase metal, individual grains tend to the same shapes regardless of their interfacial free energy. In a metal with two or more phases, the minimization of total interfacial free energy produces configurations in which high energy boundaries tend to be replaced by low energy boundaries. Thus, the shapes of grains of different phases depend on the relative magnitudes of the interfacial energies of the various types of boundaries present.

A simple type of multi-phase alloy, illustrating these principles, consists of a matrix phase in which a small amount of a second phase having a low melting point is dispersed. The second phase particles readily assume equilibrium shapes during annealing at temperatures above the melting point of the second phase.

The shapes vary depending on whether the particles occur in the interior of matrix grains, at grain boundaries, at grain edges, or at grain corners. A grain edge is the junction line where three matrix grain boundaries intersect; a grain corner is the point of intersection of four or more grain edges. When the particles are wholly included within a grain, they become spheroidal. When they are in contact with one or more of the matrix grain boundaries, their shapes are governed by their tendency to wet the grain boundary. The wetting is determined by the relative magnitudes of the interphasal and grain boundary energies.

It is convenient to characterize the "wettability" of the second phase by its "dihedral angle," the angle formed by the apex of the second phase particle penetrating the grain boundary. Under certain conditions, the dihedral angle is a function of the ratio of grain boundary and interphasal energies. The dihedral angle serves as a "boundary condition" (in the mathematical sense) on the shape of the second phase particle.

Interfacial free energies or interfacial tensions (a distinction will be made later) are thermodynamic quantities whose values depend on the thermodynamic constraints on the system. If the temperature, pressure, or the composition is varied, the resulting changes in interfacial tension are reflected in changes in microstructure via changes in the dihedral angle.

Sizable changes in interfacial tensions can occur when the composition of the system is changed. For example, a second phase consisting of a lead-bismuth alloy in copper can be made to produce dihedral angles from 15° to 60° by varying the ratio of lead to bismuth.[59] Variations in temperature can also cause changes in interfacial tensions. The

dihedral angle of lead in copper decreases from 60° to 0° as the temperature is increased from the melting point of lead to the melting point of copper.[51]

Similarly, changes in the dihedral angle are to be expected when the pressure on the system changes, because the surface tensions which determine the dihedral angle must change with pressure. The magnitude of this effect has not previously been established for systems involving metals. Changes in interfacial tensions with pressure have been observed in gas/liquid and liquid/liquid systems, however.

The shapes of such second phase particles are important primarily because they determine the extent to which the second phase can influence the bulk properties of the alloy. Many phases with low melting points are weak or brittle. When the bulk material is stressed, stress concentrations occur at these particles due to differences between phases in elastic or plastic behavior. The stress concentrations cause cracking and premature failure. These effects are most pronounced when the second phase can wet the grain boundaries and grain edges of the matrix, i.e., when the dihedral angle is low. The detrimental effects of the second phase are minimized when the dihedral angle is high. For example, lead inclusions in nickel cause the alloy to be extremely weak and brittle. This probably occurs because the dihedral angle of lead in nickel is low enough (about 50°) to allow unlimited spreading of lead along the edges between matrix grains. Lead inclusions in copper cause some decrease in strength and ductility of the alloy at room temperature, but the higher dihedral angle of lead in copper (about 65°) does not allow spreading along grain edges, hence the effect of the weaker phase is minimized.

Two other occasions may be mentioned where relative magnitudes of interfacial tensions play an important role. Sintering is sometimes carried out with a liquid phase present. When this liquid wets the solid particles, sintering rates are much more rapid. This happens because the solid particles are held together by the surface tension of the liquid during the early stages of sintering and because high rates of mass transport are possible in the liquid. The effectiveness of the liquid depends on its wettability; this can be changed, as indicated above, by changing the temperature, pressure, or composition of the system.

Secondly, it has been found that certain metals exhibit lowered fracture strengths and brittle fractures when stressed in certain liquid metal environments. Annealed copper has a fracture strength in liquid lead which is three times its fracture strength in liquid bismuth.[87] Intermediate liquid compositions produce intermediate fracture strengths. It is generally felt that this indicates that the energy required for initiation and propagation of cracks at the solid surface is lowered when the crack is exposed to certain liquid metals. This energy is identified with various interfacial tensions in the system. For a given solid metal, only a few liquid metals, if any, produce a marked decrease in fracture strength. Thus, in systems where this phenomenon is observed, rather special relations must exist between the various interfacial tensions.

In an effort to obtain information on changes in wetting with variations in the constraints on the system, experiments were undertaken to measure the effect of changes in temperature and pressure on the dihedral angle of lead in nickel. In addition, specimens were subjected to tensile and compressive stresses, and changes in the dihedral angle

were observed. These results are discussed in terms of changes taking place in the interfacial tensions of the solid nickel/liquid lead interface and the nickel grain boundary.

In the next chapter the thermodynamic description of interfaces and interfacial tensions will be discussed as a background for a review of the pertinent literature in Chapter III.

CHAPTER II

THERMODYNAMICS OF INTERFACES

In this chapter the thermodynamics of interfaces will be reviewed. This is intended to serve as a background for the literature review in the next chapter, and as a basis for treatment of the experimental results in Chapter VII.

In this review the emphasis will be on the classical description of interfaces presented by Gibbs. No rigorous derivation of the Gibbs Adsorption Equation will be presented. Instead, the various parameters used by Gibbs and others to characterize an interface will be defined, and the conditions for equilibrium and stability in systems involving interfaces will be discussed. The assumptions needed to extend the application of the Gibbs Adsorption Equation to solid surfaces will be reviewed. In the final section, the Gibbs Adsorption Equation will be written in appropriate forms for describing the dependence of interfacial tension on temperature and pressure.

1. Fundamental Definitions

It seems particularly necessary when discussing surface phenomena involving solids, to clearly define the meanings of the various quantities considered. There is little consistency in the literature, partly because great quantities of work have been done in special areas in solid surface chemistry where attention has been focused on the adsorbing substance and the properties of adsorbed films. Another major source of inconsistency has been the carry-over of concepts used to describe liquid-liquid and liquid-gaseous interfaces to interfaces involving solids. For example,

McLean[65] uses Guggenheim's expression for the dependency of the surface
tension of liquids on temperature and composition to describe temperature
and composition dependencies in metal grain boundaries. But Guggenheim
says that in solids "there is no quantity analogous to surface tension"[35]
(at least the way he defines it) which suggests that McLean's application
deserves justification which he does not provide.

The Second International Congress on Surface Activity in 1959
included presentation of nine papers under the category of the "Solid/
Liquid Interface."[112] The heated discussion which followed their
presentation indicated a basic lack of agreement on the significance
of the terms surface energy and surface tension when applied to solids,
or for that matter, when applied to liquids in some cases.

In the discussions to follow, the meanings of surface free
energy, surface tension, and surface stress will be those given by
Herring,[43] Shuttleworth,[90] and Johnson,[52] all of which are
based on the original work of Gibbs.[29,82]

Dividing Surface and Excess Quantities

Gibbs defined the various properties of a surface in terms of
excess quantities which are referred to a dividing surface separating
phases. Consider a system of bulk phases α and β separated by an
interface S. The dividing surface, according to Gibbs, is a geometrical
surface "sensibly coincident with the physical surface of discontinuity"
but having a "precisely determined position." Let a dividing surface of
some sort be chosen to separate phases α and β so that it lies between
surfaces C_α and C_β as shown schematically below. The portion of the
dividing surface under consideration is sufficiently small to be
considered plane.

$$\beta$$
$$\underline{\hspace{6cm}} \quad C_\beta$$
$$\beta'$$
$$\underline{\hspace{6cm}} \quad S \qquad \text{The dividing surface}$$
$$\alpha'$$
$$\underline{\hspace{6cm}} \quad C_\alpha$$
$$\alpha$$
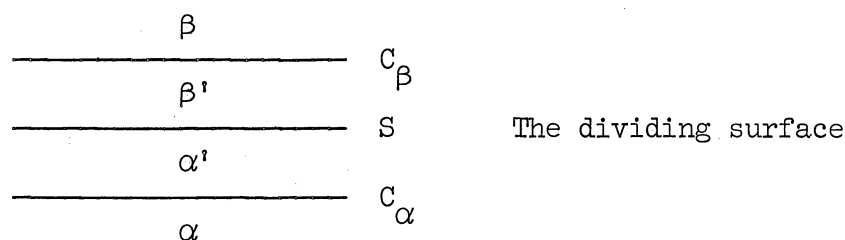
The specific properties of the material in phase α exist unchanged up to C_α, and the specific properties in β exist unchanged up to C_β. Regions α' and β' lie, respectively, between the surfaces C_α and S, and C_β and S. Let $T^{\alpha'}$ and $T^{\beta'}$ be the total quantities of some extensive variable (e.g., the mass of component i, the free energy, etc.) lying within a volume of α' and β', respectively, which is circumscribed by normal lines to a closed curve enclosing an area A in S. Then $\dfrac{T^{\alpha'} + T^{\beta'}}{A}$ may be considered to be the surface density of the variable T. Now let T^{α} and T^{β} be the quantity of the extensive variable T in the interiors of phases α and β, respectively, existing in the same volume as $T^{\alpha'}$ and $T^{\beta'}$. Then

$$T^{(s)} \;=\; \frac{(T^{\alpha'} + T^{\beta'}) - (T^{\alpha} + T^{\beta})}{A} \, , \tag{2-1}$$

where $T^{(s)}$ is the surface excess of the particular quantity T per unit area of dividing surface. In other words,

$$T^{T} \;=\; \underline{T}^{\alpha} V_\alpha \;+\; \underline{T}^{\beta} V_\beta \;+\; T^{(s)} A \tag{2-2}$$

where T^{T} is the total quantity of T in the system, $\underline{T}^{\alpha}$ and $\underline{T}^{\beta}$ the quantities of T per unit volume, V_α and V_β the total volumes of phases α and β, where the phases extend up to the dividing surface, and A the area of the dividing surface.

This analysis may be used to define excess internal energy, Helmholtz free energy, or mass of the ith component. Note, however, that since volume has been used to define the excess quantities, that $V^{(s)} = 0$, i.e., $V^T = V_\alpha + V_\beta$. One could, however, define a non-zero excess volume per mass (using a mass rather than volume basis for defining excess quantities) which is related to the surface excess of mass on the volume basis used above. Guggenheim and Adam[34] discuss alternative conventions for describing the properties of the surface.

Movement of the dividing surface in the direction of its normal affects the magnitude of the excess properties, except when the phases α, β are identical (which is the case for grain boundary between like crystals in a solid). The position of the dividing surface when α and β are not identical is usually chosen for convenience, e.g., to make the surface excess vanish for the major constituent of one of the phases. When the phases α, β are identical, the dividing surface cannot be chosen so that one of the surface excess quantities vanishes.

Surface or Interfacial Free Energy

The surface free energy $f^{(s)}$ is the excess Helmholtz free energy per unit area of dividing surface determined in the manner described above. Shuttleworth[90] points out that for a one component solid in equilibrium with its vapor in a constant volume enclosure at constant temperature, the amount of reversible work required to form a unit area of surface by a process of division is $f_i^{(s)}$. The subscript i is needed for crystalline substances because $f^{(s)}$ varies according to the crystallographic plane of division. (For liquids and glasses $f^{(s)}$ is not dependent on orientation.)

Surface or Interfacial Tension

The surface tension γ is given by Gibbs[29] as

$$\gamma = f^{(s)} - \sum_i \mu_i \Gamma_i \qquad (2-3)$$

where the subscripts i refer to various components in the system.
The chemical potentials μ_i are defined by the usual relations in either
bulk phase:

$$\mu_i = \left(\frac{\partial F}{\partial N_i} \right)_{T,V,N_j} = \left(\frac{\partial G}{\partial N_i} \right)_{T,P,N_j} \quad , \quad j \neq i \qquad (2-4)$$

Herring[43] points out that for solids, shear strains must be held
constant as well as volume in the first expression, and constant stress
should replace constant pressure in the second expression.

The quantities Γ_i are the specific surface excess quantities
of mass of component i. If $N_i^{\alpha'}$ and $N_i^{\beta'}$ are moles of the ith
component, (corresponding to $T^{\alpha'}$ and $T^{\beta'}$ above) then

$$\Gamma_i = \frac{(N_i^{\alpha'} + N_i^{\beta'}) - (N_i^{\alpha} + N_i^{\beta})}{A} \quad . \qquad (2-5)$$

Note that since Shuttleworth[90] considers only a one component
solid in equilibrium with its vapor, he may choose his dividing surface
S in such a way that the surface excess of his one component is zero.
Whenever this is so, the surface free energy and surface tension are
equal. For a two component system, however, one cannot in general choose
a dividing surface so as to make both surface excess quantities vanish.
Hence, in this case, surface tension and surface free energy are not
equal.

Herring[43] has defined surface tension in precisely the same manner as Gibbs. It must be realized, however, that when Herring defines $f^{(s)}$ as the Helmholtz free energy per unit area of surface it is the same as the surface excess free energy (surface free energy) defined above. Similarly, Herring defines $\Gamma_i = N_i^{(s)}/A$ where, in terms of quantities previously defined,

$$N_i^{(s)} = (N_i^{\alpha'} + N_i^{\beta'}) - (N_i^{\alpha} + N_i^{\beta}) \qquad (2\text{-}6)$$

For a system consisting of more than one component, γ measures the energy required to create unit area of solid surface where, as before, γ will vary with the crystallographic orientation of the new surface created.

Surface Stress

Gibbs[29] says that for solids "we may regard (γ) as expressing the work spent in forming a unit of the surface discontinuity...but it cannot properly be regarded as expressing the tension of the surface. The latter quantity depends on the work spent in _stretching_ the surface, while the quantity (γ) depends on the work spent in _forming_ the surface." In the case of liquids, the work spent in stretching or in forming a surface is the same, but for solids capable of existing in different states of strain, the quantities must be distinguished.

Following Herring[43], consider an interface S separating two bulk phases α and β, at least one of which is a solid. Then consider a plane P erected perpendicular to S, having a normal $\vec{n}$ lying in S. If we imagine P to be a cut across the bulk phases and the interface, then in order that atoms in the plane of the cut retain

the positions they had prior to cutting, external forces must be applied

acting across and in the plane P. In general, a normal force acting

in the direction of $\vec{n}$ and two perpendicular shearing forces in the

plane P will be required. The contributions to these forces resulting

from the presence of the surface is defined as the surface stress.

One can imagine that this contribution is arrived at by a process of

dividing the total forces into bulk and surface contributions as was

done in defining excess quantities earlier. When P is rotated about

an axis normal to the interface the surface stress acting across the

interface is given by $\sum_{\nu} g_{\mu\nu} \, \eta_{\nu}$ where the surface stress tensor

$g_{\mu\nu}$ has components for the two values of ν going with directions

in the plane of the interface, and components for the three values of

μ representing perpendicular directions in S and normal to S.

By considering infinitesimal deformations of the surface

which may change γ, Herring arrives at the following expression for

$g_{\mu\nu}$:

$$g_{\mu\nu} = \gamma\delta_{\mu\nu} + \frac{\partial\gamma}{\partial\epsilon_{\mu\nu}} \quad ; \qquad \begin{array}{l} \mu = 1,\ 2,\ 3 \\ \nu = 1,\ 2 \end{array} \qquad\qquad (2\text{-}7)$$

where $\epsilon_{\mu\nu}$ is the strain tensor of the deformation and $\delta_{\mu\nu}$ is the

Kronecker Delta.

Shuttleworth's treatment[90] of the same problem is simplified

because he considers only surface stresses in the external surface of

a one component solid in equilibrium with its vapor. As mentioned

before, this allows one to equate γ and $f^{(s)}$ by choosing the dividing

surface so that $\Gamma = 0$.

For this case, if one chooses x and y axes in the plane of

the interface, the surface stress may be expressed in general by three

components, g_{xx}, g_{yy} and g_{xy}. When principal axes are chosen, g_{xy} vanishes so the surface stress for an external surface can be characterized by two numbers.

Shuttleworth considers an infinitesimal deformation of a rectangle in the surface, oriented with principal surface stresses perpendicular to the sides of the rectangle (no shearing stresses). For a reversible, constant temperature deformation, the surface contribution to the work is $g_{xx}dA_x + g_{yy}dA_y = d(Af^{(s)})$ which, for the isotropic case $g_{xx} = g_{yy} = g$ reduces to

$$g = f^{(s)} + A \left(df^{(s)}/dA \right) \qquad (2-8)$$

a relation analogous to the definition above, but clearly more restricted. (Shuttleworth calls $f^{(s)}$ the surface energy and g_{ij} the surface tension. This is logical nomenclature for a one component system, but it leaves no name for γ when a multi-component system is considered. Note that Shuttleworth's symbol γ is the same as g used here.)

Alternative Treatments

Guggenheim[35] has presented treatments of interfaces not involving solids which are not based directly on Gibbs' notion of a dividing surface between phases. Guggenheim cites Van der Waals and Bakker[10] as the principal source for his development.

Consider a plane interface between bulk phases α and β and pass two planes C_α and C_β through the bulk phases α and β near the interface. C_α and C_β are placed so that the properties of the matter at or near C_α and C_β are the properties of the matter in the interior of the bulk phases α and β, respectively. (It is possible

to show that such relations as are derived for the surface are independent of the precise location of C_α and C_β as long as the above conditions are true.) The distance between C_α and C_β is τ, the thickness of the interface, which should be less than 10^{-6} cm, but is probably smaller. The interface S is treated as a bulk phase which differs from phases α and β only in the property that when the system is under hydrostatic pressure, the force across any unit area of S is different on planes parallel and perpendicular to C_α and C_β, the difference being the surface tension.

Let T^S be the total quantity of some extensive variable contained in a volume of interfacial material lying between C_α and C_β, and circumscribed by normal lines to a closed curve in, say, C_α enclosing an area A in C_α. Then the interfacial density of T is simply

$$T^\sigma = T^S/A$$

Note that this is not an excess quantity.

Guggenheim's expression for the surface tension is

$$\gamma = F^\sigma + P\tau - \sum_i \mu_i n_i^\sigma \qquad (2\text{-}9)$$

where $F^\sigma = F^S/A$ is the surface density of Helmholtz free energy, $n_i^\sigma = n_i^S/A$ is the surface density of component i, P is the pressure, μ_i the chemical potential of the ith component, and $\tau = \dfrac{V^S}{A}$ the volume of the surface phase corresponding to unit interfacial area. This expression may be reduced to Gibbs' definition of surface tension as follows:

$$F^S = F^{\alpha'} + F^{\beta'}$$

$$n_i^S = N_i^{\alpha'} + N_i^{\beta'}$$

$$\tau A = V^{\alpha'} + V^{\beta'} = V^{\alpha} + V^{\beta}$$

In terms of excess quantities:

$$F^{\sigma} = f^{(s)} + \frac{F^{\alpha} + F^{\beta}}{A}$$

$$n_i^{\sigma} = \Gamma_i + \frac{N_i^{\alpha} + N_i^{\beta}}{A}$$

Substituting in Guggenheim's expression:

$$\gamma = f^{(s)} - \sum_i \mu_i \Gamma_i + \frac{1}{A} (F^{\alpha} + PV^{\alpha} - \sum_i \mu_i N_i^{\alpha})$$

$$+ \frac{1}{A} (F^{\beta} + PV^{\beta} - \sum_i \mu_i N_i^{\beta})$$

The two terms in parentheses are zero because

$$F^{\alpha} + PV^{\alpha} = G^{\alpha} = \sum_i \mu_i N_i^{\alpha}$$

Hence the surface tensions defined by Gibbs and Guggenheim are entirely equivalent.

Guggenheim's skepticism as to the reality of surface tension in solids is undoubtedly based on the identification of γ with a real force in the surface. The distinction that Herring has made between surface tension and surface stress g_{ij} should remove this objection.

2. The Gibbs Adsorption Equation

In this section a derivation of the Gibbs Adsorption Equation applicable to a system of two fluid phases separated by an interface will be outlined following Gibbs.[29] In the next section, the criteria for

stability of an equilibrium state with respect to motion of the interfaces will be discussed and applied to systems which involve solids as well as fluids. Finally, the applicability of the Gibbs Adsorption Equation to systems involving solids undergoing changes in temperature and hydrostatic pressure will be discussed.

Gibbs[29] shows that Equation (2-10) describes the dependence of the excess internal energy of the surface U^σ, on the excess entropy of the surface S^σ, the area of the surface, A, and the excess number of moles of component i present in the surface, m_i^σ. U^σ, S^σ and m_i^σ are excess quantities for an area A of interface; they are not specific excess quantities.

$$dU^\sigma = TdS^\sigma + \gamma dA + \sum_i \mu_i dm_i^\sigma \qquad (2\text{-}10)$$

Equation (2-10) is a fundamental relation giving the internal energy as a homogeneous function of the first degree in the variables S^σ, A, m_i^σ, ..., m_n^σ. Hence, the temperature, T, interfacial tension γ, and chemical potential μ_i are homogeneous functions of zero degree in the variables S^σ, A, m_i^σ, ..., m_n^σ given by the relations

$$\left.\frac{\partial U^\sigma}{\partial S^\sigma}\right)_{A,m_i^\sigma} = T \qquad i = 1, \ldots, n$$

$$\left.\frac{\partial U^\sigma}{\partial A}\right)_{S^\sigma, m_i^\sigma} = \gamma \qquad i = 1, \ldots, n \qquad (2\text{-}11)$$

$$\left.\frac{\partial U^\sigma}{\partial m_i^\sigma}\right)_{S^\sigma, \gamma, m_j^\sigma} = \mu_i \qquad i \neq j$$

Since U^{σ} is of the first degree in its variables, then by the Euler relation

$$U^{\sigma} = TS^{\sigma} + \gamma A + \sum_i \mu_i m_i^{\sigma} \; . \qquad (2\text{-}12)$$

Differentiating Equation (2-12) we have

$$dU^{\sigma} = TdS^{\sigma} + S^{\sigma}dT + \gamma dA + Ad\gamma + \sum_i \mu_i dm_i^{\sigma} + \sum_i m_i^{\sigma}d\mu_i \; . \quad (2\text{-}13)$$

Setting Equations (2-10) and (2-13) equal to one another gives

$$S^{\sigma}dT + Ad\gamma + \sum_i m_i^{\sigma}d\mu_i = 0 \; . \qquad (2\text{-}14)$$

Dividing (2-14) by the area A and rearranging, we have

$$d\gamma = -S^{(s)}dT - \sum_i \Gamma_i d\mu_i \qquad (2\text{-}15)$$

where

$$S^{(s)} = \frac{S^{\sigma}}{A} \qquad \text{and} \qquad \Gamma_i = \frac{m_i^{\sigma}}{A} \; .$$

Equation (2-15) is the Gibbs Adsorption Equation. Note that it is obtained (up through Equation (2-14)) by the same procedure which is used to obtain the Gibbs-Duhem relation for either bulk phase. Note also that in Equation (2-15) the interfacial tension depends only on the temperature and the chemical potentials of the components present. Gibbs shows that at equilibrium the temperatures of all phases and the interface are equal, and the chemical potentials of all components are the same everywhere in the system. Thus, the interfacial tension, γ, is completely determined by intensive properties of the bulk phases.

For fluid phases separated by a curved interface, Gibbs shows that the condition for mechanical equilibrium in the system is

$$p^{\alpha} - p^{\beta} = \gamma (C_1 + C_2) \qquad\qquad (2\text{-}16)$$

where p^{α}, p^{β} are the pressures of phases α and β on either side of the interface, and C_1 and C_2 are the principal curvatures of the interface. When the interface is plane, this reduces to $p^{\alpha} = p^{\beta}$ which is the condition for mechanical equilibrium between bulk phases when interfaces are neglected.

3. Criteria for Stability of an Equilibrium State

The equilibrium conditions for a system involving an interface, i.e. uniform temperature, equal chemical potentials in all phases, etc., are derived by Gibbs from the condition that at equilibrium the energy of the system must be an extremum, when the total entropy and volume of the system, and the masses of all components are held constant.

For stable equilibrium, the energy of the system must be at a minimum. Gibbs shows that when the temperature and the chemical potentials of all components are uniform throughout the system and the surface tensions are constant over each interface, a condition for stability is that "in a stable system each surface of tension must be a surface of minimum area for constant values of the volumes which it divides, when the other surfaces bounding these volumes and the perimeter of the surface of tension are regarded as fixed." He then derives a condition of stability with reference to motion of interfaces which is sufficient, but not necessary. This condition is the basis for several methods of measuring interfacial tensions.

Consider a system composed of several bulk phases separated by interfaces of various kinds. Let the system be in equilibrium; thus the temperature and the chemical potentials of all components are every-

where constant. The total entropy and the total quantities of all components remain fixed. Gibbs shows (29, p. 252) that under these constraints, a sufficient condition for the stability of an equilibrium state with respect to motion of interfaces is: the sum of the products of the areas of the interfaces by their tensions, less the sum of the products of the volumes of the phases by their pressures, must be a minimum. This condition is expressed in Equation (2-17), where the notation indicates that the function in brackets is a minimum in the stable state.

$$\min \left[\sum_i \int \gamma_i dA_i - \sum_j \int p_j dv_j \right] \tag{2-17}$$

Now in many situations Equation (2-17) can be reduced to a simpler form. Consider a system of two bulk phases separated by an interface, the whole system being in thermal, chemical and mechanical equilibrium. The bulk phases may now be either solids or fluids. Let the volumes of the two bulk phases be held constant and let us consider changes in the mechanical work done on the system when the interface is allowed to move. Changes must in general occur in the terms $\int \gamma_i dA_i$ because the interfacial areas are being varied. If the state of stress on the bulk phases is substantially unaltered when the interfaces move*, then the terms for the bulk phases will be unchanged because the volumes of the bulk phases are constant. In particular, when all bulk phases are under a uniform hydrostatic pressure, then the terms in $\int p_j dv_j$ do

* Herring[43] points out that there must always be an inhomogeneous stress in a solid near an interface which is needed to offset the surface stress. This inhomogeneous stress will in general change as the interface changes position. Herring shows that this effect is negligible.

not change when the position of the interface is changed. Under these
conditions Equation (2-17) reduces to

$$\min \left[\sum_i \int \gamma_i dA_i \right] \qquad (2\text{-}18)$$

If the interfacial tensions are independent of crystallographic
orientation (if any of the phases is a solid), or if all phases are fluids,
application of condition (2-18) to intersecting sets of interfaces
produces the familiar "vectorial balance" of surface tensions. Herring[43]
has applied the condition (2-18) to systems in which the interfacial
tensions do depend on crystallographic orientation and obtains a more
general type of relation. These equations will be discussed more fully
in the next chapter. It must be emphasized here that all equations of
this type depend on the reduction of condition (2-17) to condition (2-18).
If for some reason this reduction is not possible, then none of the
equations expressing the balance of tensions about a point are valid.
Furthermore, the condition (2-17) is sufficient for stability, but
not necessary; hence, stable equilibrium may be possible without
satisfying either (2-17) or (2-18).

4. Application of the Gibbs Adsorption Equation to Systems Involving
   Solids

Herring[43] notes some conditions in which the Gibbs Adsorption
Equation (2-15) does not give the total change in interfacial tension
for a solid surface for all types of changes in the system. These
circumstances are: (1) when a displacement of an interface changes
its radius of curvature, (2) when the orientation of the crystalline
surface changes, and, (3) when the state of strain of a crystalline
surface is altered (other than by a simple dilation of the bulk phase
normal to the interface).

Situation (1) above can generally be disregarded because
the interfacial tension is substantially independent of curvature,
except when the radii of curvature are on the order of atomic dimensions.
Neither of the second two situations can be generally disregarded.

The dependence of the interfacial tension on crystallographic
orientation varies considerably from system to system. Studies of
small angle grain boundaries between crystals of the same phase have
shown a negligible dependence of the tension on boundary orientation,
if the crystals across the boundary have a fixed orientation with
respect to one another. The appearance of generally spherical particles
of low melting phases within solid grains indicates that the solid/
liquid interfacial tension does not have a strong dependence on the
crystallographic plane exposed. On the other hand, the development
of facets on crystals at high temperatures may be related to
significant variations in the surface tension on various crystallographic
planes, as may the occurrence of some plate-like or rod-like precipitates
in metals. (These effects, however, may also involve preferred
directions for growth.)

If the change in surface tension with a change in the constraints
on the system is measured on a large, random collection of interfaces
of all possible orientations, then the average surface tension of all
these interfaces should be independent of crystallographic changes
occurring at specific interfaces. The Gibbs Adsorption Equation can
then be applied to this average tension to describe its changes when
the constraints on the system are changed.

The final condition noted in the first paragraph seems to
seriously restrict application of the Gibbs Adsorption Equation to

solid surfaces. Gibbs says (29, p. 328) that Equation (2-15) may be applied to solid surfaces subject to the limitation "that the state of strain of the surface of the solid remains the same." He goes on to say that "this limitation may in most cases be neglected," but "if the quantity (γ) represented the true tension of the surface, as in the case of a surface between fluids, the limitation would be wholly unnecessary."

It is unfortunate that Gibbs did not expand upon this subject, because it is not at all clear in which cases changes in the state of strain of the surface may be neglected. Using Herring's expression[43] for the surface stress tensor as a function of surface tension,

$$g_{ij} = \gamma \, \delta_{ij} + \frac{\partial \gamma}{\partial \epsilon_{ij}}$$

the condition for applicability would seem to be either that the change in the state of strain is very small or that the differential coefficient $\frac{\partial \gamma}{\partial \epsilon_{ij}}$ is small compared to γ. It must be assumed that Gibbs had in mind the latter case. For example, a decrease in temperature of 50°C causes strains on the order of $-7 \cdot 10^{-4}$ in/in in nickel. (About the same amount of strain is caused by the application of 60,000 psi hydrostatic pressure.) These strains certainly result in a change in the "state of strain" of the solid surface. It seems quite unlikely that Gibbs would make the statement that Equation (2-15) was applicable to changes in solid surface tensions "in most cases," if changes in the state of strain of this order of magnitude could not be tolerated.

It will be assumed in all subsequent chapters that the Gibbs Adsorption Equation can be used to express the change in interfacial

tension with temperature and pressure for solid/solid and solid/liquid interfaces. This implies that the surface tension and surface stress do not differ significantly. Herring[43] notes that several atomistic calculations of the surface stress for homopolar crystals, alkali halide crystals and rare gas crystals indicate that the surface stress and surface tension should be significantly different. On the other hand, the conditions for equality of surface stress and surface tension in solid metals appear to be satisfied as much as 200°C below the melting point (cf. measurements of surface tension by the Udin-Shaler-Wulff method[105,41]). McLean[65] feels that the surface tension and surface stress of ordinary large angle grain boundaries should be "nearly equal...at high temperature." No experimental measurements of the difference between surface stress and surface tension in solids have been made.

To summarize, the stability conditions presented in the previous section insure that interfaces in systems involving solids under hydrostatic pressure assume a configuration such that, neglecting the influence of solid crystallography, a vectorial·balance of inter-facial tensions occurs. As will be shown later, this guarantees that ratios of interfacial tensions can be measured. However, expressing the dependence of these interfacial tensions on temperature and hydrostatic pressure by means of the Gibbs Adsorption Equation involves the assumption of equality of surface tension and surface stress.

5. Derivation of Useful Relations from the Gibbs Adsorption Equation

The dependence of surface tension on temperature, pressure and composition of a system is given by the Gibbs Adsorption Equation:

$$dy = -S^{(s)} dT - \sum_{i=1}^{n} \Gamma_i d\mu_i \qquad (2\text{-}19)$$

where $S^{(s)}$ is the surface excess entropy, and the sum is taken over all components of the system. The discussion to follow considers a two-component system consisting of two phases, α and β, and an interface separating them. For solids whose surface tension is dependent on crystallographic orientation, the following derivation is applicable for a particular set of orientation coordinates.

Let (1) and (2) designate the components of the system. The Gibbs Adsorption Equation is

$$dy = -S^{(s)} dT - \Gamma_1 d\mu_1 - \Gamma_2 d\mu_2 . \qquad (2\text{-}20)$$

The chemical potential of each component is constant throughout the system at equilibrium $\mu_1^{\alpha} = \mu_1^{\beta} = \mu_1^{(s)}$; hence $d\mu_1^{\alpha} = d\mu_1^{\beta} = d\mu_1^{(s)}$. Let x^{α}, x^{β} be the mole fractions of component (1) in phases α and β. Then $(1 - x^{\alpha})$, $(1 - x^{\beta})$ are the mole fractions of component (2). The chemical potentials in Equation (2-20) may be written:

$$d\mu_1^{\alpha} = \frac{\partial\mu_1^{\alpha}}{\partial T} dT + \frac{\partial\mu_1^{\alpha}}{\partial P} dP + \frac{\partial\mu_1^{\alpha}}{\partial x^{\alpha}} dx^{\alpha}$$

$$d\mu_2^{\alpha} = \frac{\partial\mu_2^{\alpha}}{\partial T} dT + \frac{\partial\mu_2^{\alpha}}{\partial P} dP + \frac{\partial\mu_2^{\alpha}}{\partial x^{\alpha}} dx^{\alpha} \qquad (2\text{-}21)$$

for phase α, and

$$d\mu_1^{\beta} = \frac{\partial\mu_1^{\beta}}{\partial T} dT + \frac{\partial\mu_1^{\beta}}{\partial P} dP + \frac{\partial\mu_1^{\beta}}{\partial x^{\beta}} dx^{\beta}$$

$$d\mu_2^{\beta} = \frac{\partial\mu_2^{\beta}}{\partial T} dT + \frac{\partial\mu_2^{\beta}}{\partial P} dP + \frac{\partial\mu_2^{\beta}}{\partial x^{\beta}} dx^{\beta} \qquad (2\text{-}22)$$

for phase β.

Equations (2-21) and (2-22) may be simplified using the following relations:

$$\left.\frac{\partial \mu_i^j}{\partial T}\right)_{P,x^j} = -\bar{S}_i^{\ j} \tag{2-23}$$

$$\left.\frac{\partial \mu_i^j}{\partial P}\right)_{T,x^j} = \bar{V}_i^{\ j} \tag{2-24}$$

$$x^j \frac{\partial \mu_1^j}{\partial x^j} + (1 - x^j) \frac{\partial \mu_2^j}{\partial x^j} = 0 \tag{2-25}$$

where $\bar{S}_i^j$ and $\bar{V}_i^j$ are, respectively, the partial molar entropy and the partial molar volume of component i in phase j, and Equation (2-25) is the Gibbs-Duhem relation between chemical potentials in phase j.

Inserting Equations (2-23), (2-24), and (2-25) in (2-21) and (2-22), the differentials of chemical potential in each phase are:

$$d\mu_1^\alpha = -\bar{S}_1^{\ \alpha} dT + \bar{V}_1^{\ \alpha} dP + \frac{\partial \mu_1^\alpha}{\partial x^\alpha} dx^\alpha$$

$$d\mu_2^\alpha = -\bar{S}_2^{\ \alpha} dT + \bar{V}_2^{\ \alpha} dP - \frac{x^\alpha}{1 - x^\alpha} \frac{\partial \mu_1^\alpha}{\partial x^\alpha} dx^\alpha \tag{2-26}$$

and

$$d\mu_1^\beta = -\bar{S}_1^{\ \beta} dT + \bar{V}_1^{\ \beta} dP + \frac{\partial \mu_1^\beta}{\partial x^\beta} dx^\beta$$

$$d\mu_2^\beta = -\bar{S}_2^{\ \beta} dT + \bar{V}_2^{\ \beta} dP - \frac{x^\beta}{1 - x^\beta} \frac{\partial \mu_1^\beta}{\partial x^\beta} dx^\beta \tag{2-27}$$

Either Equations (2-26) or (2-27) may now be substituted into Equation (2-20). Substituting (2-26) we have:

$$d\gamma = -\left[S^{(s)} - \Gamma_1 \bar{S}_1^\alpha - \Gamma_2 \bar{S}_2^\alpha \right] dT - \left[\Gamma_1 \bar{V}_1^\alpha + \Gamma_2 \bar{V}_2^\alpha \right] dP$$

$$- \left[\Gamma_1 - \frac{x^\alpha}{1 - x^\alpha} \Gamma_2 \right] \frac{\partial \mu_1^\alpha}{\partial x^\alpha} dx^\alpha \tag{2-28}$$

In some cases, Equation (2-28) may be considerably simplified. For example, if phase α and β have different compositions, then the dividing surface between phases can be chosen so that surface excess of one component vanishes, e.g. $\Gamma_2 = 0$. Then at constant temperature and pressure, Equation (2-28) reduces to:

$$d\gamma = - \Gamma_{1(2)} \frac{\partial \mu_1^\alpha}{\partial x^\alpha} \, dx^\alpha \qquad (2\text{-}29)$$

where $\Gamma_{1(2)}$ is the surface excess for this choice of dividing surface. Since

$$\mu_1^\alpha - \mu_1^o = RT \ln a_1^\alpha = RT \ln f_1^\alpha x^\alpha$$

where a_1^α is the activity and f_1^α the activity coefficient of component (1), then

$$\frac{\partial \mu_1^\alpha}{\partial x^\alpha} = \frac{RT}{x^\alpha} + RT \frac{\partial \ln f_1^\alpha}{\partial x^\alpha} . \qquad (2\text{-}30)$$

For solutions in which either Henry's Law or Raoult's law is valid for component (1), the second term on the right hand side of (2-30) vanishes. Under these conditions, Equation (2-29) becomes

$$d\gamma = - \Gamma_{1(2)} RT \, d \ln x^\alpha \qquad (2\text{-}31)$$

which is a commonly encountered form of the Gibbs Adsorption Equation.

Simplifications of Equation (2-28) will now be derived for the solid/liquid and grain boundary surface tensions.

Solid-Liquid Interfaces

Consider the interface between a solid and a liquid, where the solid consists almost wholly of component (1), while the liquid is

rich in component (2) with very limited solubility for component (1). The dividing surface will be chosen so that $\Gamma_2 = 0$. Then, with chemical potentials referred to the liquid phase, Equation (2-28) may be written:

$$d\gamma = -\left[S_{(2)}^{(s)} - \Gamma_{1(2)} \bar{S}_1^\ell \right] dT - \Gamma_{1(2)} \bar{V}_1^\ell dP - \Gamma_{1(2)} \frac{\partial \mu_1^\ell}{\partial x^\ell} dx^\ell. \quad (2\text{-}32)$$

At constant pressure, the variation in surface tension with temperature may now be written:

$$\frac{d\gamma}{dT} = -\left[S_{(2)}^{(s)} - \Gamma_{1(2)} \bar{S}_1^\ell \right] - \Gamma_{1(2)} \frac{\partial \mu_1^\ell}{\partial x^\ell} \frac{dx^\ell}{dT}. \quad (2\text{-}33)$$

If the activity of component (1) in the liquid is proportional to its mole fraction x^ℓ, then

$$\frac{\partial \mu_1^\ell}{\partial x^\ell} = \frac{RT}{x^\ell} \quad (2\text{-}34)$$

and

$$\frac{d\gamma}{dT} = -\left[S_{(2)}^{(s)} - \Gamma_{1(2)} \bar{S}_1^\ell \right] - \Gamma_{1(2)} RT \frac{d \ln x^\ell}{dT}. \quad (2\text{-}35)$$

Without making an assumption as to the relative magnitude of the quantities in (2-35), further simplification is not possible. If the solubility as a function of temperature and the partial molal entropy of component (1) in the liquid are known, the quantities $S_{(2)}^{(s)}$ and $\Gamma_{1(2)}$ could be determined if at least one was assumed constant with temperature and other was an assumed function of temperature. However, this would require great precision in measurements of γ vs. T.

At constant temperature, the variation of surface tension with pressure is:

$$\frac{d\gamma}{dP} = - \Gamma_{1(2)} \left[\bar{V}_1^{\ell} + \frac{\partial \mu_1^{\ell}}{\partial x^{\ell}} \frac{dx^{\ell}}{dP} \right] . \qquad (2\text{-}36)$$

Substitution of Equation (2-34) gives:

$$\frac{d\gamma}{dP} = - \Gamma_{1(2)} \left[\bar{V}_1^{\ell} + RT \frac{d \ln x^{\ell}}{dP} \right] . \qquad (2\text{-}37)$$

If the solubility as a function of pressure and the partial molal volume of component (1) in the liquid are known, $\Gamma_{1(2)}$ may be determined from measurements of γ vs. P.

In many cases, the thermodynamic properties of the liquid solution are not known. One can obtain simple expressions for $d\gamma/dT$ and $d\gamma/dP$ replacing Equations (2-35) and (2-37), if the solid can be assumed to be pure component (1). Then the differential of chemical potential referred to the solid is:

$$d\mu_1^S = \frac{\partial \mu_1^S}{\partial P} dP = \bar{V}_1^S dP = \underline{V}_1^S dP \quad \text{at constant T}$$

$$d\mu_1^S = \frac{\partial \mu_1^S}{\partial T} dT = - \bar{S}_1^S dT = - \underline{S}_1^S dT \quad \text{at constant P.}$$

Inserting these results in Equation (2-19), taking $\Gamma_2 = 0$, one has

$$d\gamma/dT = -S_{(2)}^{(s)} + \Gamma_{1(2)} \underline{S}_1^S \quad \text{at constant P} \qquad (2\text{-}38)$$

$$d\gamma/dP = - \Gamma_{1(2)} \underline{V}_1^S \quad \text{at constant T.} \qquad (2\text{-}39)$$

Since values for the molar entropy, $\underline{S}_1^S$, and the molar volume, $\underline{V}_1^S$, of the pure solid are generally available, measurement of the temperature and pressure coefficients of interfacial tension permits calculation of $\Gamma_{1(2)}$ and $S_{(2)}^{(s)}$.

Grain Boundaries

For grain boundaries between phases of the same density and composition it is not possible to choose a dividing surface so that the interfacial excess concentration of one of the components vanishes. In addition, the interfacial excess quantities are independent of the choice of dividing surface. Thus, formal simplification of Equation (2-28) is not possible by the methods previously used.

At constant temperatures and pressure, Equation (2-28) simplifies to:

$$d\gamma = - \left[\Gamma_1 - \frac{x^\alpha}{1 - x^\alpha} \Gamma_2 \right] \frac{\partial \mu_1^\alpha}{\partial x^\alpha} \, dx^\alpha \qquad (2\text{-}40)$$

Cahn and Hilliard[14] have suggested that the quantity in brackets be designated $\overline{\Gamma}_{1(2)}$. $\overline{\Gamma}_{1(2)}$ is the difference between the actual excess concentration of component (1) at the interface, and the excess concentration of (1) which would be required just to maintain the bulk composition in the boundary, given the excess concentration of component (2). Thus, $\overline{\Gamma}_{1(2)}$ indicates the direction in which the composition of the boundary deviates from the bulk composition. In the case of strongly segregating component (2) in the grain boundaries of almost pure (1), $\overline{\Gamma}_{1(2)}$ would be negative.

One could, in principle, determine $\overline{\Gamma}_{1(2)}$ from measurements of the variation in γ with x^α using a Udin-Shaler-Wulff type experiment.[105] The precision required is probably unattainable, however.

In a more general situation, this approach provides no simplifications. One can, however, obtain more usable equations if a few assumptions are made.

At constant temperature, Equation (2-28) applied to the

grain boundary gives the pressure coefficient of grain boundary tension:

$$\frac{d\gamma}{dP} = - \left[\Gamma_1 \overline{V}_1^\ell + \Gamma_2 \overline{V}_2^\ell \right] - \left[\Gamma_1 - \frac{x^\ell}{1 - x^\ell} \Gamma_2 \right] \frac{\partial \mu_1^\ell}{\partial x^\ell} \frac{dx^\ell}{dP}. \quad (2\text{-}41)$$

In this equation, the surface excess quantities refer, of

course, to the grain boundary, but the differentials of chemical potential

occurring in Equation (2-20) are now referred to the liquid phase. If

the system is in equilibrium, the chemical potentials are the same in

all phases; hence this procedure is permissible.

An expression for $\frac{\partial \mu_1^\ell}{\partial x^\ell} \frac{dx^\ell}{dP}$ is easily obtained if one assumes

that the solid is pure component (1) and the liquid is a mixture of the

two components. Then

$$d\mu_1 = \underline{V}_1^{\,S} dP \quad \text{in the solid}$$

$$d\mu_1 = \overline{V}_1^{\,\ell} dP + \frac{\partial \mu_1^\ell}{\partial x^\ell} dx^\ell \text{in the liquid.}$$

$$(2\text{-}42)$$

Equating these two expressions and rearranging gives:

$$\frac{\partial \mu_1^\ell}{\partial x^\ell} \frac{dx^\ell}{dP} = \underline{V}_1^{\,S} - \overline{V}_1^{\,\ell} \quad (2\text{-}43)$$

where $\underline{V}_1^S$ is the molar volume of the solid and $\overline{V}_1^\ell$ is the partial molal

volume of component (1) in the liquid. Substituting (2-43) in (2-41),

rearranging and using the relation $\underline{V}^\ell = x^\ell \overline{V}_1^{\,\ell} + (1 - x^\ell) \overline{V}_2^{\,\ell}$, where

$\underline{V}^\ell$ is the molar volume of the liquid, one has

$$\frac{d\gamma}{dP} = - \Gamma_1 \underline{V}_1^{\,S} - \frac{\Gamma_2}{1 - x^\ell} (\underline{V}^\ell - x^\ell \underline{V}_1^{\,S}). \quad (2\text{-}44)$$

Now if one could assume that the surface excess quantities are independent of temperature, measurement of $d\gamma/dP$ at two temperatures would allow calculation of the two surface excess quantities Γ_1, Γ_2. But, Γ_1, Γ_2 are most likely to be constant with temperature if there is little change in the liquidus composition with temperature. Since molar volume changes in the solid and liquid in this case would then be, essentially, only due to thermal expansion, the change expected in $d\gamma/dP$ would be very small. This small difference would make the computation of Γ_1, Γ_2 very inaccurate.

For the case of a grain boundary in a one component solid, the pressure coefficient of surface tension is given by

$$d\gamma/dP = -\Gamma_1 \underline{V}_1$$

where $\underline{V}_1$ is the molar volume of the solid. If the grain boundary is 10% less dense, on the average, than the grain interior and if the density of the bulk material is ρ and the boundary is 10^{-7} cm thick, then

$$\Gamma_1 = -10^{-8}\rho \text{ gms/cm}^2$$

and

$$\underline{V}_1 = 1/\rho \text{ cm}^3/\text{gm}$$

hence

$$d\gamma/dP = 10^{-8} \text{ cm}.$$

So a pressure change of 1000 atmospheres will produce an increase in the surface tension of about 10 ergs/cm^2. It will be shown later that this change is large enough to be detected from measurements of ratios of surface tensions.

When a solute is present which segregates at the grain boundary one would expect $\Gamma_1 < 0$ and $\Gamma_2 > 0$. Referring to Equation (2-44) for the saturated solution, it is apparent that $d\gamma/dP$ could be either positive or negative depending on the extent of the segregation and the thermodynamic properties of the system.

The temperature coefficient of the grain boundary tension may be expressed in an entirely analogous manner. Assuming the solid is pure component (1), then

$$\frac{\partial \mu_1}{\partial x^\ell} \frac{dx^\ell}{dT} = \bar{S}_1^{\,\ell} - \underline{S}_1^{\,s} \qquad (2\text{-}45)$$

where $\bar{S}_1^{\,\ell}$ is the partial molal entropy of component (1) in the liquid, and $\underline{S}_1^{\,s}$ is the molar entropy of the solid. The temperature coefficient is:

$$\frac{d\gamma}{dT} = -S^{(s)} + \Gamma_1 \underline{S}_1^{\,s} + \frac{\Gamma_2}{1 - x^\ell}\left[\underline{S}^\ell - x^\ell \underline{S}_1^{\,s}\right] \qquad (2\text{-}46)$$

where $\underline{S}^\ell$ is the molar entropy of the liquid.

For a grain boundary in a one component solid, (2-46) reduces to

$$d\gamma/dT = -S^{(s)} + \Gamma_1 \underline{S}_1^{\,s} .$$

Since $\Gamma_1 < 0$ one would expect the temperature coefficient of the grain boundary tension to be negative. In a two component system, it is obvious that the temperature coefficient may be either positive or negative depending on the degree of segregation at the boundary and the thermodynamic properties of the system.

CHAPTER III

LITERATURE REVIEW

The literature chosen for review may be classified under three main headings: (1) a survey of some measurements of ratios of interfacial tensions, obtained by measuring the dihedral angle, (2) a survey of measurements of changes in interfacial tension with pressure, and (3) a review of two areas, brittle fracture and liquid phase sintering, in which interfacial tensions play an important role.

1. Measurement of Ratios of Interfacial Tensions

Many methods have been devised for measuring the interfacial tension between two fluid phases. The two most common are measurements of capillary rise and measurement of drop shapes. Adam's book[1] describes these methods and their theoretical basis.

The only means of measuring with any degree of reliability the surface tension between a solid and a fluid phase is the method of Udin, Shaler and Wulff.[104] This involves suspending small weights from fine wires, measuring rates of extension, and finding (either experimentally or by extrapolation) the weight which just compensates for the tendency of the wire to contract due to surface tension. This method yields an absolute measure of the solid surface tension for polycrystalline wires if the ratio of surface and grain boundary energies is known, but is only useful to within 200°C of the melting point. Hayward and Greenough[41] have measured the surface tension of nickel by this method. Shuttleworth,[90] Herring,[43] McLean,[65] Udin,[105] and others have discussed this method. Herring concludes that surface tension and surface stress are equal in these experiments.

Measurements of ratios of surface tensions are easier to obtain. These are based on equations describing the surface tensions of three interfaces meeting at a line as a vectorial balance of forces. These equations are strictly true when all of the phases are fluids, but are not necessarily true when one or more of the phases is a solid. Thus, if phases 1, 2, 3 meet at a line, the surface tensions γ_{12}, γ_{23}, γ_{31} are given by the equations

$$\frac{\gamma_{12}}{\sin \theta_3} = \frac{\gamma_{23}}{\sin \theta_1} = \frac{\gamma_{31}}{\sin \theta_2} \qquad (3\text{-}1)$$

See figure 1(a).

If two of the phases are identical, the relation is:

$$\gamma_{11} = 2\gamma_{12} \cos \theta/2 \qquad (3\text{-}2)$$

See figure 1(b).

If the (1) phases here are metal grains, then γ_{11} is the grain boundary tension. If (2) is a gas phase or vacuum, then this expression describes the angle formed during thermal grooving at a grain boundary.[44,71] If (2) is a liquid or solid phase, then θ is termed the dihedral angle.[93] The dihedral angle is important in determining the effect of a dispersed "second phase" on mechanical properties.

When a liquid droplet is placed on a rigid, undeformable, insoluble solid, the vectorial balance of tensions only takes place in the plane of the solid, as shown in Figure 1(c).

$$\gamma_{sv} - \gamma_{ls} = \gamma_{lv} \cos \theta \qquad (3\text{-}3)$$

where θ is the contact angle of the liquid on the solid (Figure 1(c)).
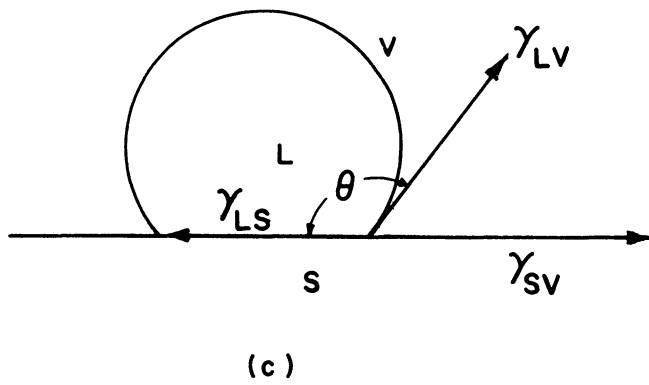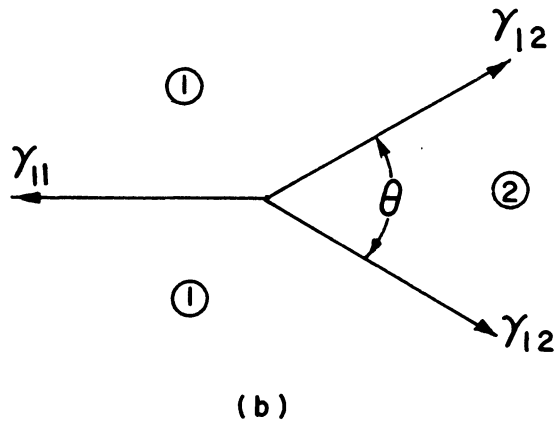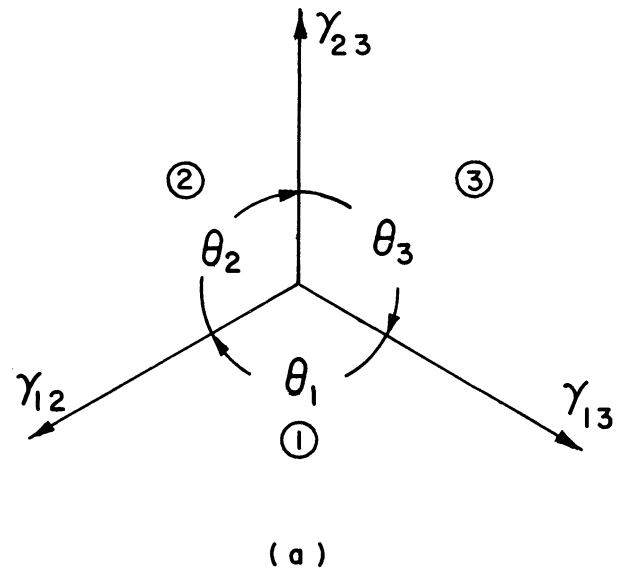
Figure 1.   Vectorial Relations Between Interfacial Tensions.

All of these relations are consequences of the necessity for minimization of the sum of the products of interfacial tensions and areas at equilibrium. (See Section 3, Chapter II.) From this principle, Gibbs[29] and Johnson[52] present derivations of Equation (3-3). Herring[43] outlines a derivation leading to (3-1) or (3-2).

It is worth noting at this point that the notion of surface tension as a physical force acting in the surface of liquids leads directly to the proper vectorial relations between tensions on intersecting surfaces. In solids, on the other hand, the surface tension is not a force per unit length but an energy per unit area. With a modification to be noted, however, the same relations between surface tensions hold for interphasal boundaries involving solids. The name "surface tension" is a misnomer for solids; it is retained because the quantity it describes has the same thermodynamic definition for all interfaces.

Herring[42] has shown that the vectorial balance of interfacial tensions given above is not strictly true when one of the phases involved is a solid whose interfacial tension depends on crystallographic orientation. By considering virtual displacements of three phase boundaries meeting at a line, the necessity for minimization of $\sum_{i=1}^{3} \int \gamma_i dA_i$ leads to the conditions[65]:

$$\gamma_{23} + \gamma_{13} \cos\theta_3 + \gamma_{12} \cos\theta_2 - \frac{\partial\gamma_{13}}{\partial\theta_3}\sin\theta_3 + \frac{\partial\gamma_{12}}{\partial\theta_2}\sin\theta_2 = 0$$

$$\gamma_{13} + \gamma_{23} \cos\theta_3 + \gamma_{12} \cos\theta_1 - \frac{\partial\gamma_{23}}{\partial\theta_3}\sin\theta_3 + \frac{\partial\gamma_{12}}{\partial\theta_1}\sin\theta_1 = 0 \qquad (3-4)$$

$$\gamma_{12} + \gamma_{23} \cos\theta_2 + \gamma_{13} \cos\theta_1 - \frac{\partial\gamma_{23}}{\partial\theta_2}\sin\theta_2 + \frac{\partial\gamma_{13}}{\partial\theta_1}\sin\theta_1 = 0$$

For derivatives with respect to θ_i clockwise rotation is positive (Figure 1(a)). Only two of the above relations are independent, and they do not suffice to determine the interfacial tensions or their derivatives with respect to rotation. For the most general case of the intersection of three grain boundaries, the situation is further complicated because five parameters of orientation are needed to describe the position of the boundary with respect to one of the adjacent crystals, and the terms $\partial\gamma/\partial\theta$ are dependent on these parameters.

If the conditions on a system involving solids are such that the stability condition for equilibrium does not reduce to simply minimization of the total interfacial free energy, then none of the Equations (3-1) to (3-4) are true.

Usually one assumes, that for anything but a small angle grain boundary or a twin boundary, the terms expressing orientation dependence in (3-4) are negligible and Equations (3-1) or (3-2) are used. This point will be expanded upon in the section on the orientation dependence of interfacial tensions.

In his classic paper on the role of interfacial energies in determining microstructures, C. S. Smith[93] noted that a vectorial balance of surface tensions at the junction of a twin boundary and a curved grain boundary would imply, in some cases, that the twin boundary had a negative surface tension. Since this is impossible, Smith thought that perhaps the twin boundary tension was so small as to be sensitive to slight variations in grain boundary tension as the grain boundary curved past the twin. Fullman[28] pointed out, however, that the behavior of coherent twin boundaries could be understood if one regarded them as "locked" in position due to the large amount of energy needed to reorient

them from their position of coherency. This, then, would only allow

a vectorial balance of surface tensions in the plane of the twin boundary.

This proposal leads to values for coherent twin boundary tension of about

0.035 of the grain boundary tension.[28] Mykura[72] has studied the thermal

grooving of twins in nickel and used Herring's equations to determine the

coefficients of orientation dependence of the surface tension. These

are on the order of 0.05 to 0.25 of the surface tension.

Measurements of relative interfacial tensions are capable

of detecting rather small changes in tensions. For example, the angle

of penetration of a liquid between solid metal grains is given by the

balance of surface tensions in Equation (3-2). If $\theta = 50°$ and $\gamma_{ss} =$

500 ergs/cm^2, then changes in γ_{ss} and γ_{sl} by 10 ergs/cm^2 produce

the changes in dihedral angle shown in Table I.

<div align="center">

TABLE I

EFFECTS OF SMALL CHANGES IN INTERFACIAL
TENSIONS ON THE DIHEDRAL ANGLE

</div>

Ratio of Tensions	Dihedral Angle
γ_{ss}/γ_{sl}	50°
$\dfrac{\gamma_{ss} + 10}{\gamma_{sl}}$	45°
$\dfrac{\gamma_{ss}}{\gamma_{sl} + 10}$	58°
$\dfrac{\gamma_{ss} + 10}{\gamma_{sl} + 10}$	54°
$\dfrac{\gamma_{ss} - 10}{\gamma_{sl}}$	55°
$\dfrac{\gamma_{ss}}{\gamma_{sl} - 10}$	40°
$\dfrac{\gamma_{ss} - 10}{\gamma_{sl} - 10}$	46°

For a dihedral angle less than 50°, the same change in the surface tensions will produce an even larger change in dihedral angle.

2. Measurement of Dihedral Angles

The most straight-forward way to measure a dihedral angle is to measure the trace of the angle on a surface normal to the line of intersection of the surfaces forming the angle. This may be done in sheet specimens where grains are allowed to grow to a width several times the thickness of the sheet. To a very good approximation, all grain boundaries become normal to the surface of the sheet during a long anneal and true dihedral angles can be measured directly.

A second method requires the measurement of a large number of angles made by the traces of grain boundaries on an arbitrary plane of polish. If there is a single dihedral angle characterizing the structure, this will give rise to a particular distribution of observed angles. From the observed distribution, one can determine the dihedral angle which generated it. The details of this method, originated by Harker and Parker,[39] are given in Appendix A.

The first method has the disadvantage that the same crystallographic surfaces will not lie in the plane of the sheet for all grains; hence, these may influence the equilibrated angle obtained. The second method has two disadvantages: a) the model for the distribution of angles observed may be inexact, and b) sampling error limits the precision of the measurements. These last disadvantages will be considered at length later.

All of the work described in the following section on the orientation dependence of surface tension was done measuring the dihedral angle directly. For some experiments, however, it is desirable to use the statistical method to determine the dihedral angle and assume that orientation differences exert a negligible influence on the distribution of measured angles.

C. S. Smith[93,94,95] and Ikeuye and Smith[51] measured the angle formed by particles of a low-melting second phase in the grain boundaries of a solid matrix phase, and studied the variation of this angle with temperature. Ikeuye and Smith[51] noted that the dihedral angle observed was dependent on the composition of the liquid phase present. When the composition of the liquid was changed either by changing the temperature or by adding alloying elements to the system, regular changes in the dihedral angle were observed. They concluded that major shifts in the dihedral angle with increasing temperature would only occur if the liquid composition varied markedly with temperature.

Van Vlack[106] also employed this technique to establish interfacial energies in the $Fe-Cu-Cu_2S$ system. Both Smith[93] and Van Vlack[106] showed conclusively that the relative interfacial tensions determined in this manner were internally consistent by comparing direct measurements and indirect calculations using other measurements to arrive at the relative tension for a particular interface.

McLean,[65] Taylor,[103] and Chalmers[16] have reviewed this work. More recently, Riegger[85] has correlated the change in dihedral angle made by a liquid phase with changes in composition of the liquid phase using a semi-empirical relation suggested by Taylor[103] based on

the Gibbs Adsorption Equation for binary systems. If one assumes that the grain boundary tension is nearly independent of temperature and composition changes in the liquid phase, then changes in the dihedral angle reflect changes in the solid/liquid interfacial tension. A plot of the solid/liquid interfacial tension obtained in this manner, versus the log of the solubility of the minor constituent in the liquid, is found to produce a linear relationship. From the slope of this curve one can then, presumably, calculate a surface excess concentration. Several other assumptions, beyond that of having the grain boundary tension constant with temperature, are also involved. Referring to Equation (2-35) it is apparent that the entropy terms must be negligible and that the activity of the solute must be proportional to its mole fraction. A constant slope with temperature, then, indicates that the surface excess varies as $1/T$. This correlation is not too helpful, because all these assumptions cannot reasonably be made without considerable experimental justification. For example, McLean's calculations (65, p. 148) indicate that the change in grain boundary tension with temperature cannot be ignored.

3. Orientation Dependence of Grain Boundary Tension

Five parameters are necessary in order to specify the orientation of a boundary between grains 1 and 2. Three determine the orientation of grain 2 with respect to axes in grain 1, and two determine the orientation of the boundary with respect to grain 1. It has proven difficult to establish orientation dependencies of grain boundary tensions because no absolute measure is available. Tensions must always be measured by means of a junction angle formed between the interface of interest and a reference interface which is assumed constant from sample to sample.

Read and Shockley[81] calculated the dependency of the energy

associated with a grain boundary formed from dislocations on the degree

of misorientation between the crystals on either side of the boundary.

They predicted that for angles of misorientation ϕ, up to about $\phi = 15°$,

the energy should be given by

$$E = E_o \phi \left[A - \ln \phi \right]$$

where E_o is a function of the macroscopic elastic constants and the

orientation of the boundary, and A is related to the energy in the

material immediately surrounding a dislocation and is also dependent on the

orientation of the boundary. This calculation was based on a model

of a simple tilt boundary in a simple cubic lattice. Since this reduces

to a two dimensional problem, only one parameter, ϕ, is needed to

specify the orientation of the grains, and another to specify the

orientation of the boundary.

Dunn and his co-workers[20,21,22] obtained the first confirm-

ation of this relationship. Dunn used oriented tricrystals of silicon

ferrite, in sheet form, all having the same crystallographic plane in

the plane of sheet. Variations in tensions with the degree of misorientation

between crystals were measured with reference to a standard interface

between crystals with a fixed degree of mismatch. Although the orientation

of the boundary could not be controlled in these experiments, the pre-

dicted relationship holds quite well. Some of the scatter in the data

is attributed to the variation in boundary orientation which occurred.[20]

Since this work, Chalmers, et al.[15,5,6,64,107] and Aust[8]

have determined this orientation dependence for Sn, Pb, Ge, Ag, and AgCl.

Friedel, Cullity, and Crussard[27] studied this effect in Al, and

Gjostein and Rhines[31] in Cu. Weinberg,[108] Chalmers,[16] Aust and Chalmers,[7] and McLean[65] have reviewed this work.

Conclusions which may be drawn are: a) the grain boundary tension is a function of misorientation between crystals, most of the variation in energy occurring between 0 and 15° for simple tilt boundaries, b) the grain boundary tension is not a strong function of the orientation of the boundary between grains of fixed orientation relative to one another, except perhaps for low angle boundaries, c) Cusps in the tension versus misorientation curve (which are predicted from the dislocation model) are not observed except, possibly, near twin orientations.

It is important to know the frequency with which low tension boundaries will be encountered in well annealed polycrystalline materials. Read and Shockley[81] estimate that "energies less than 50% of the average will be obtained in only about 3% of the cases. Consequently, observations of grain boundaries for grains selected at random would show such a small percentage of low energy boundaries that their presence would have only a slight effect on the statistics." This point will be dealt with later in the discussion of errors in the distribution of angles observed due to the presence of a range of dihedral angles in the specimen.

Several workers have determined the orientation dependence of the surface tension for metal vapor surfaces. The method involves the use of Herring's relation (Equation (3-4)) applied to thermally etched twins. By measuring various angles formed it is possible to determine the coefficients $1/\gamma \frac{\partial \gamma}{\partial \theta}$ which express the change in surface

tension with orientation. Mykura[72] showed that the surface tension changes about 6% with a rotation of about 30° from a (100) plane in nickel. Robertson and Shewmon[86] found changes of the same order of magnitude in copper. In both cases, the rate of change of tension with orientation is greatest near low index planes.

Before employing the method of statistical analysis to determine dihedral angles, it should be established that the large fluctuations in interfacial tension which occur, occur so infrequently as to be negligible, and that minor fluctuations in energy are too small to influence the distribution obtained. On the first point, reference can be made to Read and Shockley's statement above, and to similar statements by C. S. Smith[93] (It is a simple matter to show, that two adjacent grains, misoriented by a combination of tilt and twist less than 15°, occur randomly only 3.4% of the time.) Experiments on solid/ vapor interfacial tensions lead one to expect that the orientation dependence of any solid/fluid interface is small, but that a few percent variation can be expected. Hence, large fluctuations in grain boundary tension undoubtedly do not influence the distribution.

On the second point, fluctuations of a few percent seem likely in a large percentage of the grain boundary and solid/fluid interfaces one might encounter. These variations will lead to a broadening of the distribution of angles seen; a statistical analysis based on the ideal distribution (Appendix A) may be in error due to this broadening. This point will be dealt with further in the section on errors.

4. Changes in Surface Tension with Pressure

Comparatively few attempts have been made to determine the effect of pressure on surface tension. Before the importance of

adsorption was appreciated, it was believed possible to determine the molecular volume of a liquid at an interface by measuring the pressure coefficient of its surface tension. Several earlier experiments were done with this end in mind. More recent experiments have been performed on systems of interest to the petroleum industry.

The motivation for the early work was provided by an easily derived thermodynamic expression. Consider a system of n components in two bulk phases separated by an interface. For the entire system one may write:

$$dG = - SdT + VdP + \gamma dA + \sum_i \mu_i dn_i .\qquad (3\text{-}5)$$

Since dG is an exact differential, we may write

$$\left.\frac{\partial V}{\partial A}\right)_{T,P,n_i} = \left.\frac{\partial \gamma}{\partial P}\right)_{T,A,n_i} .\qquad (3\text{-}6)$$

That is, the change in surface tension with pressure is equal to the increase in volume of the system with an increase in interfacial area. Hence, in Bridgman's words,[11] "the pressure coefficient of surface tension is a measure of the difference of effective volume of a molecule in the interior and at the surface of a liquid." Lewis and Randall (1923)[61] support this view.

It was later realized[62] that this interpretation implied an over-simplified picture of the interface, as will be shown below. For a two phase, one component system, the quantity $\left.\partial\gamma/\partial P\right)_{T,A,n_i}$ cannot be determined because the pressure on the system cannot be varied at constant temperature and still retain two phases. If one has a binary system, however, consisting of a pure liquid of one component and a pure gas of another, with no mutual solubility, then one can certainly determine the quantity $\left.\partial\gamma/\partial P\right)_{T,A,n_i}$. To see the significance of the term $\left.\partial V/\partial A\right)_{T,P,n_i}$ the following illustration is helpful. Let a container fitted with a moveable

piston P be divided into two sections A and B by a sliding partition C, (Figure 2). In section A is pure vapor of substance 1 at a given temperature and pressure, and in section B is pure liquid of substance 2 at the same temperature and pressure. Assume that the properties of the liquid and vapor exist unchanged up to the partition C. Let C be slowly withdrawn and the piston P continually adjusted to maintain a constant pressure. Figures 3(a) and 3(b) show the density relationships before and after the partition is withdrawn.

Note that in this picture there is an abrupt density change clearly defining a physical "surface" at a. Also there is an "interfacial region" from a to b where the density of material (all substance 2) approaches the value of the density in the bulk liquid phase. Then the volume change of the system may be entirely ascribed to the change in density of the liquid phase in the region ab.

Now given measured values of $\partial\gamma/\partial P)_{T,A,n_i}$ and estimating a thickness for the interfacial region ab one is able to calculate an average density for the interface. Statistical mechanical models for the interfacial transition region in the liquid can then be checked directly from experimental data. This is the physical situation that Bridgman had in mind.

A somewhat more real physical situation might be imagined if adsorption of the gas were allowed at the interface, so that the density profile might look like Figure 3(c).

The change in volume of the system with creation of the interface is now the sum of volume changes which occur in the gas and liquid phases at the interface. The quantity $\dfrac{\partial V}{\partial A})_{T,P,n_i}$ cannot be broken down into

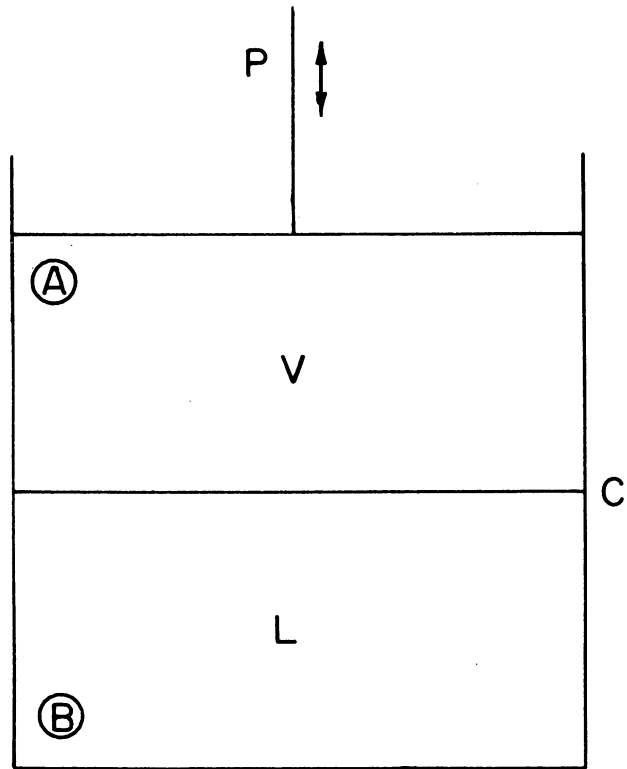Figure 2.   Thermodynamic Model for Creation
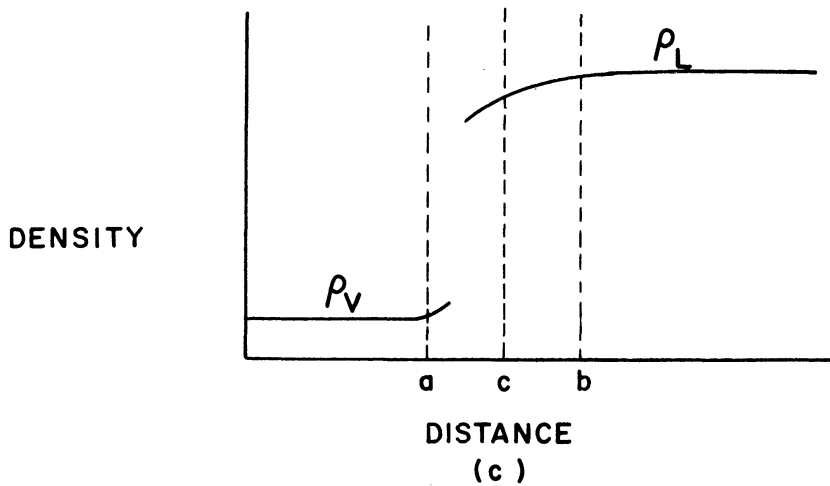of a Liquid/Vapor Interface.
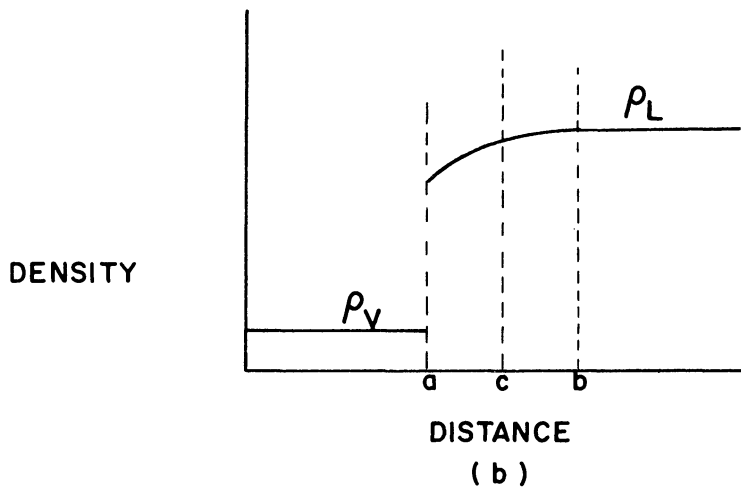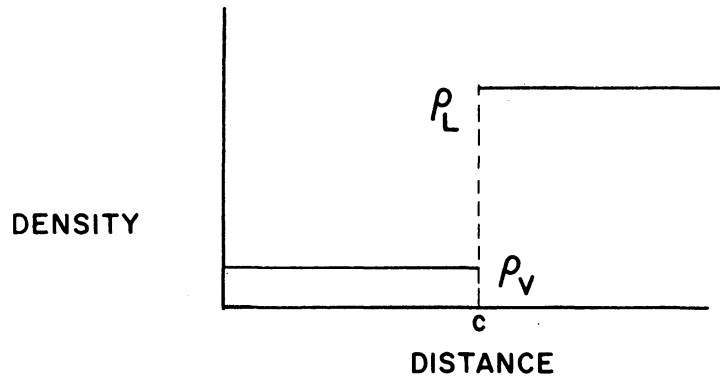
Figure 3. Density Profiles at the Liquid/Vapor Interface.
(a) Before Withdrawal of the Partition.
(b) After Withdrawal.
(c) A More Realistic Profile.

contributions from the gas and liquid phases without some information about the process occurring.

Based on the above approach, statements are often made, that since a liquid should be less dense near its surface than in its interior, the expression $\partial V/\partial A \big)_{T,P,n_i}$ will be positive and the surface tension should increase with increasing pressure. Clearly, however, with adsorption occurring, nothing can be said a priori as to whether surface tension should increase or decrease with pressure.

In any real case, where the liquid has a significant vapor pressure and the gas dissolves somewhat in the liquid, the transition in density across the interface is probably continuous (on a statistical basis, ignoring atomistics) and even less can be said about the physical meaning of the expression $\partial V/\partial A \big)_{T,P,n_i}$.

Recent workers have dealt with the change in surface tension with pressure in terms of the Gibbs Adsorption Equation. This approach emphasizes the importance of adsorption at the interface.

Recently, experiments have been performed on systems generally involving water and hydrocarbons. In oil reservoirs, recovery of oil in porous rock is affected by the displacement of oil by natural water which is in turn affected by the interfacial tension between the oil and water. But these interfacial tensions are established under conditions of very high pressure; hence it is important to know how interfacial tensions are affected by pressure. A number of experiments have been performed to determine the pressure effect on some important hydrocarbon systems.

Apparently the first measurements of the change in surface tension with pressure were performed by Kundt[60] in 1881. He measured

the change in vapor-liquid interfacial tension with pressures up to

212 atm in the systems CS_2—air, $CHCl_3$—air, C_2H_5OH—air, $C_2H_5OH-H_2$,

$(C_2H_5)_2O$—air, and $(C_2H_5)_2O$—H_2. In all cases he found the surface

tension to decrease with increasing pressure.

In 1906, Lynde[63] measured surface tension changes with

pressure in the systems mercury-water, mercury-ether, water-ether,

chloroform-water, and carbon bisulfide-water at pressures up to 5000

psi. He found increases in surface tension with pressure in the systems

mercury-ether, mercury-water, and carbon bisulfide-water and decreases

in the others. Bridgman[11] has commented on Lynde's work in connection

with determining the molecular volume at the interface by means of

Equation (3-6).

Rice[83] has discussed the effect of pressure on surface tension.

He points out that a one component liquid in equilibrium with its vapor

is "almost certainly" less dense near the surface than in the bulk;

hence $\partial V/\partial A)_{P,T,n}$ should be positive and the surface tension of a

binary system involving this liquid should increase with pressure.

Since Kundt's work shows that the surface tension decreases with increasing

pressure, Rice sought to meld the interpretation of surface energy changes

with pressure on the basis of Equation (3-6) with the interpretation

based on the Gibbs Adsorption Equation. He considers two component

vapor-liquid systems and breaks down $\dfrac{\partial V}{\partial A}\bigg)_{P,T,n}$ into two

terms: a ΔV of the gas phase arising from adsorption of gas

at the surface of the liquid, and a ΔV_σ arising from a density decrease

in the liquid near the interface. (Implicitly, his model demands that the

dividing surface to which the excess quantities refer be placed so that

on one side of the surface the properties of the gas phase are uniform.)

The volume change due to adsorption of gas in the liquid surface may be written $\Delta V = -\Gamma \underline{V}$, or for an ideal gas $\Delta V = \dfrac{-\Gamma kT}{P}$, where Γ is the surface excess of the gaseous component at the interface, with the dividing surface indicated above, and P is the total pressure on the system. So for an ideal gas

$$\left.\frac{\partial \gamma}{\partial P}\right)_{T,A,n_i} = \frac{-\Gamma kT}{P} + \Delta V_\sigma . \tag{3-7}$$

Now Rice applies this equation to Kundt's data assuming $\Delta V_\sigma = 0$ and is able to account for the fact that the surface tension decreases with increasing pressure. He obtains values for Γ as a function of pressure.

The same equation that Rice obtains may be obtained immediately from the Gibbs Adsorption Equation, avoiding the awkwardness of Rice's approach. For an ideal gas (1) above a liquid (2) the Gibbs Adsorption Equation at constant temperature is

$$- d\gamma = \Gamma_1 d\mu_1 + \Gamma_2 d\mu_2 .$$

If one chooses the dividing surface so as to make the surface excess of the liquid component vanish, i.e., $\Gamma_2 = 0$ then

$$- d\gamma = \Gamma_{1(2)} d\mu_1 \tag{3-8}$$

where $\Gamma_{1(2)}$ is the surface excess of component 1 for this choice of dividing surface. Now for the gaseous phase

$$d\mu_1 = \frac{\partial \mu_1}{\partial P} dP = \overline{V}_1 dP = \underline{V}_1 dP .$$

For a one component ideal gas, $d\mu_1 = \dfrac{kT}{P} dP$; therefore

$$d\gamma/dP = -\Gamma_{1(2)} \frac{kT}{P} \tag{3-9}$$

which is Rice's result, obtained in a more conventional manner.

Slowinski, Gates, and Waring[92] measured the effect of six

pressurized gases above water and n-hexane. The gases were CO_2, C_2H_6,

CH_4, N_2, H_2 and He. With all gases except He above either liquid,

a decrease in surface tension with pressures to 100 atm was observed.

Helium pressures to 100 atm produced a very slight increase in the

surface tension for both liquids. These results tend to confirm

Equation (3-7), which ignores any mutual solubility of the components.

From the shapes of the curves obtained it appears that over a fairly

wide range of pressures that $\Gamma_{1(2)}$ = KP; that is, the adsorbed excess

is proportional to pressure. It is interesting to note that the order

of increasing effect of a particular pressurized gas on the surface

tension of water is the same as the order of increasing gas solubility

in the water at atmospheric pressure.

Gielessen and Schmatz[30] measured the pressure dependence

of the liquid/vapor surface tension for the liquids n-hexane, heptane,

octane, nonane, a C_{13}-fraction, and cyclohexane under nitrogen.

In addition, they also considered n-hexane and nonane under pressures

of helium and argon. In all systems except those involving helium,

the surface tension was found to decrease with pressure. The data in

these systems were correlated with an empirical equation, with two

constants, formally similar to the Langmuir Adsorption Isotherm.

These authors confirm the results of Slowinski, et al.[92] for systems

involving helium; i.e. a small, linear increase in surface tension is

found.

Hassen, Nielsen, and Calhoun[40] measured the effects of

pressures to 204 atm and temperatures from 26° - 82°C on the liquid-

liquid interfacial tensions of a series of hydrocarbons with water.
The hydrocarbons used were benzene, propane, n-butane, n-pentane,
n-hexane, n-octane, and i-octane. In all cases increasing pressure
lowered the surface tension, the magnitude of decrease varying with
the liquid pair. Presumably, this data can be subjected to the same
treatment outlined above. If we choose the dividing surface so that
the surface excess of water vanishes, $\Gamma_2 = 0$, then

$$- d\gamma = \Gamma_{1(2)} \, d\mu_1.$$

Assuming the hydrocarbon liquid does not dissolve water, then

$$d\mu_1 = \frac{\partial\mu_1}{\partial P}\bigg)_T \, dP = \overline{V}_1 \, dP = \underline{V}_1 \, dP.$$

So

$$d\gamma/dP = - \Gamma_{1(2)} \, \underline{V}_1 \tag{3-10}$$

where $\underline{V}_1$ is the molar volume of the hydrocarbon liquid. Knowing
$\underline{V}_1 = \underline{V}_1 (P)$, i.e., compressibility data for the hydrocarbon, surface
excess quantities may readily be computed.

Michaels and Hauser[67] measured the liquid/liquid interfacial
tension in the systems n-decane-water and benzene-water as a function
of temperature and pressures to 700 atm. The interfacial tension
decreased with pressure in the benzene-water system and increased
with pressure in the n-decane-water system.

Hough and his co-workers[48,49,50] have measured surface tension
changes with pressure in systems involving water and methane, helium,
nitrogen or carbon dioxide at pressures up to 1000 atm. They find
rather irregular behavior in some of these systems: 1) in the water-
methane system the surface tension at 100°F and 160°F decreases with

increasing pressure to about 5000 psi, then increases; while at 74°F
it decreases continuously with pressure, 2) the surface tension in the
water-nitrogen system decreases with pressure at temperatures from 80°F
to 280°F, 3) the surface tension in the water-helium system <u>increases</u>
with applied pressure by a rather small amount at temperatures from
80°F to 280°F, 4) the surface tension in the water-CO_2 system decreases
with increasing pressure, showing an initial sharp decrease to about
3000 psi followed by a more gradual decrease thereafter.

Using the relation (3-7), Hough et al.[49,50] calculate surface
excess quantities as a function of pressure for these systems using
$\Delta V_\sigma = 0$. Although their surface tension measurements show little
scatter about a smooth curve, they are not sufficiently precise to allow
calculation of the surface excess to much more than an order of magnitude.
The plots of Γ vs P which they presented imply much better precision.

The pressure dependence of interfacial tension has been
measured for a number of systems involving crude oil, water and reservoir
gases.[47,53,102] The results are rather irregular, and because of the
multitude of chemical species present (in unknown proportions), have
little scientific value.

A certain amount of work has also been done by Russian investi-
gators on surface tension changes with pressure in hydrocarbon systems
important to the petroleum industry.[88] This work appears to be
fundamentally no different than the American work discussed above.
One exception is that differences in the wetting of solids by liquids
have been noted when the gas pressure surrounding the liquid-solid system
is increased.

In summary, the above results indicate that changes in pressure can produce measurable changes in surface tension in liquid-vapor and liquid-liquid interfaces and possibly in liquid-solid interfaces. The change in surface tension with pressure can be described by the Gibbs Adsorption Equation at constant temperature with the total differentials of chemical potential for each component expressed as functions of pressure and composition. In certain cases, especially for binary systems where one component is not present in both phases, the change in surface tension with pressure is given by the particularly simple relation

$$\frac{d\gamma}{dP} = - \Gamma_{1(2)} \underline{V}_1$$

which is rigorously true for a plane interface, with the dividing surface chosen so that $\Gamma_2 = 0$ and where $\underline{V}_1$ is the molar volume of component 1 in the phase which is assumed to be pure component 1. $\Gamma_{1(2)}$ is then the surface excess of component 1 for this choice of dividing surface.

5. Brittle Fracture

In two papers in the early 1920's[32,33] Griffith proposed a theory of rupture for isotropic brittle materials which has formed the basis for much of the subsequent work done to explain brittle and nearly-brittle failure.

The principle behind the theory is quite straightforward. If one assumes the existence of some sort of microcracks in a material, then the minimum energy that must be supplied to create a unit area of new crack surface (propagate the crack) at constant temperature is the surface tension (as defined earlier) of the crack surface. Thus, the

energy stored in the surface of a very flat elliptical crack in a plate per unit plate thickness is $W_s = 4\gamma C$ where the length of the crack is 2C.

In addition to this energy, elastic energy is stored in the material due to the action of external forces. This energy may be divided into two parts: (a) the elastic energy W_a which would be stored if the crack were absent, and (b) a correction term which accounts for the additional strain energy due to the presence of the crack. This latter term will be dependent upon the length of the crack, and is given for the plane strain problem by $W_b = \dfrac{(1 - \nu^2)\, \pi^2 C^2 \sigma^2}{E}$ where σ is the stress normal to the crack, ν is Poisson's ratio and E is Young's modulus.

For a fixed stress, the total decrease in the potential energy of the material and its surface tractions is equal to the strain energy stored in the material.[32] Hence, the potential energy of the system at equilibrium with reference to the unstressed, uncracked state is:

$$\triangle W = W_s(C) - W_a - W_b(C).$$

If the crack is to propagate, the total energy must decrease as C increases. The point at which the crack is in equilibrium with the applied stress is given by $\dfrac{d\triangle W}{dC} = 0$. When C exceeds the value given by this expression the crack may propagate without limit. Alternatively, one may also determine the stress above which a crack of length 2C will propagate. For a flat elliptical hole in a plate in a condition of plane stress, the critical stress applied normal to the crack is

$$\sigma_c = \sqrt{\frac{2E\gamma}{\pi\,C}}\,. \qquad\qquad (3\text{-}11)$$

For the plane strain problem the critical stress is given by

$$\sigma_c = \sqrt{\frac{2E\gamma}{\pi C (1 - v^2)}} \qquad .$$

(3-12)

Sack[89] has treated the corresponding three dimensional

problem of a circular "penny-shaped" crack in a solid and finds that

$$\sigma_c = \sqrt{\frac{\pi E\gamma}{2C (1 - v^2)}}$$

(3-13)

where σ_c is the critical stress normal to the plane of the crack.

Griffith's theory adequately explains the fracture behavior

of glasses and some ionic solids.[3]

In recent years, the Griffith theory has been modified to account

for the plastic deformation associated with cleavage-type fractures in

metals which have some ductility. Thus, Orowan[77] suggests that γ

in Griffith's expression be replaced by $\gamma + p$, or simply p, where

p represents the energy stored in plastic deformation per unit area of

crack surface formed, and is about 1000 times as large as γ. The

presence of deformed metal layers on fracture surfaces lends support

to this suggestion.[25]

Griffith's theory does not explain how microcracks originate

in metals, or how they grow to a critical size. The answer to this

problem has been provided by the development of theories of crack nucleation

based on dislocation models. Stroh has been a major contributor in this

field, and has written an excellent review of many aspects of metal

fracture.[100]

According to the model developed by Stroh, cracks are nucleated

in polycrystalline metals by the pile-up of dislocations in a slip band

at a grain boundary. The grain boundary is usually an effective obstacle

to the propagation of slip because the orientation of adjacent grains across the boundary is different. That is, slip in one grain cannot readily be extended to a neighboring grain because there is no slip system properly oriented to accomodate it. This situation produces a pile-up of dislocations in the slip band at the grain boundary.

When a sufficient amount of slip has taken place in a grain, the total stress field arising from the piled-up dislocations becomes large enough to create a crack. Stroh's relation for the resolved shear stress on the slip plane needed to produce a crack is:[100]

$$\sigma_s = \sqrt{\frac{3\pi\gamma G}{8(1-\nu)L}} \tag{3-14}$$

where G is the rigidity modulus and L is the length of piled-up dislocations in the slip plane. (L is usually taken to be of the order of the grain diameter.)

As Stroh points out,[100] the above relation for crack nucleation does not contain a dependence on the crack length, thus the crack may grow with an overall decrease in energy until it has consumed the dislocations which produced it. Once this occurs further growth of the crack is dependent upon the normal stress across the crack and the ability of the material to yield plastically to reduce the stress concentration at the crack tip. For an ideally brittle material, Griffith's criteria now determines whether or not the crack will propagate; for a material with some ductility Orowan's modification may be appropriate.

The theories outlined above explain many aspects of fracture behavior. Fracture, however, is a very complicated subject. Reference to a recent symposium on fracture[9] shows that many modifications and refinements of the foregoing notions are needed to explain the many phenomena observed.

It is apparent from the preceding discussion that the surface

tension of the crack surface is of paramount importance in fracture theory

because it occurs in every expression (3-11) to (3-14) for the critical

stress for crack nucleation or growth. Changes in the state of the system

which change this surface tension can produce changes in the fracture

behavior of a metal. But not all changes in surface tension produce

identifiable changes in fracture strength. For example, changes in

temperature and pressure (or stress) produce changes in the surface

tension, but they have a much more pronounced effect on the generation

and movement of dislocations; hence any effect of surface tension changes

from these sources is masked by changes in the modes of deformation.

Changes in composition, on the other hand, change the surface tension

and may not radically change the mechanism of crack nucleation and growth.

Petch[80] has developed this last idea to explain the hydrogen

embrittlement of iron. Using Stroh's criteria for the nucleation of a

cleavage crack due to dislocation pile-up, Petch corrects the surface

energy term for adsorption of hydrogen on the crack surfaces. He

employs the Gibbs Adsorption Equation, written for the adsorption of an

ideal gas, and substitutes the Langmuir Adsorption Isotherm to express

the surface excess concentration as a function of pressure. Although

sufficient data is not available to allow a precise calculation to be

made, it is clear that the lowering of surface tension due to adsorption

should produce a drop in strength which is of the same order of magnitude

as that which is observed.

6. Intergranular Fracture

The dislocation model of crack nucleation proposes that the

nucleating crack is transgranular, but there are many occasions where fractures are observed to proceed along grain boundaries rather than across grains. The minimum energy required to form a unit area of grain boundary crack at constant temperature is $2\gamma_s - \gamma_{gb}$ and the energy required to form a transcrystalline crack is $2\gamma_s$, where γ_s is the surface tension of the crack surface formed and γ_{gb} is the surface tension of the grain boundary.[65] One usually assumes that a crack propagates so as to expend the least amount of energy; this suggests that variations in the quantity $2\gamma_s$ are important in determining the fracture path. While it is always true that $\dfrac{2\gamma_s - \gamma_{gb}}{2\gamma_s} < 1$, γ_s is generally much larger than γ_{gb}. This ratio is on the order of 0.9, so other factors probably determine whether the fracture will proceed intergranularly or transgranularly, or show a mixture of the two. But if γ_s is caused to decrease, e.g., by changes in composition, then the ratio $\dfrac{2\gamma_s - \gamma_{gb}}{2\gamma_s}$ is smaller and preference for the inter- granular path is now marked.

One of the ways in which γ_s can be significantly lowered has been mentioned above in the case of hydrogen embrittlement. And indeed, intergranular fracture is observed in this case.[100] This is at best, however, a qualitative correlation; no theory has yet explained all that is involved in the choice of fracture path.

The work of Eborall and Gregory[23] and Rostoker[73,74,75,17,87] on embrittlement by liquid metals lends itself to interpretation on the basis of changes in interfacial tension. Eborall and Gregory showed that small amounts of lead present in β-brass and tin bronze produced a large drop in the hot ductility of these alloys. (Experiments were conducted above the melting point of lead.) They pointed out that

for intergranular cracking, the surface energy that must be supplied
to propagate a Griffith crack in the presence of a liquid phase is
$2\gamma_{sl} - \gamma_{gb}$ where γ_{sl} is the surface tension of the solid-liquid
interface. As a rule, $\gamma_s > \gamma_{s(l)} > \gamma_{sl}$ i.e., the surface tension
of the pure metal surface is greater than its surface tension in the
presence of the liquid's vapor, and the latter is in turn greater than
the solid-liquid interfacial tension. Hence, if the liquid fills the
crack tip, a Griffith crack can propagate at a much lower stress. It
is likely, in this case, that the lead particles existing in the grain
boundaries of this material acted as pre-existing Griffith cracks.

Rostoker and his associates have published several papers
(73,74,75,17) and a book[87] on the embrittling effect of liquid metals.
The features they have observed are characteristic of many types of
embrittlement; for example: (1) a ductile-brittle transition temper-
ature, (2) delayed failure behavior, (3) dependence of embrittlement
on grain size, and (4) intergranular, rather than transgranular cracking.

They have observed that cracking commences at the surface of
a metal stressed in a liquid metal environment. Hence, the environment
probably influences not only crack propagation but nucleation as well.
This supposition has been confirmed,[75] and by use of the Stroh-Petch
relation between grain size and fracture stress, the effective surface
tensions for the nucleation and propagation of cracks have been estimated.
While the interpretation of the results in terms of surface tensions
depends on the model chosen for the initiating crack, the data suggest
that the initiating and propagating steps are characterized by different
surface tensions.

Brittle, intergranular failures are also observed when a casting fails by "hot-tearing." Hot tears may occur whenever stresses are produced in the casting due to either thermal gradients or constraints on the cooling metal from complicated mold shapes. In either case, severe hot tearing is usually associated with the presence of a low melting phase, e.g. an iron sulfide-iron eutectic in steels. In the absence of this liquid, tearing seldom occurs because the metal plastically deforms to reduce the magnitude of the stresses present. With some liquid present, these stresses are reduced by cracking. It seems likely that the mechanism Eborall and Gregory propose to explain the detrimental effect of lead in brass and bronze is also applicable here.

7. Liquid Phase Sintering

Liquid phase sintering is a process in which a liquid phase, permeating the interstices between solid particles, accelerates the densification of the compact. As in all sintering, interfacial tension plays a dominant role in this process, and the lowering of the total free energy of the system by the motion of interfaces (and resulting change in particle shape) provides the driving force for densification.

Although liquid phase sintering has been a successful industrial technique for many years, the theoretical development of the subject has lagged. Recently, however, Kingery[56,57,58] has proposed a densification mechanism for liquid phase sintering which conforms to experimental observations of the importance of major process variables.

Liquid phase sintering begins, typically, with a pressed compact of low and high melting materials. When the compact is raised

to a temperature sufficient to melt the low melting phase, an initial

densification occurs due to the rearrangement of the solid particles

into a more closely packed configuration. In order to obtain the

accelerated densification characteristic of liquid phase sintering,

several criteria must be satisfied: (1) there must be sufficient

liquid present to fill most of the interstices of the solid particles,

(2) the solid must be appreciably soluble in the liquid, and (3) the

liquid must wet the solid completely.

The structure of a compact which has been liquid-phase sintered

generally shows rounded solid particles outlined by the totally wetting

liquid phase. (If the solid is non-metallic, e.g., a carbide, euhedral

grain shapes will often be preserved.) If insufficient liquid is

present or if the liquid does not wet the solid completely, bridges

may form between the solid particles, and the sintering rate slows to

that characteristic of conventional solid state sintering. The solid

particles change shape by a process of solution and reprecipitation,

mass transport taking place through the liquid phase; hence the

requirement that the solid be soluble in the liquid phase.

After the initial readjustment when the liquid phase melts,

the solid particles change shape so as to: a) round off sharp edges,

b) flatten points of contact (or points of nearest approach), and

c) increase in size. Kingery[56] proposes that step (b) is most

important in promoting densification, and derives an expression for

the rate of densification due to this process.

Several requirements on interfacial tensions may be inferred

from the above requirements for successful liquid phase sintering.

(a). The solid-liquid interfacial tension must be less than or equal to half the solid-solid grain boundary tension for the liquid phase to wet the solid particles.   (b). Following Kingery's model, it is necessary that the contact angle, formed by the balance of liquid-vapor, solid-vapor and solid-liquid interfacial tensions, be acute, which implies that the solid-vapor tension is greater than the solid-liquid tension.

Equilibrium measurements of relative interfacial tensions of a liquid-solid pair should indicate whether liquid phase sintering is possible for this system. In practice, however, if the liquid is not saturated initially with the solid (and vice versa) the wetting characteristics may deviate far enough from equilibrium behavior so that relative interfacial tensions determined at equilibrium are a poor guide to the actual sinterability of the system.[58, discussion] In addition, surface active impurities present in small amounts may also influence wettability.

Since surface tensions vary with the pressure on the system, it is possible that some of the benefits of sintering under pressure (hot-pressing), with or without a liquid phase present, are due to pressure induced changes in surface tensions.

8. Summary

The effects of temperature and composition on surface and interfacial tensions have been widely studied and are generally appreciated. Relatively few investigations have been made of the effect of pressure on interfacial tensions, mainly because pressures beyond the customary range of laboratory experimentation or commercial application must be

applied to produce a significant change. This is particularly true
for interfaces between condensed phases.

The tension of a solid/liquid or solid/solid interface is
difficult to measure absolutely. Ratios of these tensions, however,
can be more easily determined. Complications which arise due to the
crystallographic and elastic properties of the solid are frequently
resolved by assuming that metals behave as liquids. This assumption
is warranted in many cases, but the departures from liquid-like behavior
(e.g., the dependence of grain boundary tension on the misorientation
of grains across the boundary, the behavior of coherent twin boundaries)
have provided a most fruitful field for research.

A study of changes in interfacial tensions in metals is
profitable because many properties of the metal depend indirectly
on interfacial tensions. For example, interfacial tensions are the
major controlling factor determining the shapes of grains in annealed
polycrystalline metals. The magnitudes of certain of these tensions
and the relative magnitudes of tensions at various types of interfaces
must also be considered in theories of brittle fracture and theories of
sintering. Changes in interfacial tensions arising from changes in
composition have been shown to significantly influence such properties
as fracture strength and ductility. It is likely that changes in
interfacial tensions caused by changes in pressure (or state of stress)
or temperature may also influence these properties, although the effect
may be masked by changes in the mode of deformation.

CHAPTER IV

EXPERIMENTAL PROCEDURE

1. Sample Preparation

All specimens of leaded nickel were made using high-purity

(99.99+%) lead obtained from the American Smelting and Refining Company.

Table II is the spectrographic analysis provided with this material.

TABLE II

SPECTROGRAPHIC ANALYSIS OF LEAD USED FOR ALLOY

Bi	0.0008 *	Fe	0.0002
Cu	0.0003	Zn	N.D.
Sb	N.D.	Cd	N.D.
As	N.D.	Ag	N.D.
Sn	N.D.	Te	N.D.
Ni	N.D.	Pb	99.99+% by difference

N.D. = None Detected   * Weight Percent

Mond Nickel shot (99.95% Ni + Co), obtained from the International

Nickel Company, was used in all but two melts. All specimens with the

letters B, C, or D in their designation were from heats made using

Mond Nickel. Specimens from heats E and F were made using Sherritt

Gordon Grade "E" Nickel Powder. A typical analysis provided with the

latter material is given in Table III.

TABLE III

TYPICAL ANALYSIS OF SHERRITT GORDON
GRADE "E" NICKEL POWDER

Ni	99.9*	Fe	0.004
Co	0.03	S	0.002
Cu	0.01	C	0.03

* Weight Percent

Heats B, C, D, consisting of about 4 lbs. of Ni and Pb were

induction melted in a LECO zirconia crucible under a protective atmosphere

of tank argon. The system was evacuated and flushed with argon before

melting and while the system was being heated. From 8 - 12 psig argon

pressure was kept above the melt to keep the lead from boiling off.

Melts were allowed to solidify in the crucible under argon pressure.

In all cases ingots showed no sign of oxidation during melting.

Heats E and F were prepared by compacting mixed lead

and nickel powders and sintering at 1500°F for about 18 hours in purified

flowing hydrogen. The sintered compacts were then melted under a pressure

of about 3 psig purified flowing hydrogen in a small globar furnace.

The melt was contained in a small Morganite, recrystallized alumina

boat. The hydrogen gas was purified by passage through a DeOxo unit,

a Drierite dessicant, and a liquid nitrogen cold trap. Pressure was

maintained on the system by bubbling the outlet gas through about

7 inches of mercury.

Analyses were performed on a sample of material from Heat D

by Chicago Spectro Service Laboratory. The results are shown in

Table IV.

TABLE IV
ANALYSIS OF HEAT "D"

Pb	1.98*	C	0.02
Cu	0.001	S	0.013
Fe	0.002	O	0.004
Si	0.001		

* Weight Percent

Since the analysis of Heat D showed a sulfur content which

was not negligible, heats E and F were made to obtain specimens with

a low sulfur level. A sulfur analysis on Heat F performed by the Research

Laboratory of the International Nickel Company indicated 3 ppm sulfur,

which is considerably lower than the sulfur content of the Nickel used

for the melt.

Sufficient information as to the free energies of formation of the nickel sulfides is not available. Thus, the partial pressure of H_2S in equilibrium with them cannot be calculated. However, the data that are available[24] indicate that the free energy of formation of these sulfides is not much different from the free energy of formation of H_2S, per mole of sulfur. It is probable that the partial pressure of H_2S in the flowing hydrogen stream was kept low enough to result in removal of sulfur from the nickel in heats E and F.
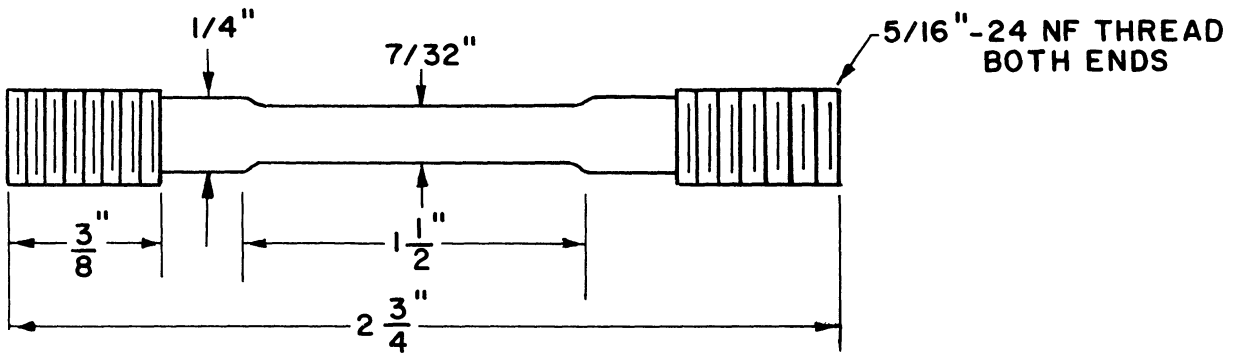
Test Specimens

Test specimens were machined from ingots according to the dimensions shown in Figure 4.

Specimens used in hydrostatic testing and for equilibration at various temperatures varied in dimensions. Most were small cylinders, 3/16 inches diam., 1/2 inches long.

Tensile specimens were copper plated before use. A flash coat of copper was applied using a cyanide bath, at low current density. Subsequently a heavier coat, about 0.001 inches thick, was applied from a sulfate bath at higher current density. Plating conditions and solutions used are given by Kehl.[54]

Heat Treatment

Specimens were equilibrated at temperatures from 371°C to 816°C at times varying from 24 hours to one week. All specimens subjected to hydrostatic, tensile, or compression loading at 371°C were annealed for one week at 371°C prior to testing. Specimens hydrostatically tested at 593°C were annealed for five days at 593°C prior to testing.

(a)
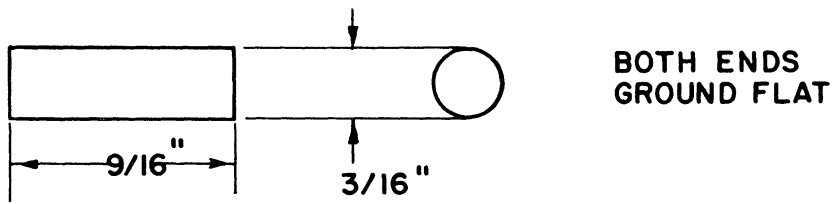
(b)

Figure 4. Tension and Compression Test Specimens.
(a) Tensile Specimen. (b) Compression Specimen.

The only exceptions were specimens from heats E and F which were annealed three days at 593°C.

Annealing was done in a vycor tube which was fitted with a ground glass joint and a stopcock. Samples were positioned in the tube using ceramic pieces so that when the vycor tube was placed in a tube furnace, the specimens were at a determinable position in the hot zone. Previous calibration of the furnace insured that the annealing temperature was within ± 5°C of the desired temperature during the course of the run.

The portion of the annealing tube not occupied by the specimen was filled with clean uranium turnings and cerium chips. Prior to placing the tube in the furnace, it was evacuated, flushed repeatedly with argon or helium, then evacuated again. The tube was placed in the furnace while still open to the vacuum system. After about 15 minutes of pumping while the tube was at the desired annealing temperature, the stopcock was closed and the vacuum system detached.

This proved to be a very satisfactory method for long time anneals. The presence of the very reactive metals, U and Ce, insured that residual amounts of gases were removed.

At the completion of the anneal, the vycor tube was quickly withdrawn from the furnace and quenched in water. This seemed to provide a satisfactory quench for the temperature range covered. It probably would not give a rapid enough quench from temperatures much higher than 816°C, however.

In every case, the specimens annealed in this manner were as bright as when they were placed in the furnace. The U and Ce present

were usually covered with a light coating of reaction products. This
was easily removed by cleaning in nitric acid. The same uranium turnings
were used for more than a dozen long time equilibrations.

The average matrix grain diameter after annealing for heats
B, C, D was about 0.5 mm. Lead was present largely as spherical
shapes within grains and as lenticular and elongated shapes in grain
boundaries. Figure 5 is typical of the appearance of the lead in these
alloys. Heats E and F were different. The average matrix grain
diameter in F was about 0.2 mm. The lead was distributed as in the
previous heats except that no elongated lead particles were observed
in grain boundaries. No significant change in matrix or particle grain
size occurred with heat treatment in the temperature range used.

Recrystallization of samples did not occur during heat treatment.
If the specimens were sufficiently deformed to cause recrystallization,
they were so badly cracked as to be unusable. Failure to have a recrystal-
lized matrix structure did not appear to introduce any systematic sampling
error in dihedral angle measurement.

2. Hydrostatic Pressure Testing

All tests under hydrostatic loading were carried out in a
hydrothermal unit, model HR-1B, manufactured by Tem-Press Research, Inc.
A schematic drawing of this apparatus is shown in Figure 6.

Each reactor vessel, about 8 inches long, with 1/4 inch bore
and 3/8 inch thick walls, was mounted so that a vertical tube furance
could be raised into a position around it. After completing a run,
the furnace could be quickly dropped, and a quenching bath placed about
the reactor. Specimens were successfully quenched from 593°C and 50,000 psi
by this method.

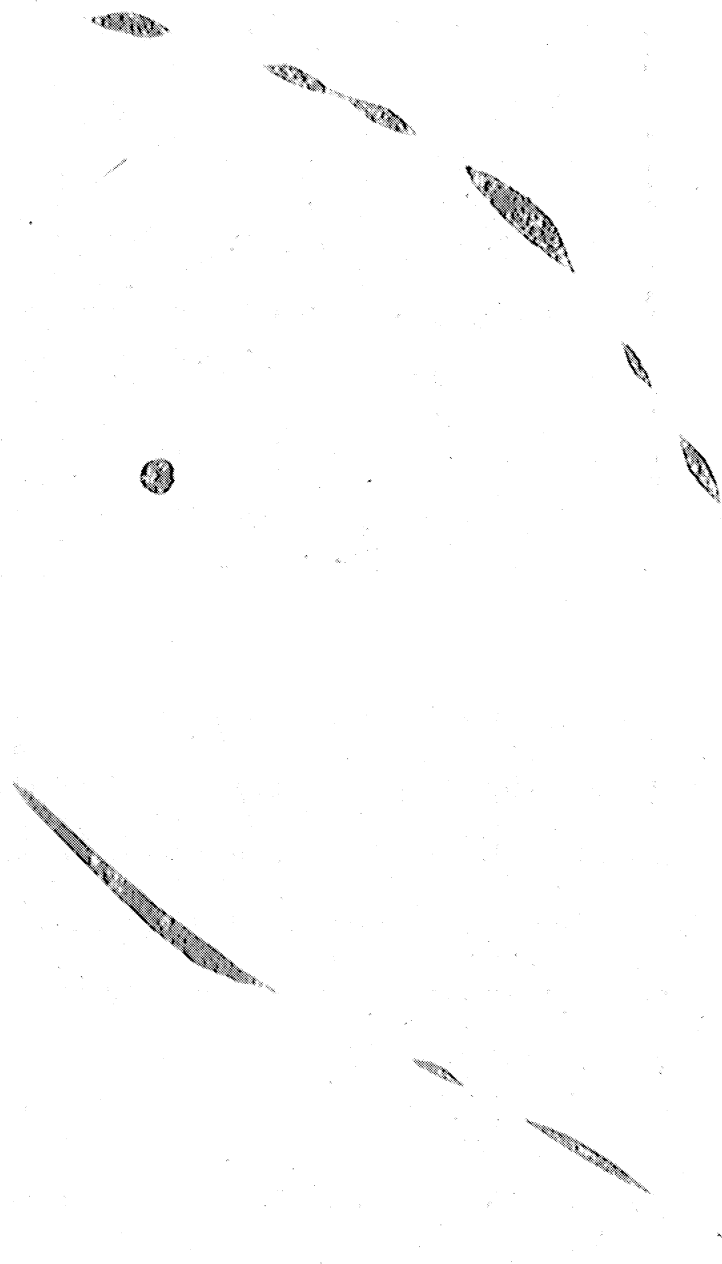Figure 5. Photomicrographs of Specimen DP8.
1000 X. Not Etched.

Figure 5 (cont'd). Photomicrographs of Specimen DP8. 1000 X. Not Etched.

The unit above is built to operate using water as a pressure medium. The procedure used for a typical run was: (1) The specimen was placed in reactor vessel and the vessel was filled with water, assembled and installed in the unit. (2) The pressure was raised on the vessel using the water pump. (3) The furnace was raised over the reactor and the vessel brought to the desired test temperature. (4) Excess pressure was bled from the system during heating and when stabilized at the test temperature. When the desired test temperature and pressure were obtained, the system was isolated by closing the appropriate valve. When the system was adequately pressure tight, week-long runs could be made with no significant pressure drop occurring.

The temperature of the vessel was measured by a thermocouple inserted in a well on the outside of the reactor vessel opposite the specimen. A calibration showed that temperatures recorded at this point were about 2°C higher at 371°C and 593°C than temperatures inside the reactor vessel after the system had become stabilized at a particular temperature. The temperature of the furnace was regulated by a thermo-couple inserted in the furnace windings. A West Model JP controller was used.

Pressures were followed during a run by means of the pressure gauges shown in Figure 6. The two units with 0-50,000 psi gauges were used for runs of less than 30,000 psi. If the pressure on the system was suddenly removed, the resulting jar to the gauge needle often changed the indicated zero point. Over the several months that these units were used, several zero point calibrations of the pressure gauges were necessary. These were made by attaching a dead weight gauge tester directly to the system. The calibration of the gauges was otherwise unaffected.
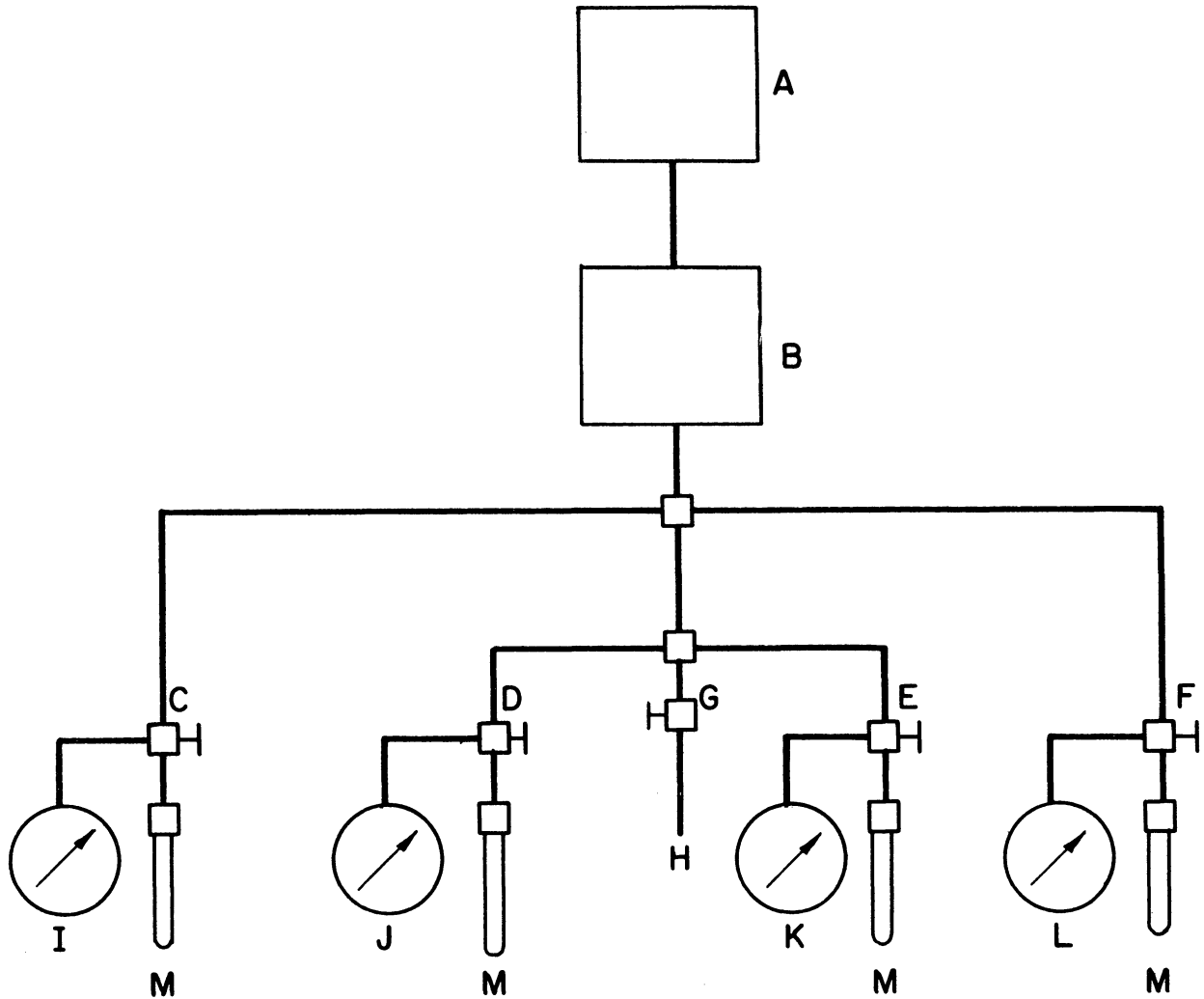
Figure 6. Schematic Drawing of Hydrothermal Unit. Key:
A--Water Reservoir. B--High Pressure Air Driven
Water Pump. Max Output Pressure 28,000 psi.
C, D, E, F, G--High Pressure Valves. K, L--0-100,000
psi Pressure Gauges. M--Reactor Vessel.

It was found that no oxidation of specimens occurred in the course of a run, if all dissolved oxygen was removed from the water in the unit. This was accomplished by using freshly boiled distilled water in the reactor vessel and by placing a few uranium turnings or cerium chips in the reactor. These reactive metals prevented any specimen oxidation; any metal left after reaction with the dissolved oxygen (or nitrogen) was converted to oxide by reaction with the water.

Two runs, (Specimens E1 and F1) only one of which was completely successful, were made using argon as a pressure medium. To obtain sufficiently high argon pressures at 593°C, it was necessary to begin the run with the reactor vessel filled with liquid argon. This was readily done by placing the reactor vessel in liquid nitrogen, and running in tank argon until the vessel was filled. When the reactor was installed in the unit and allowed to warm to room temperature a pressure of 25-30,000 psi was obtained. Subsequent heating produced higher pressures. It was also necessary in these runs to add reactive metals to the reactor vessel to remove oxygen and nitrogen from the argon. Enough water was left in the line leading to the pressure gauge to insure a proper pressure reading.

3. Testing in Tension and Compression

All tests in tension and compression were done at 371°C (700°F) in a helium atmosphere. Direct dead weight loading was used. A sketch of the apparatus with a tensile specimen in place is shown in Figure 7. A split wound tube furnace, 1 1/4" ID, 12" long was placed around the tube. All threaded fittings inside the furnace tube were loose fitting; this provided the necessary flexibility to prevent bending of the specimens.
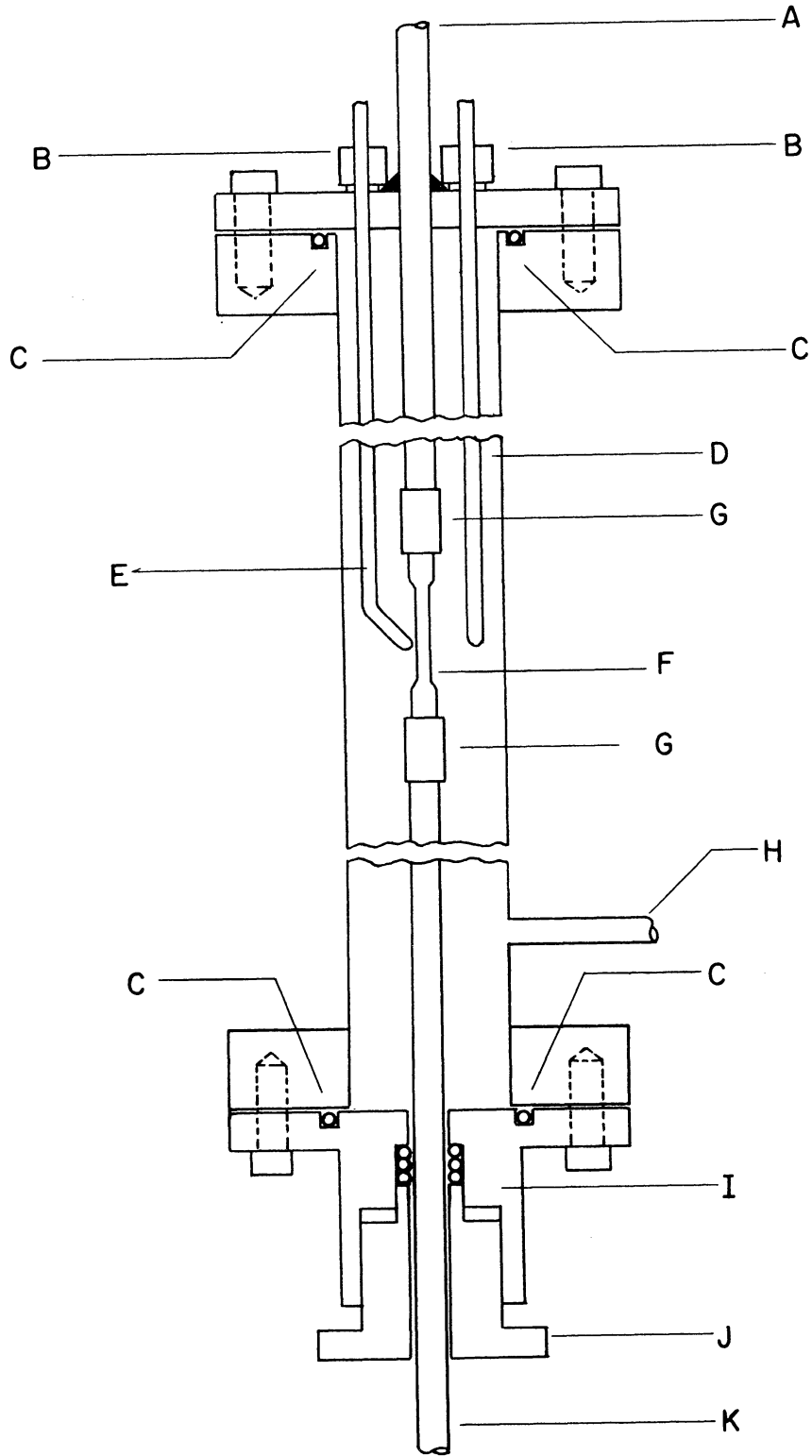
Figure 7. Furnace Tube and Fittings for Tensile Testing. Key:
A--Pull Rod to Framework. B--Conax Seals
C--"O"-Ring Seals. D--Furnace Control Thermocouple.
E--Thermocouple. F--Specimen. G--Threaded Fittings.
H--Helium Supply. I--"O"-Ring Packing Gland.
J--Packing Gland Nut. K--Pull Rod to Weight Pan.

Prior to starting a run, the furnace tube was evacuated and flushed several times with helium. During the run a positive pressure of 1-2 psig helium was maintained in the furnace tube. This kept oxidation of the specimens to a minimum, but never eliminated it entirely.

The temperature of the furnace was controlled using the control thermocouple shown in Figure 7. A "Celectray" controller, manufactured by C. J. Tagliabue Manufacturing Company, was used for temperature control. Temperatures during runs were checked using a thermocouple which touched the specimen. The temperature gradient along the specimen was less than 2°C. Temperature variation during a run was about ± 2°C.

The lower pull rod attached to the specimen passed through a packing gland which consisted of 3 teflon "O" rings. The packing gland nut was used only to keep the "O" rings in position; they were not compressed. A high polish was kept on the pull rod. It was found that the 1-2 psig helium pressure inside the furnace tube was sufficient to push the rod through the packing gland. The load placed in the weight pan plus the weight of the pan and fittings was taken to be the true load on the specimen. In other words, it was assumed that the helium pressure maintained inside the furnace tube just offset the frictional forces in the packing gland. At most, this could result in a 2% error in the effective load on the specimen.

Before each run, three sets of scribe marks were placed on the specimen. The distance between marks was at least one inch. Measurement of the distance between these marks before and after each run revealed no indication that bending occurred. For runs made at the heavier loads, about $2 \cdot 10^{-4}$ permanent strain was indicated, but this is less than the

error with which the distances between scribe marks could be measured on successive trials. Hence, one can conclude that no sizable permanent elongation occurred during these runs.

A compression run (DC1) was made in the same apparatus using fittings which permitted tensile loading to achieve compression of the specimen. Two interlocking "U" shaped fittings, one of which is shown in Figure 8, were used.

One run in compression was carried out. Microscopic inspection after the run showed no signs of bending.

4. Measurement of Dihedral Angles

Specimens were prepared for metallographic examination using conventional metallographic techniques applied with some care.

Specimens were generally cylindrical in shape, 1/2 to 3/4"long, 5/32 to 7/32" diameter. Most specimens were copper plated using solutions recommended by Kehl,[54] prior to mounting in bakelite. This prevented rounding of the specimen edges during polishing.

After mounting, specimens were ground using 60C silicon carbide paper, so that the final plane of polish bisected the cylinder along its axis. Some of the tensile specimens were also examined on transverse sections. Following this, 240C and 600C grit papers were used; 6 micron diamond on a silk cloth was used to remove the scratches from the 600 paper.

Typically, at this point it appeared that the nickel matrix had been smeared to such an extent that only the largest lead particles were visible. Since no etchants were used, (because of preferential attack of either the lead phase or the interfaces in the system) this flowed metal had to be removed by careful polishing with a Linde A
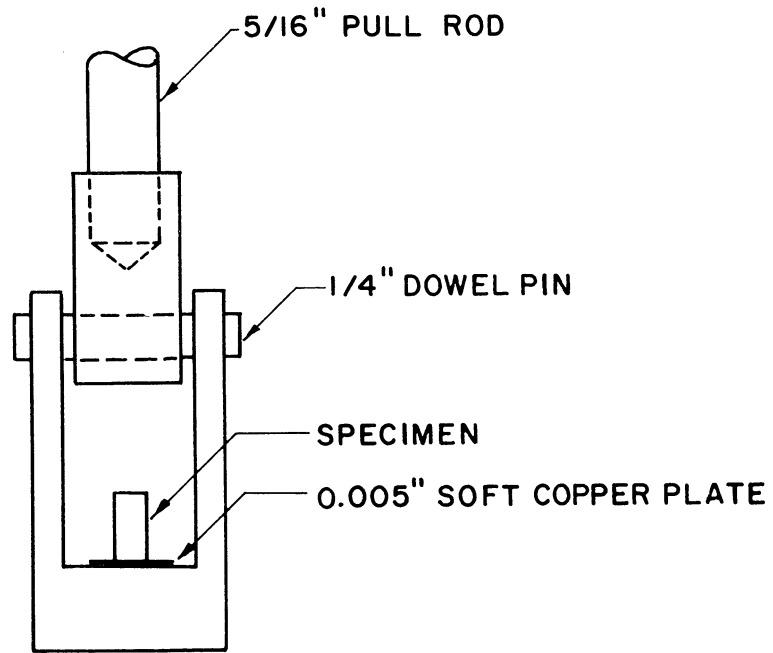
Figure 8. Fitting for Compression Testing.

Al_2O_3 suspension, followed by two or more hours of mechanical polishing using a Syntron vibrating polisher with Linde B Al_2O_3 suspended in water.

In both of the final polishing steps, well-worn Buehler Microcloths were used. The high nap on a new cloth tended to remove lead from the structure.

This polishing treatment did not produce "relief" polishing in the sense that adjacent nickel grains were at different levels. It did, however, cause all grain boundaries to be lower than the matrix grains. It is not felt that this in any way distorted the shape of the lead particles present. On the contrary, unless this situation obtained, the lead particles were often partially obscured by smeared nickel.

Angles were measured on a Baush and Lomb Research Metallograph equipped with a rotating stage. By means of a vernier attached to the stage, angles could be read to the nearest $0.1°$. All angles were recorded to the nearest $0.1°$ even though the probable accuracy of measurement varied from ±0.5 to $\pm5°$ from one angle to another.

An 80X, oil immersion objective was used for all measurements with a 15X filar eyepiece. For angles measured on tension and compression specimens (and on sample D, a blank), the distance from the edge of the specimen was recorded for each angle. In addition, the angle which the grain boundary made with the axis of tension (or compression) was measured. The accuracy of the latter measurement was probably about $\pm5°$.

The distance from the specimen edge was also recorded for all specimens equilibrated at various temperatures or subjected to hydro-static loading with the exception of specimens from heats E and F. The specimens used in these cases were irregular in shape which made such a measurement difficult.

In every case, specimens were repolished at least once so that angle measurements were made on more than one polished section. This was done to minimize any systematic error due to the quality of polish. As experience was gained, good quality polishes could be produced consistantly.

CHAPTER V

STATISTICS OF DIHEDRAL ANGLE MEASUREMENTS

The statistical problem involved in the determination of a dihedral angle from a sampling of observed angles should be a problem in determining a best estimator, $\hat{\theta}$, for the dihedral angle θ , which is the single parameter in the theoretical cumulative frequency function (Appendix A) which describes the population from which the sample is drawn.

Straightforward solution of the problem is difficult because of the complexity of the analytical form of the distribution function. More important, however, is the fact that the distribution function does not, in all likelihood, accurately characterize the population from which the sample is drawn. For these reasons, a less direct approach is required.

It has been shown[84] that the median angle of the theoretical distribution always lies within 1° of the dihedral angle, θ . Given a value of the median angle one can apply a correction which will produce the dihedral angle. One must then consider the factors which are likely to cause the actual distribution to depart from the theoretical distribution and determine their effect on the median angle. If the effect on the median angle is predictable, then it is still possible to determine the dihedral angle from the median angle by applying several corrections.

Since the actual form of the distribution function for the population is unknown or exceedingly complex, the most satisfactory way to determine the probable errors in the value of the median angle obtained is to apply methods of non-parametric statistics to the sample.

This will allow one to establish a confidence interval for the median
of the population. Other non-parametric methods will allow comparisons
for significance to be made between different samples.

The sections to follow elaborate on these points and discuss
the calculations made.

1. A Discussion of Errors Affecting the Distribution of Observed Angles

The statistical analysis of observed angles to determine a
true dihedral angle was first employed by Harker and Parker[39] in 1945.
A few years later, Smith[93] and Ikeuye and Smith[51] used this analysis
to determine the dihedral angle of dispersed second phase particles
lying in grain boundaries of a matrix phase, e.g., lead in copper.

These authors, and most subsequent workers who have employed
this technique, have observed that in general the distribution of angles
observed departs considerably from the expected distribution, in that
the peaks observed at the modal angle are blunter and broader than one
would expect. Figure 9 illustrates this point with data from the
Nickel-Lead system, (Specimen D). Application of a Chi-Squared test
to this data indicates there is virtually no chance that the sample
of angles obtained came from a population with the theoretical distribution
shown. Application of the Chi-Squared Test to other data in the litera-
ture shows some data which fits the theoretical distribution better than
the data shown, but no cases of good fits.

Several reasons have been advanced to explain this discrepancy.
Harker and Parker[39] suggested that a) the presence of a range of
dihedral angles in a specimen rather than a unique dihedral angle would
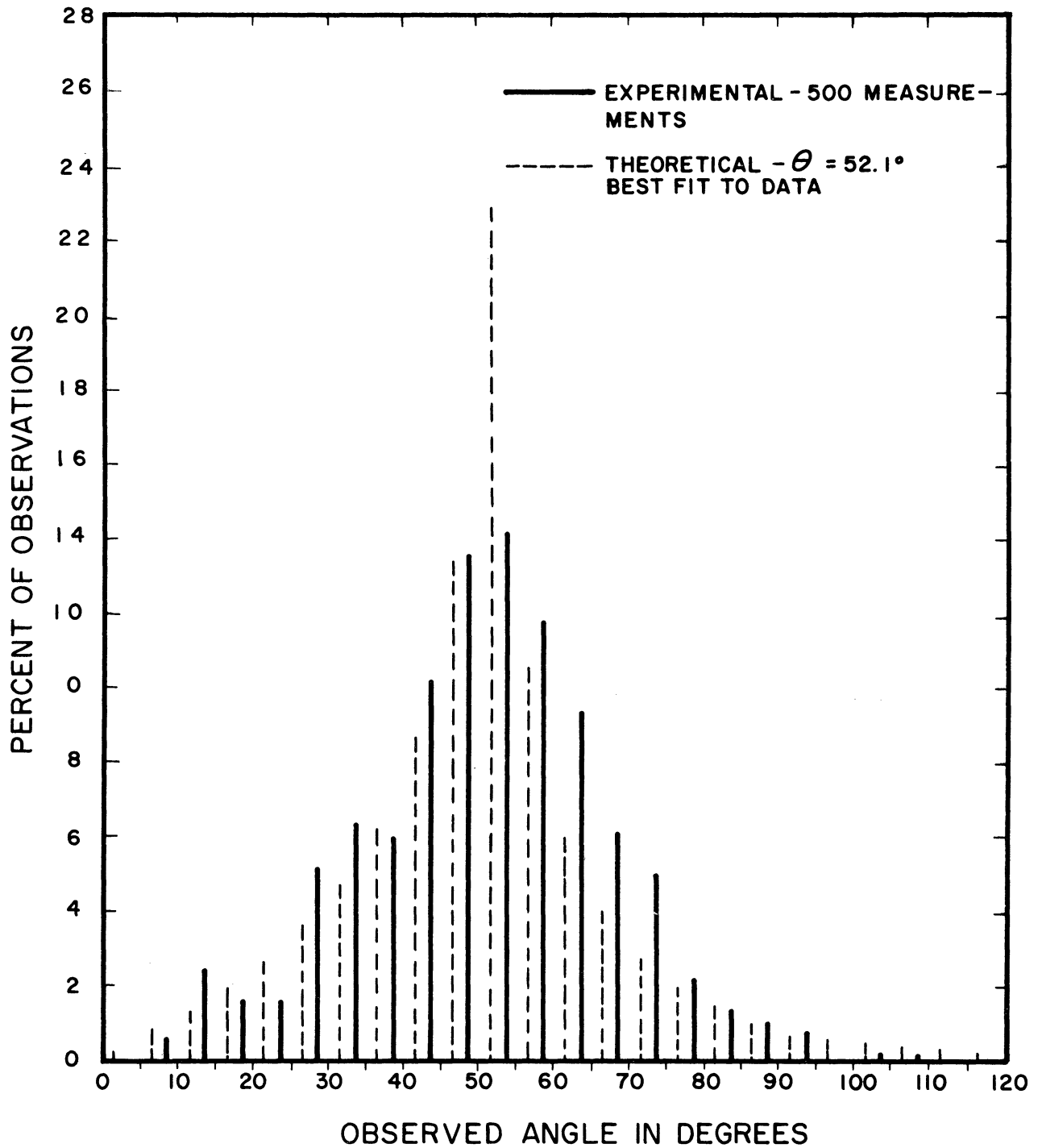cause a spreading of the distribution function, b) a non-random selection

Figure 9. Frequency Plot - Theoretical and Observed.

of orientations with respect to the plane of polish would distort the
distrubution function, e.g., arising from a columnar grain structure.
This is more likely to be a problem when measuring the angle at which
matrix grains meet, as in Harker and Parker's experiment, c) "bad luck"
in sampling. The last cause can be ruled out because the effect is
invariably observed.

Smith[95] and Ikeuye and Smith[51] suggest that failure to
observe the expected peak frequencies is due to either a) differences
in grain boundary energy due to orientation effects, or b) failure
to obtain equilibrium. For well annealed specimens, such as they used,
Ikeuye and Smith do not consider the latter effect to be important.
They ascribe the bulk of the peak broadening to the first cause even
though "there is only a small probability that two grains will meet
each other at an angle that gives a boundary of low energy".[95]

Another possible source of this discrepancy is the contribution
of measuring error. If the errors in measurement are sizable, then
even if they occur randomly they will change the effective distribution
function for the population of observed angles. Increasing the sample
size only insures that the sample distribution approaches the effective
distribution of the population, not the "true" distribution.

In measurements performed on dispersed second phase particles,
another type of error can arise from an improper selection of particles.
It is easier to measure the angles from a particle whose section size in
the plane of polish is large. This same particle can be sectioned to
produce a variety of section sizes, and it can be shown that if the
difficult measurements on small section sizes are omitted, then a systematic
error in the sample distribution can result.

The following three sections show the effects of three sources
of error on the effective distribution function of observed angles.
The calculations were performed with aid of an IBM 7090 computer.

2. Effect of a Non-Unique Dihedral Angle on the Distribution of Observed Angles

Blunting of the distribution peak has usually been ascribed
to variations in grain boundary tensions arising from the dependence of
grain boundary tension on orientation parameters. It is undoubtedly
true that the few orientations which produce very low grain boundary
tensions contribute negligibly to a sample of observed angles. However,
minor fluctuations in composition due to segregation (influencing
adsorption at the boundary) might very well produce a range of dihedral
angles. Smith[93] points out that the general occurrence of particles
with nearly spherical symmetry within matrix grains argues against any
significant dependence of solid-liquid tension on interface orientation.
This may be so, but variations in interface tension by a few percent
might not noticeably affect the sphericity of these particles, but
would have significant effect on the dihedral angle.

For the moment, we will assume that fluctuations in tensions
only occur for grain boundaries. If the grain boundary tension is
uniformly distributed over a range $\gamma \pm 0.015\gamma$, then if the dihedral
angle corresponding to γ is $50°$, the range in dihedral angles will
vary from about $46°$ to $54°$. If the range is $\gamma \pm 0.03\gamma$ the dihedral
angles will vary from $42°$ to $58°$. The spread in the frequency function
peak for each of these cases is indicated in Table V. Comparison with
the sample presented in Figure 9 shows that a uniform distribution of
dihedral angles from at least $42°$ to $58°$ would be needed to explain
the peak depression.

TABLE V

EFFECT OF NON-UNIQUE DIHEDRAL ANGLE ON THE DISTRIBUTION OF OBSERVED ANGLES

Observed Angle	Theoretical Cumulative Frequency for $\theta = 50°$	Cumulative Frequency for $\theta = 50^{\pm}2$	Cumulative Frequency for $\theta = 50^{\pm}4$	Cumulative Frequency for $\theta = 50^{\pm}8$
5	0.29	0.29	0.29	0.30
10	1.18	1.18	1.19	1.22
15	2.70	2.71	2.73	2.80
20	4.94	4.95	4.98	5.12
25	8.00	8.02	8.08	8.32
30	12.09	12.12	12.22	12.62
35	17.51	17.57	17.72	18.38
40	24.82	24.92	25.19	26.42
45	35.23	35.44	36.10	39.31
48	44.42	45.04	46.67	48.63
49	48.60	49.74	50.71	51.75
50	54.73	54.75	54.78	54.84
51	60.75	59.68	58.77	57.88
52	64.69	64.13	62.62	60.86
55	72.80	72.62	72.03	69.24
60	80.94	80.85	80.61	79.55
65	85.95	85.90	85.76	85.17
70	89.33	89.30	89.20	88.81
75	91.73	91.70	91.63	91.36
80	93.48	93.47	93.41	93.21
85	94.81	94.80	94.76	94.60
90	95.83	95.82	95.79	95.67
95	96.63	96.63	96.60	96.51
100	97.27	97.27	97.25	97.17
105	97.79	97.78	97.77	97.71
110	98.20	98.20	98.19	98.14
115	98.55	98.54	98.54	98.50
120	98.83	98.83	98.82	98.79
Median Angle	49.3	49.1	48.8	48.4

Relative frequencies near Peak of Frequency Plot

40-45	10.41	10.53	10.91	12.89
45-50	19.49	19.31	18.67	15.53
50-55	18.07	17.87	17.25	14.40
55-60	8.14	8.24	8.58	10.32

If this factor is important, then no unique dihedral angle exists. If the number obtained for the median angle of the population is corrected to obtain the dihedral angle, the latter can only be regarded as a number representing the central tendency of an existing range of dihedral angles.

3. The Contribution of Measuring Error

According to the theoretical distribution (Appendix A), if one has a dihedral angle of 50°, then 20.3% of the angles observed should lie between 48° and 52°. But if the reproducibility of measurement is on the order of 1°, then even if the sampling is perfect, errors in measurement would not allow one to observe such a large percentage of angles in such a small range. The following discussion presents an approximate method for determination of the amount of peak broadening due to errors in measurement.

Let ψ^* designate the variable which is measured experimentally. Then, when errors in measurement exist

$$\psi^* = \psi + y \tag{5-1}$$

where ψ is the value of the variable which would be observed in the absence of errors, and y is the contribution of error. Let y be normally distributed with mean 0 and standard deviation σ, and let ψ be distributed according to Harker and Parker's expression. Then, what is required is an expression for the distribution function of ψ^*.

The distribution function for ψ^* may be calculated according to the following scheme. Let the fraction of angles less than or equal to ψ be called C_ψ, where C_ψ is determined from the theoretical distribution equation. Let the fraction of angles between ψ and $\psi + \Delta\psi$ be designated $f_{\psi + \frac{\Delta\psi}{2}}$, where

$$f_{\psi + \frac{\Delta\psi}{2}} = C_{\psi + \Delta\psi} - C_\psi . \qquad (5\text{-}2)$$

Errors in measurement cause the fraction $f_{\psi + \frac{\Delta\psi}{2}}$ to be normally

distributed over all ψ. (Since the range of ψ is finite, the normal

distribution is a good approximation except for ψ near 0 or 180°.)

The fraction of $f_{\psi + \frac{\Delta\psi}{2}}$ which is greater than $\psi + \frac{\Delta\psi}{2} + x$ or

less than $\psi + \frac{\psi}{2} - x$ is

$$f_{\psi + \frac{\Delta\psi}{2}} \left[\frac{1}{\sqrt{2\pi}} \int_{x/\sigma}^{\infty} e^{-t^2/2} \, dt \right] .$$

Hence the cumulative frequency corrected for measuring error is C_ψ^*

where

$$C_\psi^* = C_\psi + \sum_{n=0}^{K} \left[f_{\psi + (n + 1/2)\Delta\psi} - f_{\psi - (n + 1/2)\Delta\psi} \right]$$

$$\frac{1}{\sqrt{2\pi}} \int_{\frac{(n + 1/2)\Delta\psi}{\sigma}}^{\infty} e^{-t^2/2} \, dt . \qquad (5\text{-}3)$$

The summation is carried out up to $n = K$, where K is high

enough so that the value of the error integral is very small. This will,

of course, depend on the value chosen for σ and for $\Delta\psi$. For the

calculations that were made, $\Delta\psi$ and σ were adjusted so that $K = 40$,

which meant that the smallest value of the error integral used was 0.00004.

The results of this calculation for $\sigma = 2$ and $\sigma = 5$ are shown

in Table VI. Computed values are shown only for the central portion

of the distribution, since the assumed normal distribution of error

cannot hold for very large or very small angles. Although a pronounced

blunting of the distribution peak occurs for $\sigma = 5$, neither the modal

angle nor the median angle is much affected. While both of these criteria

remain relatively unbiased for this type of error, neither the sample

TABLE VI

EFFECT OF MEASURING ERROR ON THE
DISTRIBUTION OF OBSERVED ANGLES

Observed Angle	Theoretical Cumulative Frequency θ =50°	Cumulative Frequency for σ=2 θ =50°	Cumulative Frequency for σ=5 θ =50°
20	4.94	5.00	
25	8.00	8.09	8.53
30	12.09	12.20	12.78
35	17.51	17.66	18.52
40	24.82	25.06	26.60
45	35.23	35.81	38.48
48	44.42	45.81	47.63
49	48.60	50.06	50.88
50	54.73	54.74	54.15
51	60.75	59.03	57.38
52	64.69	63.12	60.53
55	72.80	72.17	69.04
60	80.94	80.70	79.10
65	85.95	85.83	85.05
70	89.33	89.25	88.81
75	91.73	91.68	91.39
80	93.48	93.45	93.26
85	94.81	94.79	94.65
90	95.83	95.82	95.72
95	96.63	96.62	96.55
100	97.27	97.26	97.21
105	97.79	97.78	97.74
110	98.20	98.20	98.17
115	98.55	98.54	98.52
120	98.83	98.83	98.81
Median Angle	49.3	49.0	48.8

Relative Frequencies near Peak of Frequency Plot

40-45	10.41	10.75	11.89
45-50	19.49	18.93	15.66
50-55	18.07	17.43	14.90
55-60	8.14	8.53	10.06

mode nor median will be as reliable as calculations based on the theoretical distribution would suggest.

The standard deviation σ of the error in measurement depends on the magnitude of the angle, the size of the particle being measured relative to the magnification, and the quality of the metallographic preparation. Thus, while a single value for σ really does not exist, the assumption of a fixed value is valid for estimating the magnitude of the effect.

For most samples measured in this work, a conservative estimate of σ would be 2.0°. From the results of the above calculations one can see this would have s small effect on the shape of the distribution, and a negligible effect on the median or modal angles.

4. The Effect of Observed Particle Size

The two types of errors previously discussed probably account for most of the departure observed from the theoretical distribution of angles. A third type of error may on occasion arise due to biased sampling which occurs because of differences in the section size of dispersed particles.

For example, if the dispersed second phase consists mainly of lenticular shapes lying in matrix grain boundaries, measurement of only the largest sections seen on a plane of polish introduces a bias toward a higher median angle. This occurs because sections through a lens which are of a smaller apparent size have angles which are on the average, smaller.

To see this, consider a single such particle in the form of a lens with surfaces which are portions of spheres[93] meeting in a dihedral

angle θ and having a diameter d in the central plane. Then, passing planes of random orientation through the particle gives rise to observed grains whose apparent length ℓ is such that $\ell \leq d$.

If one is measuring angles observed on a plane of polish at a particular magnification, the ease of measurement is dependent upon the particle size. For particles whose diameters lie between d and d + Δ d, there will always be a length ℓ_o below which it is not possible to make an accurate measurement. However, disregarding particles which are too small to measure gives rise to a systematic error in the distribution of angles obtained, whose net effect is to raise the median angle of the distribution.

It is worthwhile to determine the value of ℓ_o/d which will allow one to disregard particles having $\ell/d < \ell_o/d$ without appreciably affecting the distribution of angles obtained. This in turn gives one a qualitative guide to the magnification needed to satisfactorily measure dispersed particles having a certain size range.

Let N be the normal to the plane intersecting a lens having its central plane lying in the XZ plane. The normal has direction cosines $(\cos \beta \sin\alpha, \sin\beta \sin \alpha, \cos \alpha)$ where α, β are the usual spherical coordinates. Thus, the equation of the intersecting plane is $\cos \beta \sin \alpha \, x + \sin\beta \sin \alpha \, y + \cos \alpha \, z = 0$, and the trace T of this plane on the XZ plane is the line $\cos \beta \sin \alpha \, x + \cos \alpha \, z = 0$. The equation of the circle C in the central plane of the lens is $(x - r)^2 + z^2 = r^2$. Solving the latter two equations for x, and expressing the length of the chord ℓ in terms of x results in the following expression:

$$\ell/d \quad = \quad \ell/2r \quad = \quad \frac{1}{\sqrt{1 + \cos^2\beta \, \tan^2\alpha}} \, . \tag{5-4}$$

Rearranging (5-4) and using the trigonometric substitution

$$\tan^2\alpha \quad = \quad \frac{\sin^2\alpha}{1 - \sin^2\alpha}$$

one has

$$\sin^2\alpha \quad = \quad \frac{K}{K + \cos^2\beta} \tag{5-5}$$

where $K = (d/\ell)^2 - 1.$

Harker and Parker[39] have shown that the probability of observing an angle less than or equal to ψ for a given dihedral angle θ is given by the areas to the left of curves of constant ψ on a graph of $\sin^2\alpha$ vs. β. Superposition of curves of constant ℓ_o/d from (5-5) on the curves of constant ψ will indicate the portion of the distribution not obtained when particles having $\ell/d < \ell_o/d$ are ignored.

For $\theta = 50°$, the probability plot of $\sin^2\alpha$ vs β is given in Figure 10 with the curves for three ratios of ℓ_o/d superimposed. The fraction of the population of observed angles having $\ell_o/d < 0.1$ is about 0.5%, for $\ell_o/d < 0.3$ about 4.6%, and for $\ell_o/d < 0.5$ about 13.4%. The data for the frequency plots thus obtained are given in Table VII and the median angle for each case is indicated. Note that the modal angle is about the same for each case. Clearly, if all particles with $\ell/d > 0.1$ can be measured, no significant error in the distribution will result. On the other hand, if only 85% of the particles present are large enough to measure, the distribution of angles obtained will be in error.

Two considerations prohibit the application of these results in any quantitative manner. First, a distribution of particle sizes
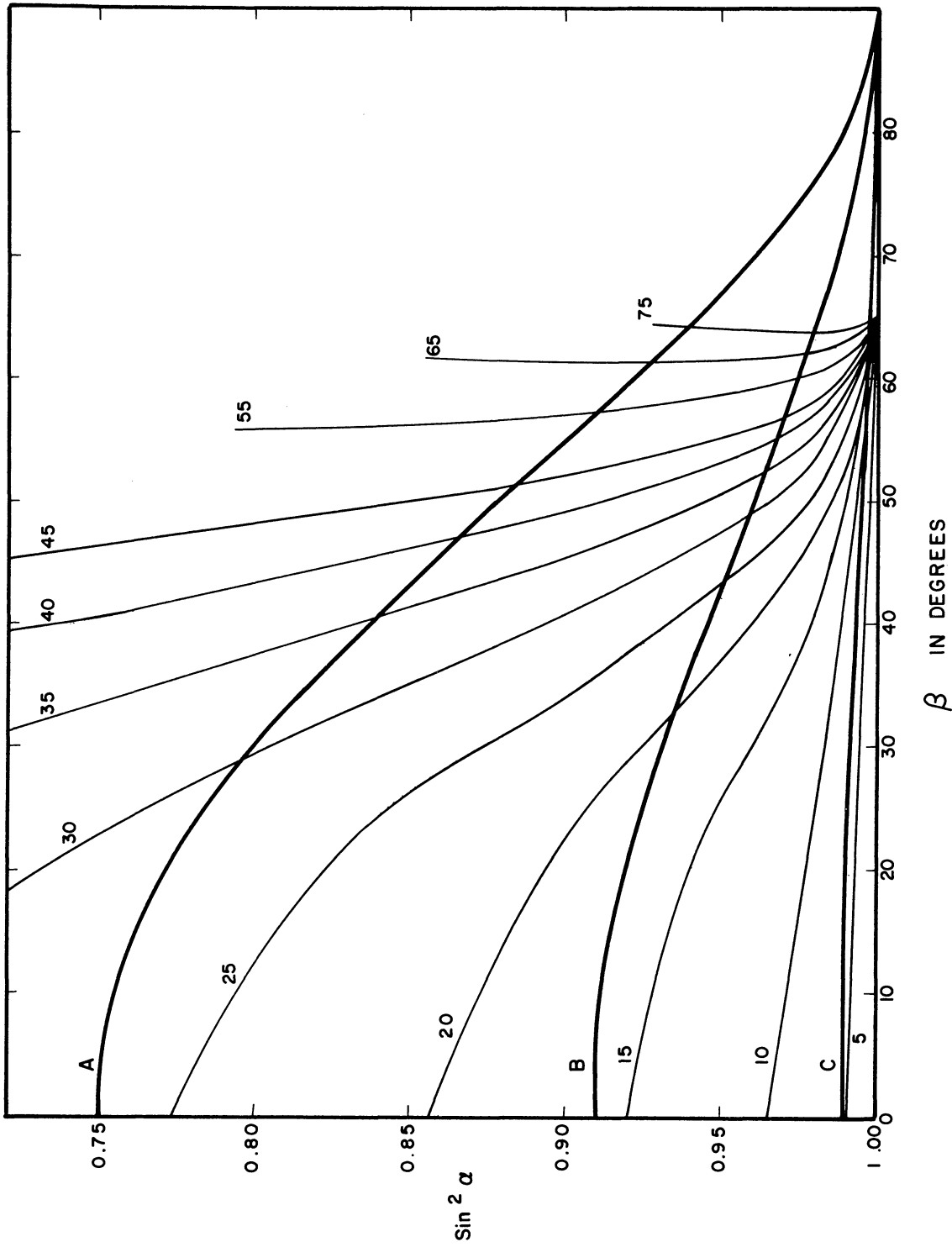
Figure 10. Probability Plot Showing Regions Where Section Size of Lenticular Particles
is Small. Dihedral Angle is 50°. Curve A: $\ell o/d$ = 0.5.
Curve B: $\ell o/d$ = 0.3. Curve C: $\ell o/d$ = 0.1.

TABLE VII

EFFECT OF IGNORING ANGLES FROM SMALL SECTION SIZES ON THE DISTRIBUTION OF OBSERVED ANGLES FROM LENTICULAR PARTICLES

Observed Angle	Theoretical Cumulative Frequency θ =50°	Cumulative Frequency $\ell/d=0.1$ θ =50°	Cumulative Frequency $\ell/d=0.3$ θ =50°	Cumulative Frequency $\ell/d=0.5$ θ =50°
10	1.18	0.73	0	0
15	2.70	2.24	0	0
20	4.94	4.48	1.25	0
25	8.00	7.56	4.16	0
30	12.09	11.67	8.30	1.95
35	17.51	17.12	13.90	7.18
40	24.82	24.46	21.51	15.06
45	35.23	34.93	32.39	26.73
48	44.42	44.16	42.01	37.19
49	48.60	48.36	46.38	41.96
50	54.73	54.52	52.81	49.00
51	60.75	60.57	59.12	55.92
52	64.69	64.53	63.24	60.43
55	72.80	72.68	71.73	69.70
60	80.94	80.86	80.25	78.96
65	85.95	85.90	85.49	84.65
70	89.33	89.30	89.02	88.46
75	91.73	91.70	91.52	91.15
80	93.48	93.47	93.35	93.12
85	94.81	94.80	94.73	94.60
90	95.83	95.83	95.80	95.73
95	96.63	96.63	96.63	96.61
100	97.27	97.28	97.29	97.31
105	97.79	97.79	97.82	97.87
110	98.20	98.21	98.25	98.31
115	98.55	98.56	98.61	98.68
120	98.83	98.84	98.90	98.97
Median Angle	49.3	49.3	49.6	50.1

Relative Frequencies Near Peak of Frequency Plot

40-45	10.41	10.46	10.88	11.67
45-50	19.49	19.59	20.41	22.27
50-55	18.07	18.16	18.93	20.70
55-60	8.14	8.18	8.52	9.26

is always present. This means that for relatively large particles, nearly all orientations of the particle with respect to the plane of polish produce sections large enough to measure, while for particle sizes at the other end of the spectrum, a large proportion will produce sections too small to measure. Without knowing the distribution of particle sizes, no correction can be applied. It is probably true, however, that if the magnification used is adequate to resolve all but a few percent of the particles present, no significant error should result. When a fine dispersion of particles is present and the best magnification available cannot resolve a large proportion of them, the distribution of angles obtained is sure to be in error. An approximation to the true dihedral angle can, however, still be obtained from the modal angle. The median angle of the measured distribution will be too high.

In the alloys used in this work, lenticular shapes were predominant. However, this is often not the case. When the matrix grain size is small relative to the dispersed particle size (as in powder compacts sintered with a partially-wetting liquid phase present), more particles will lie in grain edges and in corners where four grains meet than when the matrix grain size is relatively large. Obviously, the same considerations that have been dealt with above for lenticular shapes apply here, too, but the more complex geometry of these particle shapes would make a similar calculation difficult.

5. Establishing a Confidence Interval for the Median Angle

Two criteria have been proposed to determine the dihedral angle from a sample distribution of angles; a) the modal angle, and b) the median angle. Smith[93] pointed out that the modal angle in the theoretical

frequency function is the dihedral angle. If a range of dihedral angles

exists, the mode then tends to a central value in the distribution of dihedral

angles. Unfortunately, the mode is a clumsy tool; the sample size must

be large and the value of the modal angle depends on the classification

of the data. The value of the modal angle is insensitive to many types

of error, but the frequency of the mode is not.

Riegger and Van Vlack[84] proposed use of the median angle to

characterize the distribution. They show that the median angle of the

theoretical distribution is always within 1° of the true dihedral angle,

(see Figure 25). The median angle is obviously determined more easily

than the mode, and with a greater precision. Riegger and Van Vlack

estimate the sampling error in using the median angle of a sample

(drawn from a population having the theoretical distribution) to obtain

the median angle of the population. They assume that the theoretical

distribution function of observed angles approximates a normal distribution.

Then, the standard deviation of the median angle is given as an asymptotic

approximation for large n by the relation

$$\sigma_{med} \approx 1.253 \frac{\sigma_p}{\sqrt{n}}$$

where σ_p is the standard deviation of the population. They then apply

this relation to show that 25-50 angle samples characterized by means of

the median angle give the same accuracy in determining the dihedral angle

as much larger samples characterized by the mode. These last results may

be criticized on three points: (1) the theoretical distribution deviates

from a normal distribution at small and large values of the dihedral

angle; the useful range of this assumption is probably $20° < \theta < 160°$;

(2) the approximation used to obtain the standard deviation of the median

angle is valid for large samples. It has not been shown that a 25-50 angle

sample is sufficiently "large"; (3) the population from which the sample

is drawn is almost certainly not characterized by the theoretical frequency

function (or a normal distribution with the same mean and standard deviation);

the standard deviation of the actual population is larger.

A better approach is to use a non-parametric method to establish

a confidence interval for the median. Such a method has the virtue of

being independent of the distribution function assumed for the population.

S. S. Wilks[110] derives the following probability relationships.

A sample of size n from a given population may be ordered according to

the magnitude of the elements in the sample. Thus, the sample may be

represented $(x_{(1)}, \ x_{(2)}, \ \ldots, \ x_{(n)})$ where $x_{(k)} \leq x_{(k+1)}$. Then

a confidence interval for the median of the population $\underline{x}$ is given by:

$$P\left(x_{(k_1)} < \underline{x} < x_{(k_1 + k_2)}\right) = I_{0.5}\left(k_1, \ n - k_1 + 1\right)$$

$$- I_{0.5}\left(k_1 + k_2, \ n - (k_1 + k_2) + 1\right)$$

(5-6)

where $I_p\left(v_1, \ v_2\right)$ is the Incomplete Beta Function. Tabulated values

of this function have been prepared by Pearson[78] for p = 0.01 to 1.00,

and for $v_1, \ v_2$ = 0.05 to 50. For large samples, an asymptotic approxi-

mation using a normal distribution permits a similar calculation. Table VIII

shows 90% and 95% confidence intervals for samples of five different sizes.

TABLE VIII

CONFIDENCE INTERVALS FOR VARIOUS SAMPLE SIZES

Sample Size	90% Confidence Interval	95% Confidence Interval
25	8 - 17	7 - 18
50	19 - 32	18 - 33
75	30 - 45	29 - 46
250	112 - 138	110 - 140
500	232 - 268	228 - 272

Using this method, one can then say, for example, that for a sample size of 500, there is only one chance in twenty that the median of the population has a value lying outside the values of the 228th and 272nd members. Thus, without making any assumptions as to the distribution function of the population, the median of the population can be established to within fairly close limits.

Although this method gives an interval in which the median of the population is likely to occur, it gives no best estimate for the median of the population. For purposes of further calculation, the median of the population is taken to be the median of the sample. An equally valid choice for the median of the population would be the mean of the limits of the confidence interval. For large sample sizes, there is no significant difference between these two figures.

To obtain the dihedral angle from the median, the factor obtained by Riegger and Van Vlack[84] is added to the median angle. From the calculations of the previous sections one could also apply a correction for measuring error. A value of $\sigma = 2$ is a conservative estimate for the measuring error of any specimen; this would mean an additional factor of about 0.3° should be added to the median angle. This last correction was not applied because it is small and computations show it is independent of the size of the median angle in the range of interest. Furthermore, the measuring error was probably not the same for all specimens.

6. Summary

Three types of errors have been considered which will change the effective population of observed angles and thereby the distribution function for that population: (1) Existence of a range of dihedral angles,

distributed in an unknown manner, (2) errors in measurement, and
(3) a range of apparent particle sizes, some of which are too small to
measure.

One should be able to avoid the third type of error by using
sufficiently high magnification on a sufficiently coarse distribution
of particles. This type of error is most likely to show itself when
comparing results of samples taken from two different dispersions.

Both of the first two effects must always be present, however,
to some extent. The resulting samples with flattened peaks represent a
superposition of both effects. A reasonable estimate of the error in
measurement, $\sigma = 2$, cannot account for all of the peak broadening.
One must conclude, therefore, that a range of dihedral angles exists in
the specimen. If one assumes that this range of dihedral angles is rec-
tangularly distributed, then the above calculations suggest a spread of
dihedral angles from 8° to 16° wide is present.

The median angle of the population of observed angles can be
determined. To relate this to a dihedral angle one must retain the con-
venient fiction that a single dihedral angle exists. This assumption leads
to the calculation of ratios of interfacial tensions which are some sort
of averaged values. While it is important to realize that all interfaces
may not have the same tensions, conclusions made as to how the averaged
tensions vary with the constraints on the system must also be true for
the individual tensions.

In the following section, a brief description is given of
another method for determining a dihedral angle from a sample of observed
angles. In the second section, the results of non-parametric tests for
statistical differences between certain pairs of samples are given.

7. Another Method for Obtaining Dihedral Angles

In a previous section, a non-parametric method for establishing a confidence interval for the median angle of the population was discussed. For large samples, the 95% confidence interval is small enough so that the probable error involved in identifying the median angle of the sample with the median angle of the population is tolerable. In addition, however, one would like to know how well the samples fit the theoretical distribution equation.

An alternative method for choosing a value of dihedral angle likely to produce the observed sample was devised which is applicable to samples of any size. This method is empirical and does not give an indication as to the accuracy of the values obtained, but it does give an indication as to how well the sample fits the distribution equation.

Given a sample $(\psi_1, \ldots, \psi_n)$ ordered so that $\psi_i \leq \psi_{i+1}$, one can construct a cumulative distribution function for the sample

$$F^*(\psi) = \begin{cases} 0, & \psi \leq 0 \\ \dfrac{2i-1}{2n}, & 0 < \psi < \psi_i \;; \quad i = 1, \ldots, n. \\ 1, & \psi > \psi_n \end{cases} \quad (5\text{-}7)$$

If $F(\psi; \theta)$ is the distribution function given in Appendix A which describes the population, then one can define a parameter J given by:

$$J = \sum_{i=1}^{n} \left[F(\psi_i; \theta) - F^*(\psi_i) \right]^2. \quad (5\text{-}8)$$

Thus, a value of J for a sample can be computed for any choice of the parameter θ. The value of θ which gives the smallest value to J, thus giving the "best" fit to the data, is taken to be the dihedral angle. The value of J for this "best" fit, is an index as to how well the sample fits the theoretical distribution.

This empirical method for choosing the parameter θ is based on the Cramér-von Mises test for "goodness-of-fit."[18] According to this test, if the theoretical distribution function is known, the "goodness-of-fit" of a data sample can be established by means of the parameter $n\omega^2$

$$n\omega^2 = \frac{1}{12n} + \sum_{j=1}^{n} \left[F(x_j) - \frac{2j - 1}{2n} \right]^2$$

where $F(x)$ is the distribution function of the population, and $\frac{2j - 1}{2n}$ is the distribution function for the sample. Tables of the probability that a sample has $n\omega^2 \leq Z$ for various values of Z are given by Anderson and Darling.[4]

While there is no assurance that the above method of minimizing J produces an estimate of θ which is any way better than a value of θ determined via the median angle, one does obtain in the minimum value of J an indication as to how well the data can be made to fit a theoretical distribution. As was pointed out in the discussion of errors, the distribution function of Appendix A does not satisfactorily describe the population distribution, a fact which may be confirmed by the Cramér-von Mises test. Nevertheless, the minimum values of J obtained allow judgments to be made as to the relative reliability of various samples.

For purposes of comparison, an index of fit, I, is defined as follows:

$$I = \sqrt{J/n} = \sqrt{\sum_i \left[F(\psi_i, \theta) - F^*(\psi_i) \right]^2 / n} \qquad (5\text{-}9)$$

where $F(\psi_i; \theta)$ and $F^*(\psi_i)$ are expressed as percentages. This index is not dependent on sample size, as is J. Typically, "good data" gives values of I less than 5.

The values of the dihedral angle found by this method are up to 1° higher (and never lower) than those obtained by using the corrected median angle. One would expect this result, because (1) measuring error has been shown to decrease the median angle, and (2) a range in dihedral angles probably decreases the median angle.

In subsequent calculations, the dihedral angle used was the one obtained by correcting the median angle. No significant difference in any of the results is obtained by using the dihedral angles which fit the data best according to the above criteria.

8. Statistical Tests for Differences Between Samples

Since the form of the distribution function for the population of "observed angles" is unknown, it is desirable to use non-parametric methods to establish whether or not certain samples could have come from the same population. The methods used are described in reference (91).

Two types of "two-sample" tests are suitable: (1) the median test, and (2) the Kolmogorov-Smirnov test. In the median test the hypothesis being tested (null hypothesis) is that the samples come from populations with the same median. Used as a one-tailed test, rejection of this hypothesis implies that the medians are different in the manner predicted.

In the Kolmogorov-Smirnov test, the null hypothesis is that for any X, $F_{(1)}(X) = F_{(2)}(x)$, where $F(X)$ is the distribution function for the population from which the sample is drawn. Subscripts refer to the two samples being tested. Used as a two-tailed test, rejection of the null hypothesis implies that the distribution functions are different in central tendency, dispersion, or skewness. Used as a one-tailed test, rejection implies that $F_{(1)}(X) > F_{(2)}(X)$ for X near the center of the distribution.

The one-tailed test is most sensitive to differences in the central tendency of the distribution.

The Kolmogorov-Smirnov test is more sensitive to differences, and is the preferred test.[91] Some results of these comparisons are presented in Table IX. The level of significance at which the null hypothesis is rejected is the probability of rejecting the null hypothesis when it is in fact true. In each case, the lowest level of significance at which the null hypothesis can be rejected is indicated. The median test applied to the same data does not allow rejection of the null hypothesis with as high a degree of certainty.

TABLE IX

COMPARISON OF PAIRS OF SAMPLES FOR SIGNIFICANT
DIFFERENCES. KOLMOGOROV-SMIRNOV TWO-SAMPLE TEST

	Sample Pair	Level of Significance at which Null Hypothesis is rejected	
		Two-Tailed Test	One Tailed Test
1	D11-7 D11-8	0.10	0.05
2	D 1 D 3	Not rejected	Not rejected
3	C2A 1 C2A 3	0.025	0.01
4	C1 1 C1 3	0.01	0.01
5	D1 1 D1 3	0.05	0.05

Reference to Tables X and XI in the next chapter will show that all the samples in each pair in Table IX, except the second pair, should have come from different populations. The Kolmogorov-Smirnov test indicates that it is likely that the samples in each pair, except the second, do come from different populations. For example, the results of the two-tailed test for pair (1) show that there is only one chance in ten that the samples are drawn from the same population.

1. The Nickel-Lead Phase Diagram

Figure 11, the phase diagram for the Nickel-Lead System, is taken from Miller and Elliot.[69] It is based on Hansen,[37] with corrections from the more recent data of Fleisher and Elliott,[26] and Alden, Stevenson, and Wulff.[2] Figure 12 shows the solubility of Ni in liquid lead from reference (2). It is not known whether a eutectic or peritectic reaction occurs near the melting point of pure lead.

No information is available as to how the phases present change composition with changes in pressure. A rough calculation can be made to indicate the order of magnitude of the change of nickel solubility in liquid lead.

Assume that the solid is pure nickel and the liquid is a dilute solution of nickel in lead. Then since

$$d\mu_{Ni}^{s} = d\mu_{Ni}^{\ell} \tag{6-1}$$

and

$$d\mu_{Ni}^{s} = \underline{V}_{Ni}^{s} \, dP \tag{6-2}$$

$$d\mu_{Ni}^{\ell} = \overline{V}_{Ni}^{\ell} \, dP + \frac{\partial \mu_{Ni}^{\ell}}{\partial x_{Ni}^{\ell}} \, dx_{Ni}^{\ell} \qquad \text{T constant}$$

one has

$$\frac{\partial \mu_{Ni}^{\ell}}{\partial x_{Ni}^{\ell}} \frac{dx_{Ni}^{\ell}}{dP} = \underline{V}_{Ni}^{s} - \overline{V}_{Ni}^{\ell} \qquad \text{T constant} \tag{6-3}$$

where μ_{Ni} is the chemical potential of nickel, $\underline{V}_{Ni}^{s}$ is the molar

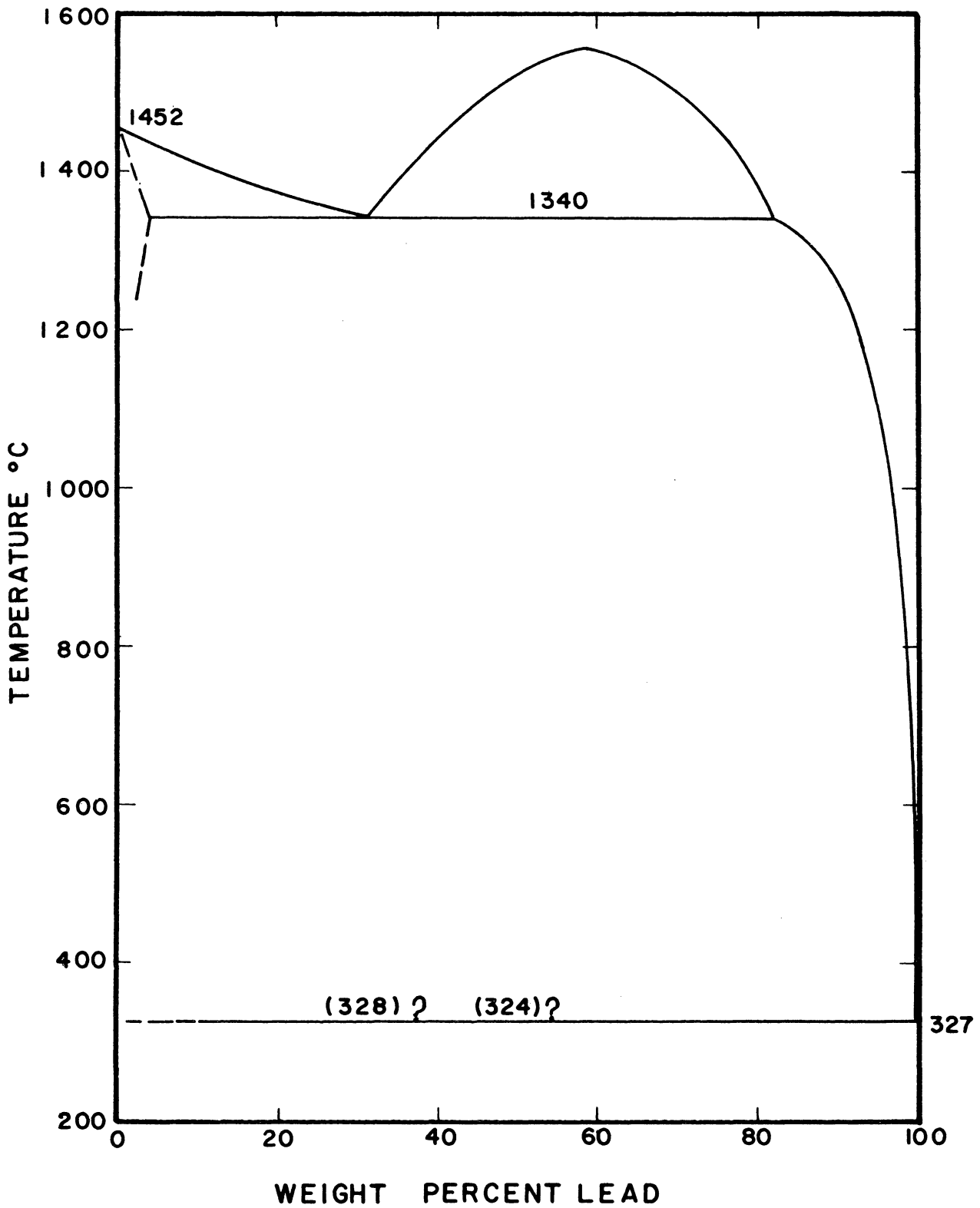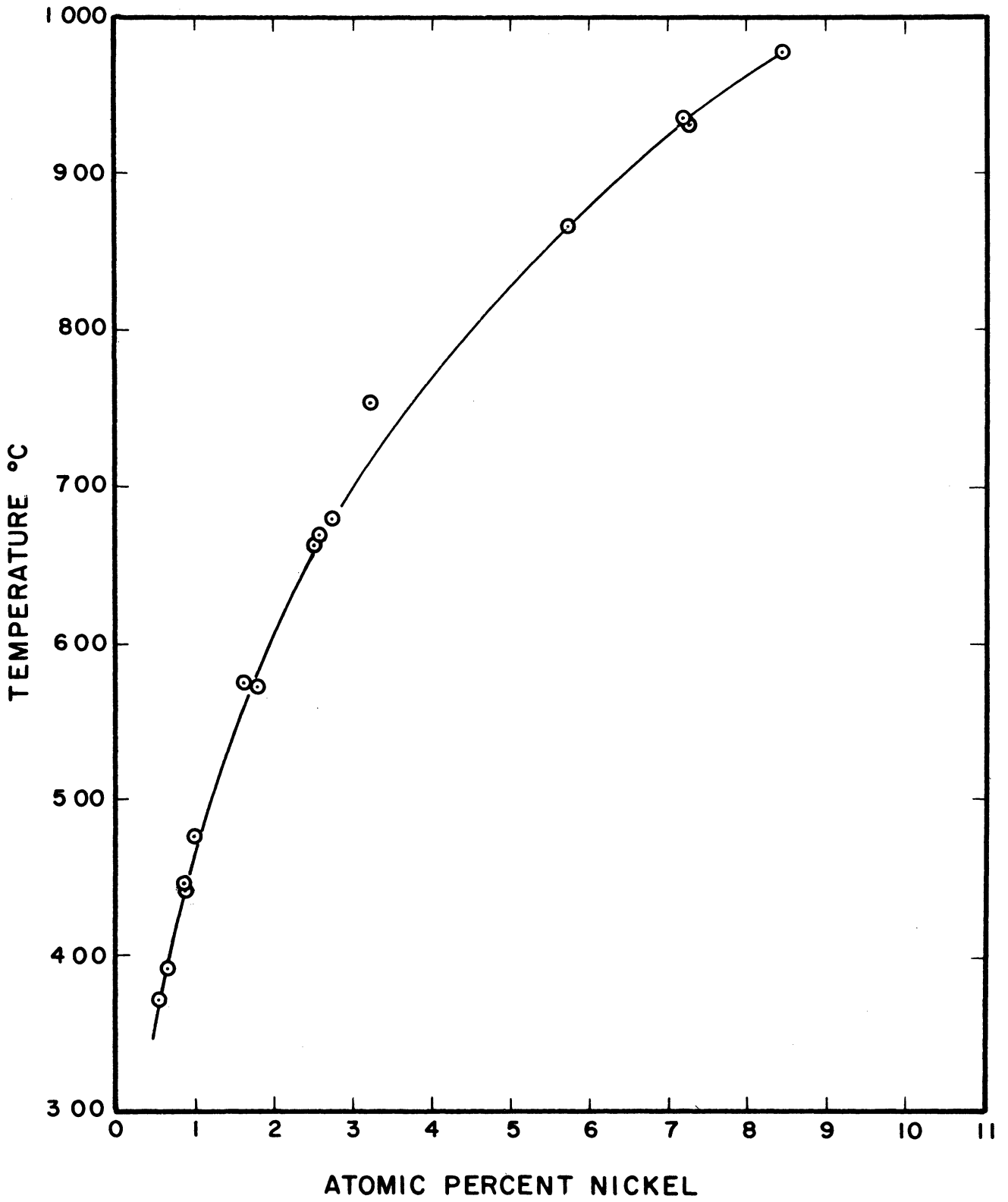Figure 11. The Nickel-Lead Phase Diagram.

Figure 12. Solubility of Nickel in Liquid Lead. Reference (2).

volume of nickel in the solid, $\overline{V}^{\ell}_{Ni}$ the partial molar volume of nickel

in the liquid, and x^{ℓ}_{Ni} the mole fraction of nickel in the liquid.

If the activity of nickel in liquid lead is proportional to

its mole fraction, then

$$\frac{\partial \mu^{\ell}_{Ni}}{\partial x^{\ell}_{Ni}} = \frac{RT}{x^{\ell}_{Ni}} \quad . \tag{6-4}$$

So

$$\frac{d \ln x^{\ell}_{Ni}}{dP} = \frac{V^{s}_{Ni} - \overline{V}^{\ell}_{Ni}}{RT} \quad . \tag{6-5}$$

From (66, 96) the molar volume of solid nickel at 600°C is

6.66 cc/mol. From (98) the partial molal volume of nickel in liquid

lead at 600°C in in the range 3.2 to 5.5 cc/mol. Taking the value which

will produce the greatest change in solubility one has:

$$\frac{d \ln x^{\ell}_{Ni}}{dP} = 4.8 \cdot 10^{-5} \ atm^{-1} \quad . \tag{6-6}$$

The solubility of nickel in lead at 600°C is 1.85 atomic

percent. From Equation (6-6), 3000 atm (44,000 psi) pressure increases

the solubility to 2.14 atomic percent. From the data available, this

must be regarded as an upper limit to the solubility change which occurs.

One can conclude that pressures in the range used in these

experiments exert very little influence on the phase diagram.

2. Temperature and Pressure Data

Specimens of leaded nickel were equilibrated at temperatures

from 371°C to 816°C (700°F to 1500°F) in a vacuum. Other specimens were

equilibrated at pressures up to 50,000 psi at 371°C (700°F) and 593°C

(1100°F). The results of 500 angles measured on each specimen are shown in Table X.

All of the specimens with designation D were cut from the same ingot, and had about the same grain size, impurity content, etc. All of these specimens were hydrostatically tested in water. The only inconsistent values from this data are from DP2 and DP3. The first gave an abnormally low value for the dihedral angle and the second an abnormally high value. (Compare with specimens DP5 and DP9, respectively.) Re-measurement of these specimens produced virtually the same dihedral angles. These two specimens were among the first ones run in the hydro-thermal unit and neither was quenched after the run as were all other specimens. DP2 was cooled in an air blast, and DP3 was cooled in an air blast until the pressure dropped to about 25,000 psi, then quenched in water. It is not clear why failure to give a rapid quench should produce a low angle in one case and a high angle in another. This seems to be the only difference, however, in the way these two specimens were treated, so one must assume that the cause of the unusual values is the quenching rate. Neither of these two specimens will be considered in the analysis of the results.

As was mentioned in Chapter IV, heat D proved to have an undesirably high sulfur level. Sulfur is known to be surface active in liquid iron[36] and there is indirect evidence which suggests it might segregate to nickel grain boundaries.[76] Oxygen is also surface active in liquid nickel.[55] For these reasons, heats E and F were prepared in such a manner as to insure low sulfur and oxygen contents.

TABLE X

SUMMARY OF TEMPERATURE AND PRESSURE DATA
500 ANGLES MEASURED ON ALL SPECIMENS

Sample	Pressure psi	Temp °F	Time Hours	Dih. ∡ from Median	Median Angle	95% Conf. Limits on Median		Dih. ∡ from Computer	Index of Fit
D	0	700	186	51.9	51.0	52.2	49.1	52.1	3.21
D900	0	900	168	46.5	45.5	47.0	44.1	47.0	3.95
D1100	0	1100	168	41.1	40.2	41.9	38.8	42.2	5.82
D1300	0	1300	120	36.8	36.0	37.6	34.8	37.8	5.54
D1500	0	1500	120	32.3	31.6	33.3	30.6	33.6	6.94
DP1	10,600	706	168	47.7	46.7	48.4	45.3	48.2	3.66
DP2	24,000	716	161	40.1	39.2	40.7	37.9	41.0	5.00
DP3	33,500	708	144	44.8	43.8	44.4	42.1	44.8	3.75
DP5	19,700	709	167	45.0	44.0	45.7	42.7	45.5	4.76
DP6	41,000	712	168	40.9	40.0	41.5	39.0	41.7	5.74
DP8	50,200	703	168	38.6	37.7	38.8	36.6	39.2	4.73
DP9	31,000	703	83	42.6	41.6	43.1	39.8	43.0	4.39
D11-1	23,200	1096	124	36.1	35.3	36.8	34.3	37.3	3.85
D11-2	11,500	1098	120	38.9	38.0	39.1	36.7	39.3	4.14
D11-6	33,100	1096	120	34.7	33.9	34.9	32.5	35.5	4.38
D11-7	42,000	1097	120	33.6	32.8	33.9	31.3	34.3	5.52
D11-8	52,600	1096	52	32.1	31.4	32.6	30.1	32.8	7.81
E	0	1100	72	43.5	42.5	43.8	41.3	44.5	5.27
E1	23,500	1098	28	39.5	38.6	39.8	37.5	40.4	4.39
F	0	1100	72	42.1	41.1	43.0	40.2	43.6	5.28
F1	30,200	1097	30	35.8	35.0	36.3	33.7	36.5	4.17
F1A	0	1100	36	42.1	41.1	42.5	40.2	42.6	3.79

Due to the melting practice used, heat E contained only a few percent lead which was very finely dispersed throughout the nickel matrix. The median length of lenticular particles was about 3.4μ. Heat F contained 8-10% lead with a median particle length of about 5.4μ. Particles in heat D were larger; a median particle length of about 7μ was measured. Any particle less than about 2μ in length is too small to measure with any degree of accuracy at the magnification used (1200X). Particles from $2-4\mu$ in length can be measured, but the measuring error is probably high.

The measurements from specimens E, F, and D1100 show decreasing median angles with increasing particle size. In the light of the errors discussed in the previous chapter, it is felt that a high median angle was obtained from E because of biased sampling due to the omission of measurements on small particles. The same tendency may have been present in F; but the results from F and D1100 are not sufficiently different (nor are the particle sizes sufficiently different) to warrant such a conclusion.

Specimen E1 was hydrostatically tested using argon as a pressure medium. However, a slow leak in the system allowed the argon pressure to drop about 6000 psi during the course of the run. Hence, the measurements made on E1 have little significance.

Specimen F1 was also hydrostatically tested in argon. The resulting change in median angle from F to F1 checks well the change in median angle from D1100 to D11-6. These results allow one to conclude that, (1) composition differences (particularly sulfur content) do not significantly influence the results, at least at these impurity

levels, (2) hydrostatically testing in water rather than an inert medium does not influence the results, (3) the length of time allowed to obtain equilibration at 1100°F for all specimens from heat D was more than adequate.

The reversibility of the change in dihedral angle is shown by specimens F, F1, and F1A. Specimens F and F1 were heat treated at 1100°F for 72 hours. Angles on F were then measured. Specimen F1 was then subjected to hydrostatic pressure at 1100°F for 30 hours. After angle measurements were completed on F1, it was reannealed at 1100°F for 36 hours. The angles then measured are designated by F1A. It is clear that there is no significant difference between F and F1A.

The results of the temperature and pressure measurements are summarized in Figures 13 and 14. The ratio of surface tensions is related to the dihedral angle by: $\gamma_{gb}/\gamma_{sl} = 2 \cos \theta/2$, where θ is the dihedral angle. Points designated by squares in Figure 14 are picked off the smooth curves of Figure 13.

3. Tension and Compression Data

The angle measurements made on stressed specimens were treated in the same manner as similar measurements made on specimens equilibrated at different combinations of temperature and pressure. For purposes of characterizing a sample of angles obtained from these specimens, the median angle will be used. The problem of relating this to a dihedral angle expressible as a ratio of interfacial tensions will be left to the next chapter.

Preliminary experiments on leaded copper[59] suggested that the median angle decreased when a tensile stress was applied. The exact
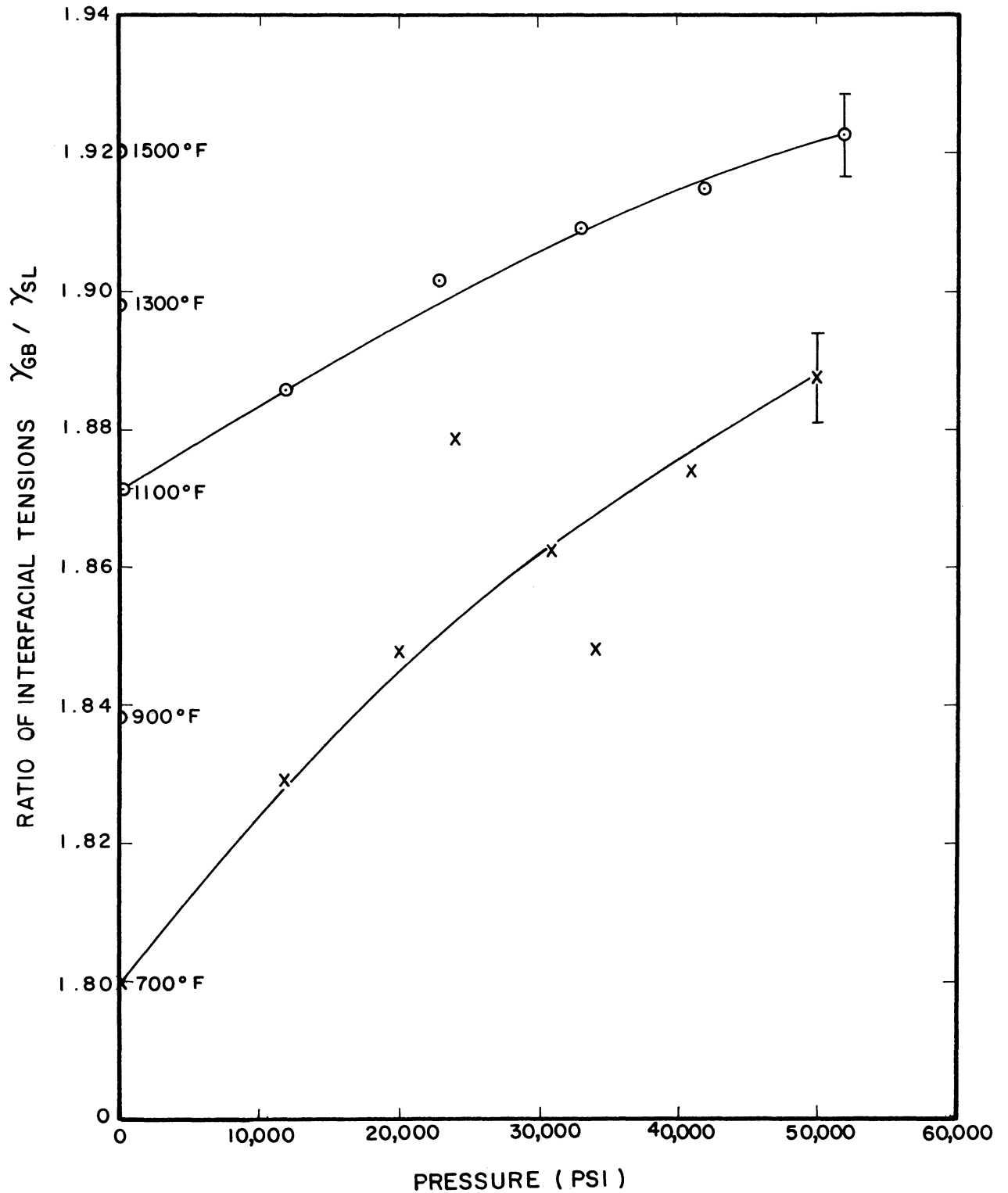
Figure 13. Ratio of Interfacial Tensions as a Function of Pressure.
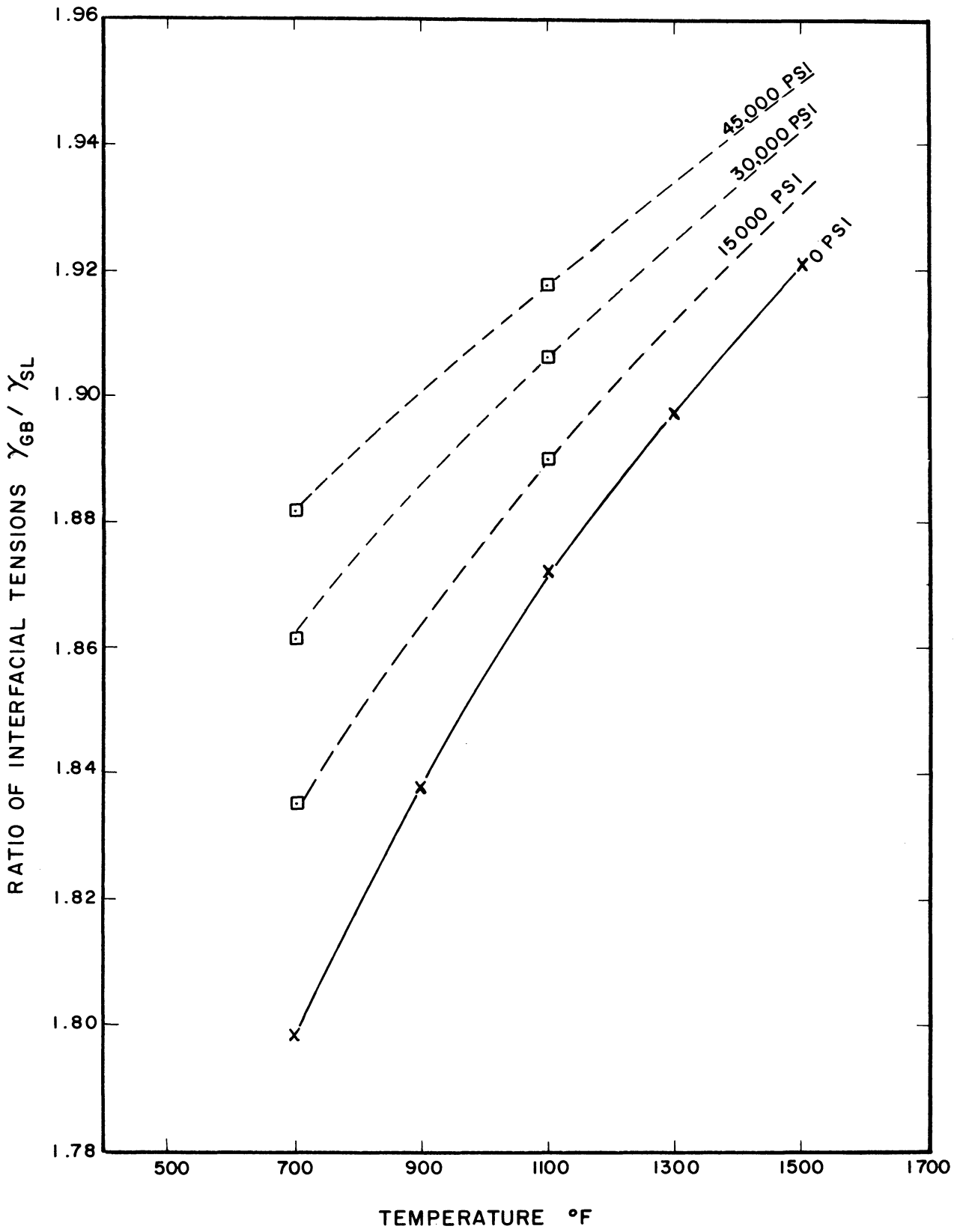95% Confidence Intervals Are Shown for Two Data Points.

Figure 14. Ratio of Interfacial Tensions as a Function of Temperature.

nature of the variation was not established by the preliminary work, so these experiments were repeated using leaded nickel. All tension and compression testing was done at 371°C in an inert atmosphere for 48 hours, with the exception of one specimen run for 120 hours.

Two specimens were run at stresses of 1000 and 1500 psi. Both showed a lower median angle than an unstressed specimen treated at the same temperature, but the decrease in both cases was about the same. The angle measurements were then grouped on the basis of the distance from the edge of the specimen at which the angle was observed. It was found that the median angle was lower (by 5-6°) in the center two thirds of each specimen than it was in the outer third of the specimen. This confirmed the observations made in reference (59). The median angle in the outer third of the specimen was almost the same as the median angle of the unstressed alloy.

Observations of the polished section showed some cracks occurred. These began at the specimen surface and followed grain boundaries into the interior of the specimen. On the order of 30 cracks per inch along the section edge were observed, the longest running 0.015-0.020" into the specimen. The portion of the specimen showing unchanged median angles was about 0.035" thick.

It was postulated that the applied stress was indeed affecting the median angle observed, but that cracks occurring at the surface relieved the stress in the outer portion of the specimen. This produced a median angle in the outer portion of the specimen characteristic of the unstressed material. Since observations of crack depth can only be made in the plane of polish, it was considered likely that some cracks were at least 0.035" deep.

To test this hypothesis, subsequent specimens were plated
with about 0.001" thick copper plate prior to tensile testing. This
soft plate was applied to eliminate crack initation at the surface.
In every subsequent tensile test with plated specimens, no dependence
of the median angle on distance from the surface was noted. On the
basis of these results, the suggestion put forward in reference (59)
that diffusion of oxygen from the atmosphere along grain boundaries was
responsible for this behavior must be rejected.

In a tensile test on this sort of material, the liquid lead
particles probably behave very much like stress-free holes in a solid
matrix. Stress concentrations occur at the particles; particles lying
in planes normal to the axis of tension must have a concentrated normal
stress at the apex of the particle tending to cause cracking. It was
considered possible that lead filled cracks originating at these particles
might have been measured and were responsible for the overall decrease
in median angle observed in stressed specimens.

To check this possibility, the angle that each lead particle
made with the axis of tension was recorded along with the apex angles.
The data was classified into three groups on the basis of angle off
the axis of tension. This was done for all tensile specimens. A sum-
mary of all the data on plated tension specimens, classified in this
manner, is presented in Table XI and in Figures 15 to 17.

The data show that for all but one tensile test the median
angles taken from particles lying normal to the axis of tension are
larger than the median angle from particles lying along the axis of
tension. Non-parametric tests for statistical significance indicate

TABLE XI

SUMMARY OF TENSION AND COMPRESSION DATA TEMPERATURE 700°F

Run	Stress psi	Angle Off Axis	Time Hours	Median Angle	No. Angles Measured	95% Conf. Interval For Median		Dihedral Angle From Computer	Index of Fit
Tension									
D 1	0	0-29.9	186	51.1	143	53.8	48.4	52.4	3.12
2		30-59.9		51.1	165	53.8	47.9	52.1	4.67
3		60+		50.9	191	52.4	48.7	51.8	2.50
D1 1	2010	0-29.9	48	38.6	233	41.9	34.9	40.8	7.88
2		30-59.9		38.8	299	41.2	36.5	41.0	8.27
3		60+		42.9	452	44.8	40.7	44.3	8.73
D2 1	975	0-29.9	120	42.9	205	44.8	40.8	44.6	4.56
2		30-59.9		46.5	206	48.5	43.0	47.5	4.88
3		60+		47.8	191	50.1	44.9	49.2	4.21
C1 1	1500	0-29.9	48	40.6	231	42.6	39.4	42.6	4.12
2		30-59.9		42.5	173	45.2	40.8	44.4	4.35
3		60+		44.2	187	46.7	43.3	45.8	2.41
C2 1	995	0-29.9	48	43.8	182	46.4	41.9	45.5	3.19
2		30-59.9		46.3	147	48.2	42.6	47.4	4.78
3		60+		47.4	167	49.9	45.1	49.2	5.06
B1 1	2350	0-29.9	48	37.9	150	40.5	34.8	39.7	7.90
2		30-59.9		37.1	145	38.8	33.2	38.0	7.86
3		60+		31.7	141	34.8	26.7	33.6	9.64
Compression									
DC1 1	1500	0-29.9	48	45.7	182	47.6	42.1	46.6	4.62
2		30-59.9		42.3	206	44.6	39.2	43.8	5.00
3		60+		39.6	212	43.4	36.0	41.6	7.68
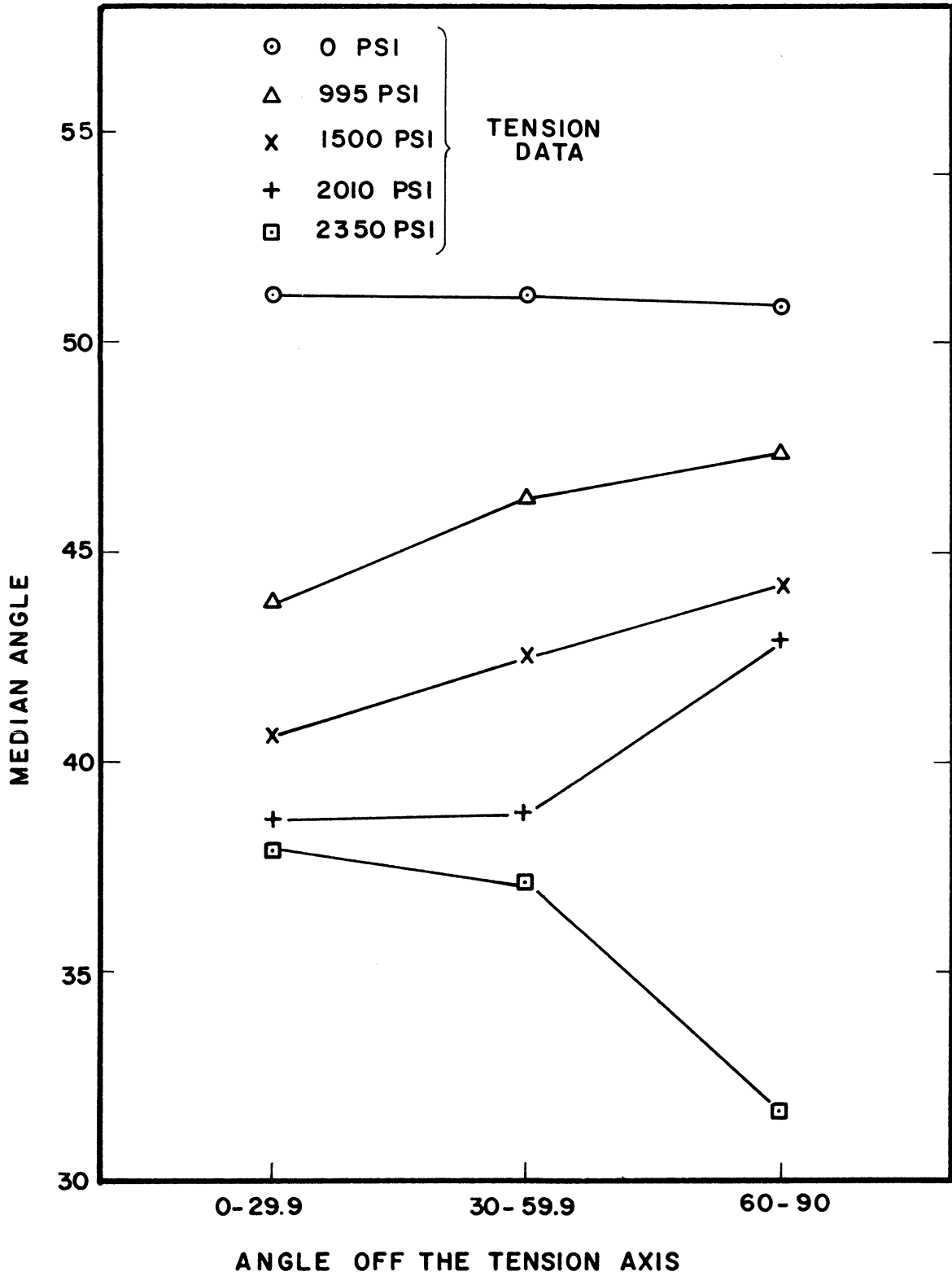
Figure 15. Median Angle Observed in Tensile Testing as a Function of Orientation with Respect to the Axis of Tension.
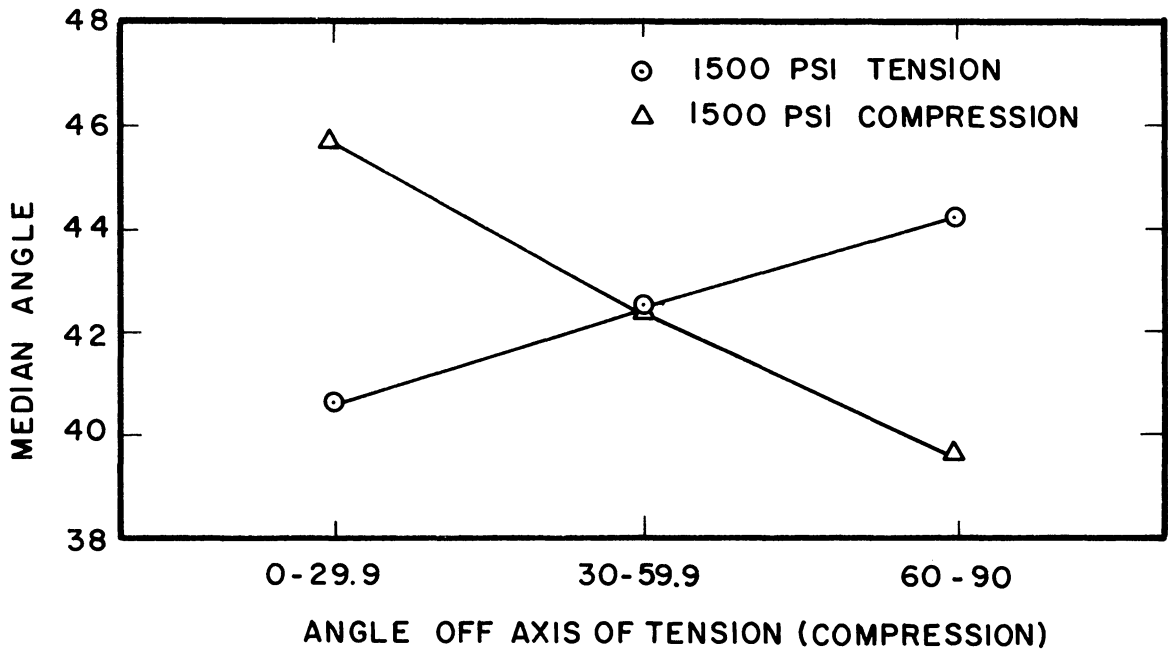
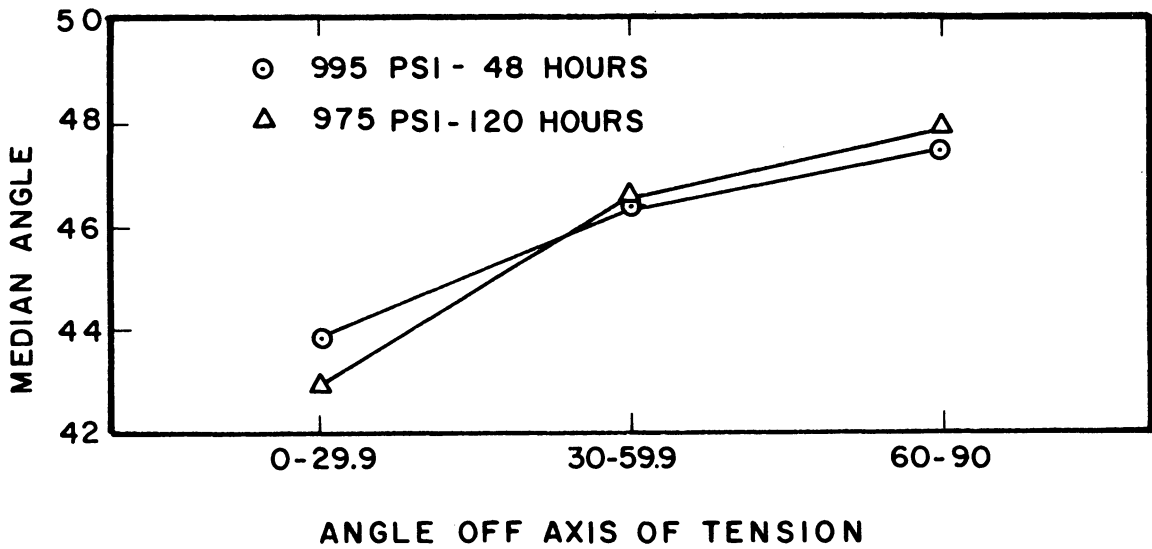Figure 16. Comparison of Results of Testing in Tension and Compression

Figure 17. Comparison of Tensile Tests Run for 48 and 120 hours.

that the differences indicated perpendicular to and along the axis of tension are significant. The only specimen which shows a smaller median angle perpendicular to the axis of tension is B1 which was run at the highest stress. Attempts made to run specimens at still higher stresses all resulted in fracture soon after the load was applied. (In fact, some specimens loaded at a lower stress than B1 also fractured.)

One must conclude from these results that the lowered median angle observed in tension is not influenced by crack formation at the lead particles at stresses below the observed fracture stress of these alloys.

Specimen D2 was run for a longer time to determine whether the median angles changed with time. Comparison with specimen C2 run at the same stress shows no significant change in the median angle between the two specimens.

One specimen (DC1) was subjected to compressive loading under the same conditions that were used in tensile testing. The specimen was not plated. The median angles measured for this specimen were also lower than for the unstressed material, but the lowest angle was now observed normal to the axis of compression. The changes observed in compression were not much different than the changes occurring at the same tensile stress (specimen C1), but the dependence of the median angle on the angle off the axis of tension is reversed.

Comparison of the data from Table XI and the data from hydrostatic testing at 371°C in Table X shows that a pressure of 50,000 psi is required in hydrostatic loading to produce the same drop in median angle as was observed with a 2000 psi tensile stress.

It is probable that the variation in median angle observed in these specimens depends on the orientation with respect to the axis of tension of the plane of the grain boundary in which the lead particle occurs. The angle off the axis of tension measured in the plane of polish, ψ , is related to the spherical co-ordinates (θ, ϕ) of the normal to the grain boundary by the relation

$$\cos \psi = \frac{\sin \theta \sin \phi}{\sqrt{1 - \sin^2 \theta \cos^2 \phi}} \qquad (6\text{-}7)$$

The orientation parameter θ represents the angle between the normal to the grain boundary and axis of tension. When ψ is allowed to range from 0 to 30°, θ can take on values from 60 to 90°. For $30° < \psi < 60°$, then $30° < \theta < 90°$, and for $60° < \psi < 90°$, then $0 < \theta < 90°$. Thus the grouping of angles occurring 60-90° off the axis of tension can arise from particles occurring in planes with any inclination from 0 to 90° with the tension axis. The majority, however, will have inclinations from 0 to 30°, so the variations observed are still qualitatively correct.

The significance of this data will be discussed in the next chapter.

CHAPTER VII

DISCUSSION OF RESULTS

1. A Method for Obtaining Variations in Interfacial Tensions from Variations in the Dihedral Angle

Changes in the dihedral angle with changes in temperature and pressure are the net results of changes in interfacial tensions at the solid/solid and solid/liquid interfaces. If one can obtain, however, the change in interfacial tension occurring at each interface, then the thermodynamic equations developed in Chapter II from the Gibbs Adsorption Equation can be applied and some properties of the interfaces may be calculated.

In order to do this, one must make an assumption as to the dependence of $d\gamma/dT$ on temperature and of $d\gamma/dP$ on pressure. The simplest assumption one can make is that for both interfaces $d\gamma/dT$ is independent of T, and $d\gamma/dP$ is independent of P. Since one cannot show, in general, that the thermodynamic quantities which determine these coefficients are independent of temperature or pressure, the worth of this assumption can only be measured by how well the data can be correlated on this basis.

Assume that the tension of each interface changes according to the expression:

$$\gamma = \gamma^\circ + \frac{d\gamma}{d\chi} \Delta\chi = \gamma^\circ + \gamma'\Delta\chi \tag{7-1}$$

where χ represents either temperature or pressure, $\Delta\chi = \chi - \chi^\circ$, γ° is the interfacial tension at χ°, and $d\gamma/d\chi = \gamma'$ is independent of χ. Then at any value of χ one may write:

$$\frac{\gamma_{gb}}{\gamma_{sl}} = \frac{\gamma^{\circ}_{gb} + \gamma'_{gb}\,\Delta\chi}{\gamma^{\circ}_{sl} + \gamma'_{sl}\,\Delta\chi} \qquad\qquad (7\text{-}2)$$

where subscripts gb, sl refer to the solid/solid and solid/liquid interfaces respectively. Subtracting $\gamma^{\circ}_{gb}/\gamma^{\circ}_{sl}$ from both sides, dividing by 2 and rearranging gives:

$$\frac{\gamma_{gb}}{2\gamma_{sl}} - \frac{\gamma^{\circ}_{gb}}{2\gamma^{\circ}_{sl}} = \frac{\gamma^{\circ}_{gb}\gamma^{\circ}_{sl} + \gamma'_{gb}\gamma^{\circ}_{sl}\Delta\chi - \gamma^{\circ}_{gb}\gamma^{\circ}_{sl} - \gamma^{\circ}_{gb}\gamma'_{sl}\Delta\chi}{2\gamma^{\circ}_{sl}(\gamma^{\circ}_{sl} + \gamma'_{sl}\Delta\chi)}$$

or

$$\frac{\gamma_{gb}}{2\gamma_{sl}} - \frac{\gamma^{\circ}_{gb}}{2\gamma^{\circ}_{sl}} = \frac{(\gamma'_{gb}\gamma^{\circ}_{sl} - \gamma^{\circ}_{gb}\gamma'_{sl})\,\Delta\chi}{2\gamma^{\circ}_{sl}\gamma^{\circ}_{sl} + 2\gamma^{\circ}_{sl}\gamma'_{sl}\,\Delta\chi} \qquad (7\text{-}3)$$

taking the reciprocal, assuming $\gamma^{\circ}_{gb}/\gamma^{\circ}_{sl} \neq \gamma'_{gb}/\gamma'_{sl}$

$$(7\text{-}4) \qquad \frac{1}{\dfrac{\gamma_{gb}}{2\gamma_{sl}} - \dfrac{\gamma^{\circ}_{gb}}{2\gamma^{\circ}_{sl}}} = \frac{2\gamma^{\circ}_{sl}\gamma'_{sl}}{(\gamma'_{gb}\gamma^{\circ}_{sl} - \gamma^{\circ}_{gb}\gamma'_{sl})} + \frac{2\gamma^{\circ}_{sl}\gamma^{\circ}_{sl}}{(\gamma'_{gb}\gamma^{\circ}_{sl} - \gamma^{\circ}_{gb}\gamma'_{sl})}\left(\frac{1}{\Delta\chi}\right)$$

Now when the ratio of interfacial tensions is such that $0 < \gamma_{gb}/2\gamma_{sl} < 1$, then a dihedral angle θ exists, $0 < \theta < 180°$. So the ratios of interfacial tensions on the lefthand side of (7-4) may be represented in terms of the dihedral angle. The first term on the righthand side of (7-4) is independent of χ and the coefficient of $1/\Delta\chi$ in the second term is independent of χ. Thus Equation (7-4) may be written:

$$(\cos\,\theta/2 - \cos\,\theta^{\circ}/2)^{-1} = b + m\left(\frac{1}{\Delta\chi}\right). \qquad (7\text{-}5)$$

If the assumption that $d\gamma/d\chi$ is independent of χ is true, then a plot of $(\cos\,\theta/2 - \cos\,\theta^{\circ}/2)^{-1}$ vs $(\Delta\chi)^{-1}$ will yield a straight line with slope m and intercept b. If m and b are determined from such a plot, then they may be used to find γ'_{gb} and

γ'_{sl} in terms of either γ°_{sl} or γ°_{gb} and cos $\theta^{\circ}/2$. This is done by solving the equations for m and b simultaneously and using the relation:

$$2 \cos \theta^{\circ}/2 = \gamma^{\circ}_{gb}/\gamma^{\circ}_{sl} .$$

The results are:

$$\gamma'_{sl} = \frac{b}{m} \gamma^{\circ}_{sl} = \frac{b \gamma^{\circ}_{gb}}{2m \cos \theta^{\circ}/2} \tag{7-6}$$

$$\gamma'_{gb} = \frac{2\gamma^{\circ}_{sl}}{m} (1 + b \cos \theta^{\circ}/2) = \frac{\gamma^{\circ}_{gb}}{m} (\frac{1}{\cos \theta^{\circ}/2} + b) .$$

Thus $d\gamma_{sl}/d\chi$ and $d\gamma_{gb}/d\chi$ are determined in terms of the surface tension of either the solid/solid or solid/liquid interface and the dihedral angle θ° at χ°.

Using the above technique the coefficients $d\gamma/dP$ and $d\gamma/dT$ can be determined for each interface from measurements of the dihedral angle as a function of pressure and temperature, respectively. In Appendix C, the change in dihedral angle with temperature is correlated on this basis for data obtained from the literature.

The dihedral angle at zero pressure was measured at five temperatures from 371° to 816°C. This data is presented in Table X.

Using a reference temperature of 371°C, a plot of $(\cos \theta/2 - \cos \theta^{\circ}/2)^{-1}$ vs $(\Delta T)^{-1}$ is shown in Figure 18. The line drawn through these points is a weighted least squares line. The reasons for using a weighted least squares fit are discussed in Appendix D. The method for fitting weighted least square lines is described in reference (68).

It is interesting to note that this plot extrapolates to a zero dihedral angle at the monotectic temperature (1340°C). If one takes the monotectic temperature as a reference and constructs a
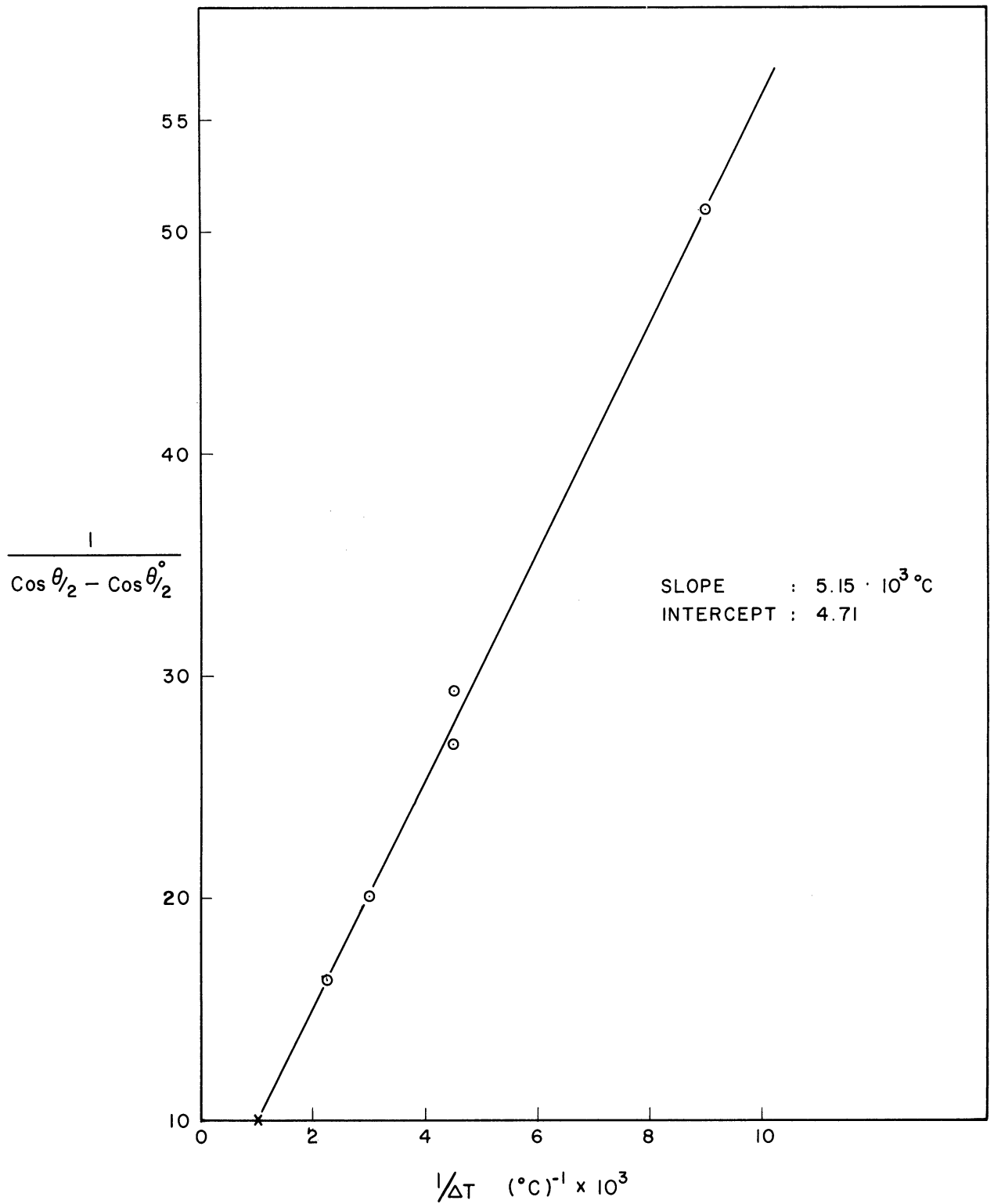
Figure 18. R-plot for Temperature Data at 0 Pressure. The Line Shown is a
Weighted Least Squares Line. The Line Extrapolates to a 0°
Dihedral Angle at 1340°C, the Monotectic Temperature, Indicated
on the Abscissa.

$(\cos \theta /2 - \cos \theta°/2)^{-1}$ vs $(\Delta T)^{-1}$ plot, the data is linear and the calculated temperature coefficients of surface tension agree to within one standard deviation with the temperature coefficients obtained using 371°C as a reference. The variance of the coefficients obtained is about the same in both cases.

An attempt to quench a specimen equilibrated at the monotectic temperature produced a specimen with a small but finite dihedral angle. Angles appeared to be smallest at the surface of the specimen, indicating that the quenching rate is an important variable. Ikeuye and Smith[51] show the dihedral angle going to zero at the monotectic temperature in the Cu-Pb system, and it is possible that this occurs in the Ni-Pb system, too.

A slope and intercept may be determined from Figure 18 and used to compute the temperature coefficients of the surface tension at each interface. The results are:

$$\frac{d\gamma_{sl}}{dT} = 5.09 \; (\pm 2.76) \cdot 10^{-4} \; \gamma(371°) \quad ergs/cm^2 \text{-}°C$$

$$\frac{d\gamma_{gb}}{dT} = 11.32 \; (\pm 5.06) \cdot 10^{-4} \; \gamma(371°) \quad ergs/cm^2 \text{-}°C$$

where $\gamma(371°)$, is the grain boundary tension at 371°C and 0 pressure. The standard deviation of the coefficient is indicated in parentheses $(\pm X)$. For purposes of comparison, all data will be expressed in terms of the grain boundary tension at 593°C. From Equation (7-1)

$$\gamma(593°) = \gamma(371°) + 11.32 \cdot 10^{-4} \; \gamma(371°) \quad (593 - 371)$$

$$\gamma(593°) = 1.252 \; \gamma(371°)$$

Hence, the temperature coefficients become:

$$\frac{d\gamma_{sl}}{dT} = 4.07 \ (\pm 2.20) \cdot 10^{-4} \ \gamma(593°) \qquad ergs/cm^2\text{-}°C$$

$$\frac{d\gamma_{gb}}{dT} = 9.04 \ (\pm 4.05) \cdot 10^{-4} \ \gamma(593°) \qquad ergs/cm^2\text{-}°C.$$

(7-7)

Note that both surface tensions are increasing with increasing temperature.
For pure liquids, surface tensions invariably decrease with increasing
temperature, but, as McLean points out,[65] positive or negative temperature
coefficients are possible in two component systems. Reference to
Equation (2-28) clearly indicates that the temperature coefficient is
dependent not only on adsorption at the interfaces, but also on the
thermodynamic properties of the two component phases present. The
assumption is often made in treating changes in dihedral angles with
temperature, that the grain boundary tension is constant with changing
temperature. If this were so in this system, then the intercept of the
above plot should equal - sec $\theta°/2$ or -1.1. It is clear from
Figure 18, that such an intercept is improbable.

Changes in the dihedral angle with pressure were measured
at 371° and 593°C. This data is presented in Table X and plotted as
(cos $\theta/2$ - cos $\theta°/2$)$^{-1}$ vs P^{-1} in Figures 19 and 20. The reference
points are the zero pressure values of the dihedral angle at these
temperatures. The lines drawn are weighted least squares lines.

From the slope and intercept of these plots, pressure coef-
ficients of interfacial tension are determined:

$$\frac{d\gamma_{sl}}{dP} = 2.00 \ (\pm 0.82) \cdot 10^{-10} \ \gamma(371°) \qquad cm$$

$$\frac{d\gamma_{gb}}{dP} = 3.90 \ (\pm 1.53) \cdot 10^{-10} \ \gamma(371°) \qquad cm$$

at 371°C (7-8)
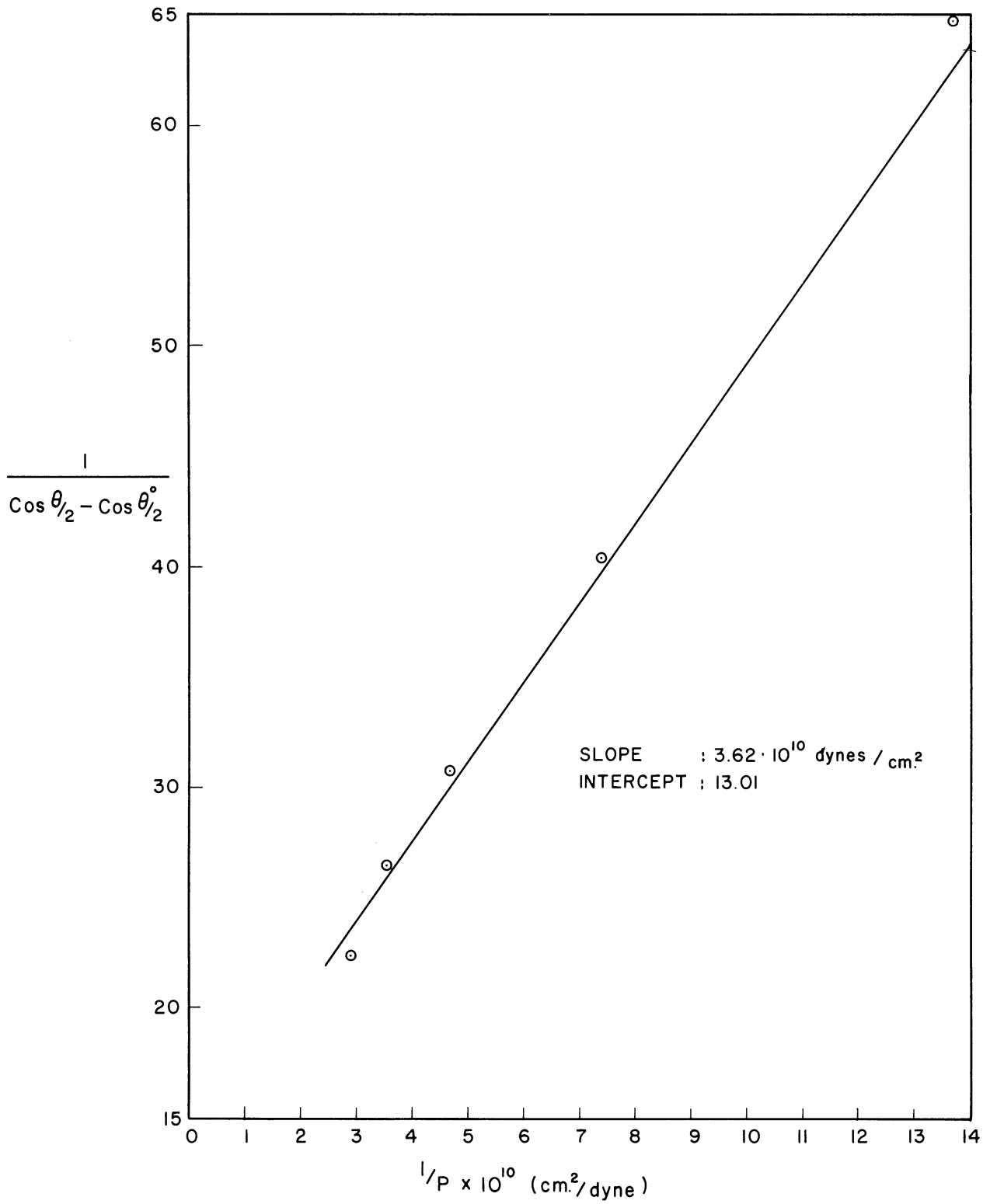
Figure 19. R-Plot for Pressure Data at 371°C. The Line Shown is a Weighted
Least Squares Line.
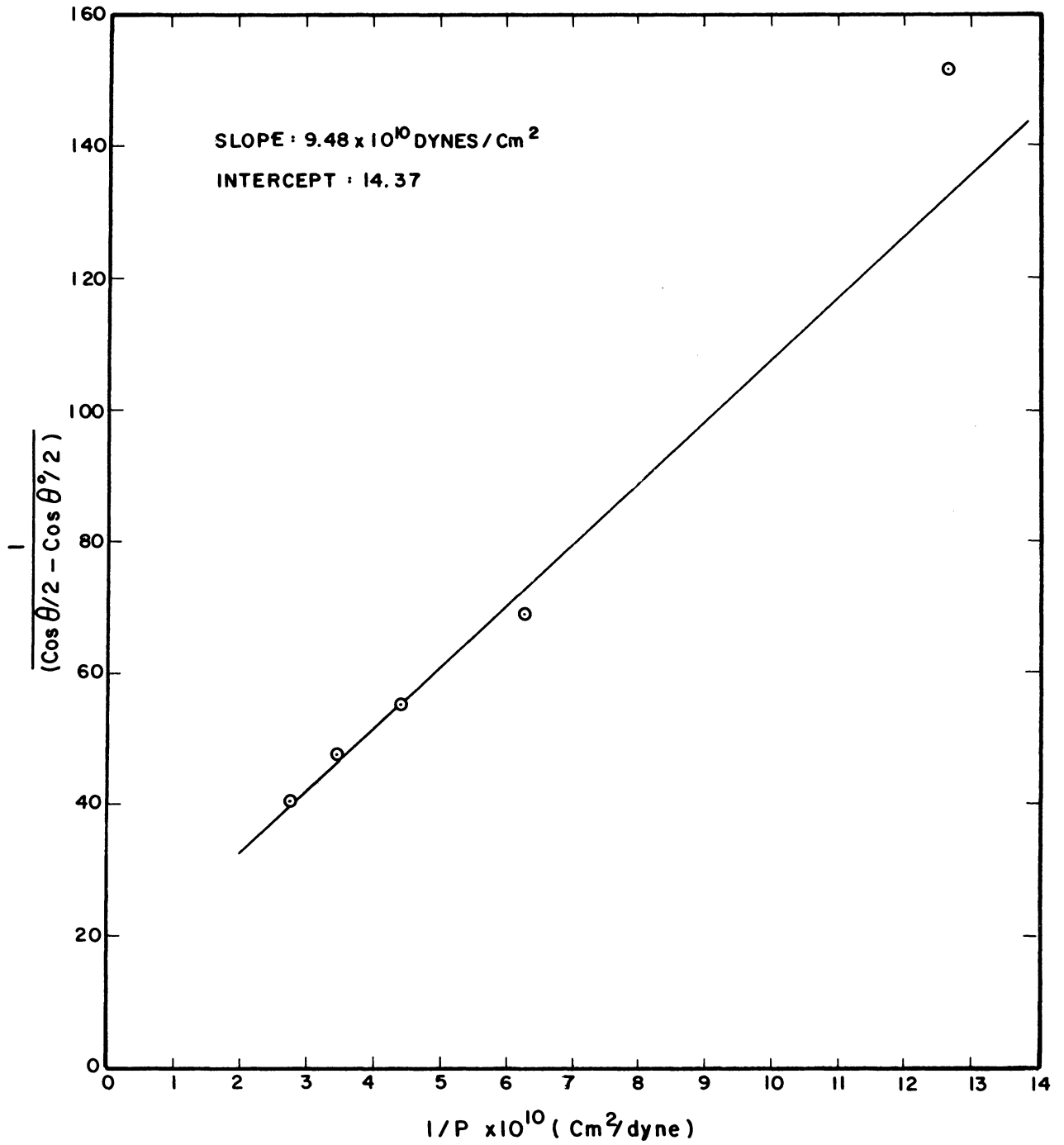
Figure 20. R-Plot for Pressure Data at 593°C. The Line Shown is a Weighted
Least Squares Line.

$$\frac{d\gamma_{sl}}{dP} = 0.81 \ (\pm 0.63) \cdot 10^{-10} \ \gamma(593°) \quad cm$$

at 593°C   (7-8)

$$\frac{d\gamma_{gb}}{dP} = 1.63 \ (\pm 1.32) \cdot 10^{-10} \ \gamma(593°) \quad cm \ .$$

Referring the measurement at 371°C to the grain boundary

tension at 593°C, as before, one has

$$\frac{d\gamma_{sl}}{dP} = 1.60 \ (\pm 0.65) \cdot 10^{-10} \ \gamma(593°) \quad cm$$

at 371°C   (7-9)

$$\frac{d\gamma_{gb}}{dP} = 3.12 \ (\pm 1.22) \cdot 10^{-10} \ \gamma(593°) \quad cm \ .$$

The calculated pressure and temperature coefficients in

Equations (7-7) to (7-9) are rather inaccurate; the reason for this

is discussed in Appendix D. It should be emphasized here that the

properties of the interfaces to be calculated from these coefficients

in the next sections are at least equally uncertain, i.e., they are

reliable to an order of magnitude, but not much more.

2. The Solid/Liquid Interface

From the measured pressure coefficient of interfacial tension,

it is possible to determine the surface excess of Ni, $\Gamma_{Ni(Pb)}$, by

using Equation (2-39). The only other information needed is the molar

volume of solid nickel at 371° and 593°C, which is readily obtained.

From reference (66), the density of Ni at 20°C is 8.902 g/cc.

Smithells[96] gives data for the linear coefficient of thermal expansion

between 20°C and the temperature of interest. Using these data, the

molar volumes of solid Ni at the temperatures of interest are:

$$\underline{V}_{Ni} = 6.70 \quad cc/mol \quad \text{at } 371°C$$

$$\underline{V}_{Ni} = 6.77 \quad cc/mol \quad \text{at } 593°C \ .$$

(7-10)

The compressibility of Nickel is on the order of $10^{-7}(psi)^{-1}$. Since the maximum pressure used in these experiments was about 50,000 psi, the maximum change in $\underline{V}_{Ni}$ with pressure is on the order of 0.5% or less. This change is small enough to be ignored.

From the data in (7-8), (7-9) and (7-10) and using Equation (2-39), the excess concentration of Ni at the solid/liquid interface may be computed. The results are:

$$\Gamma_{Ni(Pb)} = -2.39 \cdot 10^{-11} \; \gamma(593°) \; mole/cm^2 = -14.4 \cdot 10^{12} \; \gamma(593°)$$
$$atoms/cm^2 \quad at \; 371°C \qquad (7\text{-}11)$$

$$\Gamma_{Ni(Pb)} = -1.19 \cdot 10^{-11} \; \gamma(593°) \; mols/cm^2 = -7.17 \cdot 10^{12} \; \gamma(593°)$$
$$atoms/cm^2 \quad at \; 593°C \; .$$

The excess entropy of the interface, $S_{(Pb)}^{(s)}$ can be determined from the temperature coefficient of interfacial tension, using the results in (7-11) above. This can be done in two ways. First, one can assume that the solid is pure nickel, and express the differential of chemical potential of nickel in terms of the solid phase. The expression for the temperature coefficient of interfacial tension is then:

$$d\gamma_{sl}/dT \;=\; -S_{(Pb)}^{(s)} \;+\; \Gamma_{Ni(Pb)} \; \underline{S}_{Ni} \qquad (7\text{-}12)$$

where $\underline{S}_{Ni}$ is the molar entropy of solid nickel.

From reference (101) the molar entropy of solid nickel is:

$$\underline{S}_{Ni} \;=\; 12.65 \; cal/°C\text{-}mol \;=\; 5.30 \cdot 10^{8} \; ergs/°C\text{-}mol \quad at \; 371°C$$
$$(7\text{-}13)$$
$$\underline{S}_{Ni} \;=\; 14.88 \; cal/°C\text{-}mol \;=\; 6.23 \cdot 10^{8} \; ergs/°C\text{-}mol \quad at \; 593°C \; .$$

Then using Equation (7-12) and the data from (7-7), (7-11), and (7-13) the excess entropies are:

$$S_{(Pb)}^{(s)} = -1.30 \cdot 10^{-2} \, \gamma(593°) \quad ergs/cm^2 \text{-} °C \quad at \, 371°C$$

$$S_{(Pb)}^{(s)} = -0.785 \cdot 10^{-2} \, \gamma(593°) \quad ergs/cm^2 \text{-} °C \quad at \, 593°C \quad .$$

$$(7\text{-}14)$$

The second method of obtaining the excess entropy requires that the differential of chemical potential of nickel be expressed in terms of the liquid phase. This leads to Equation (2-33). No simplifying assumption is necessary here as to the composition of the phases, but values are required for the partial molar entropy of nickel in liquid lead, $\overline{S}_{Ni}$ and for $\left. \dfrac{\partial \mu_{Ni}}{\partial x} \right)_{T,P} \dfrac{dx}{dT}$, both evaluated in the saturated solution. Sufficient experimental data is not available to allow calculation of these quantities, but they may be estimated from a "sub-regular" solution model. The necessary calculations are shown in Appendix E.

Using the results of Appendix E, the terms $\Gamma_{Ni(Pb)} \overline{S}_{Ni}$ and $\Gamma_{Ni(Pb)} \dfrac{\partial \mu_{Ni}}{\partial x} \dfrac{dx}{dT}$ occurring in Equation (2-33) are computed, giving the following:

$$\Gamma_{Ni(Pb)} \, \overline{S}_{Ni} = -2.20 \cdot 10^{-2} \, \gamma(593°) \, \frac{dynes/cm}{°C} \quad at \, 371°C$$

$$\Gamma_{Ni(Pb)} \, \overline{S}_{Ni} = -1.12 \cdot 10^{-2} \, \gamma(593°) \, \frac{dynes/cm}{°C} \quad at \, 593°C$$

$$(7\text{-}15)$$

$$\Gamma_{Ni(Pb)} \left. \frac{\partial \mu_{Ni}}{\partial x} \right)_{T,P} \frac{dx}{dT} = -5.53 \cdot 10^{-3} \, \gamma(593°) \, \frac{dynes/cm}{°C} \quad at \, 371°C$$

$$\Gamma_{Ni(Pb)} \left. \frac{\partial \mu_{Ni}}{\partial x} \right)_{T,P} \frac{dx}{dT} = -3.58 \cdot 10^{-3} \, \gamma(593°) \, \frac{dynes/cm}{°C} \quad at \, 593°C.$$

Using (7-11), (7-15), (7-7), and Equation (2-33), the excess entropy at the solid/liquid interface is:

$$S_{(Pb)}^{(s)} = -1.61 \cdot 10^{-2} \, \gamma(593°) \quad ergs/cm^2 \text{-} °C \quad at \, 371°C$$

$$(7\text{-}16)$$

$$S_{(Pb)}^{(s)} = -0.721 \cdot 10^{-2} \, \gamma(593°) \quad ergs/cm^2 \text{-} °C \quad at \, 593°C$$

These results check well with (7-14).

From the values of excess entropy obtained, some inferences may be drawn as to the thickness of the solid/liquid interfacial region. If one calculates the entropy per unit volume in the solid and liquid phases, then the excess entropy of the interface can never be larger than the difference between these values. This assumes no maxima or minima in the entropy per unit volume as one moves across the interfacial region. From reference (101) the molar entropy of the liquid lead solution and of solid nickel can be determined. Using the molar volumes of these phases at 371°C and 593°C, the entropies per cubic centimeter in each phase are:

$$\underline{S}_{Pb}^{V} = 4.86 \cdot 10^{7} \text{ ergs/cc-°C at } 371°C$$

$$\underline{S}_{Pb}^{V} = 5.16 \cdot 10^{7} \text{ ergs/cc-°C at } 593°C$$

$$\underline{S}_{Ni}^{V} = 7.91 \cdot 10^{7} \text{ ergs/cc-°C at } 371°C$$

$$\underline{S}_{Ni}^{V} = 9.16 \cdot 10^{7} \text{ ergs/cc-°C at } 593°C .$$

$$(7-17)$$

The maximum negative differences in entropies at each temperature are: $-3.05 \cdot 10^{7}$ ergs/cc-°C at 371°C and $-4.0 \cdot 10^{7}$ ergs/cc-°C at 593°C. These may be set equal to $S_{\binom{s}{Pb}}/\tau$ at each temperature, and the minimum possible thicknesses, τ_{min}, are:

$$\tau_{min} = 1.70 \cdot 10^{-7} \text{ cm at } 371°C$$

$$(7-18)$$

$$\tau_{min} = 0.78 \cdot 10^{-7} \text{ cm at } 593°C .$$

These are computed assuming that $\gamma(593°) = 400$ in Equation (7-16). (See Appendix B for a justification of this assumption.) At both temperatures the minimum thickness corresponds to 3 - 6 atom layers.

These figures are not unreasonable for the solid/liquid interface; they are, of course, no more reliable than the numerous assumptions and estimations that have been made up to this point in the discussion.

Such a diffuse interface is also to be expected on the basis of the excess concentrations of nickel in Equation (7-11). Again using $\gamma(593°) = 400$,

$$\Gamma_{Ni(Pb)} = -5.76 \cdot 10^{15} \text{ atoms/cm}^2 \quad \text{at } 371°C$$

$$\Gamma_{Ni(Pb)} = -2.87 \cdot 10^{15} \text{ atoms/cm}^2 \quad \text{at } 593°C. \qquad (7-19)$$

Since there are about $2 \cdot 10^{15}$ atoms of Ni on a close packed plane in the solid, an interface of about 3 - 4 atom layers would be necessary to obtain these values.

It is generally felt that the thickness of a grain boundary between identical phases is on the order of 3 atom layers thick.[65] For interfaces between dissimilar phases, this is probably not the case. Cahn and Hilliard[12,45] for example, predict diffuse interfaces between dissimilar phases from calculations based on a necessarily simplified model.

3. The Solid/Solid Interface

It was pointed out in section (5), Chapter II, that one cannot express the temperature and pressure coefficients of grain boundary tension in a form that permits the direct calculation of the excess concentrations and excess entropy at the interface. It is possible, however, to make some inferences as to the signs of the excess properties.

Equations (2-44) and (2-46) are given below:

$$d\gamma/dP = -\Gamma_{Ni} \underline{V}^S_{Ni} - \frac{\Gamma_{Pb}}{1 - x^\ell_{Ni}} (\underline{V}^\ell - x^\ell_{Ni} \underline{V}^S_{Ni}) \qquad (7-20)$$

$$dy/dT = -S^{(s)} + \Gamma_{Ni} S^s_{Ni} + \frac{\Gamma_{Pb}}{1 - x^\ell_{Ni}} \left[\underline{S}^\ell - x^\ell_{Ni} \ \underline{S}^s_{Ni} \right]. \quad (7\text{-}21)$$

If one substitutes into these equations the molar volumes and entropies of the saturated phases at 371°C and the experimentally derived coefficients, one obtains two equations involving three interfacial quantities Γ_{Ni}, Γ_{Pb} and $S^{(s)}$.

$$3.12 \cdot 10^{-10} \ \gamma(593) = -\Gamma_{Ni} \ 6.70 - \Gamma_{Pb} \ 19.5 \quad (7\text{-}22)$$

$$9.04 \cdot 10^{-4} \ \gamma(593) = -S^{(s)} + \Gamma_{Ni} \ 5.30 \cdot 10^8 + \quad (7\text{-}23)$$

$$\Gamma_{Pb} \ 9.44 \cdot 10^8 \ \text{ergs/cm}^2\text{-°C} \quad .$$

No solution of these equations for the interfacial quantities is possible, but certain observations can be made. Rewriting Equation (7-22) one obtains:

$$\Gamma_{Ni} = 2.91 \ \Gamma_{Pb} - 4.66 \cdot 10^{-11} \ \gamma(593) \ . \quad (7\text{-}24)$$

One can now show that the surface excess of nickel must be negative, because the surface excess of lead cannot have a sufficiently large negative value to make the righthand side of (7-24) negative. Let the grain boundary be 10^{-6} cm thick, and suppose the solubility of lead in solid nickel is one atom percent. Then, the smallest value of Γ_{Pb} occurs when the grain boundary is void of lead. The molar density of solid nickel is 0.149 moles/cc, so

$$\Gamma_{Pb}^{min} = -1.49 \cdot 10^{-9} \ \text{moles/cm}^2 \ .$$

A negative value larger than this would require either a thicker boundary region or a larger solubility of lead in nickel; neither event is likely.

Inserting Γ_{Pb}^{min} in (7-24) we see that as long as $\gamma(593°) > 95$ ergs/cm^2, Γ_{Ni} must be negative.

Since the lead atom is much larger than the nickel atom, one expects segregation of lead to the grain boundary, i.e., $\Gamma_{Pb} > 0$. The positive segregation of lead implies a negative segregation of nickel. The above result, $\Gamma_{Ni} < 0$, confirms this.

If Equations (7-22) and (7-23) are combined to eliminate Γ_{Pb}, one obtains:

$$S^{(s)} = -1.60 \cdot 10^{-2} \, \gamma(593°) + 2.06 \cdot 10^8 \, \Gamma_{Ni} \text{ ergs/cm}^2\text{-°C}. \quad (7-25)$$

Since $\Gamma_{Ni} < 0$, Equation (7-25) shows that the excess entropy of the grain boundary is negative. This result requires some explanation.

The entropy per mole for atoms in the grain boundary is undoubtedly higher than for atoms in grain interiors. But the excess entropy of the boundary is determined by a comparison of the entropies in equal volumes of material in the boundary and in the bulk phase. Thus, the difference between the molar densities of the boundary and the bulk phase is also important.

For a one-component system, a negative excess grain boundary entropy could only occur if the boundary region was considerably less dense than the grain interior. With two kinds of atoms present, quite different in size, a positive segregation of large atoms to the boundary implies a much greater negative segregation of small atoms. The excess entropy of the interface can then decrease as segregation increases, if the ratio of partial molar entropy to partial molar volume is smaller for the large atoms than for the small atoms.

Some crude calculations can be made to justify the existence of a negative excess interfacial entropy for nickel grain boundaries with lead present. Assume that the solubility of lead in solid nickel is zero; then the excess entropy of the interface is:

$$S^{(s)} = \tau \left(n'_{Ni} \, \overline{S}'_{Ni} - n_{Ni} \, \underline{S}_{Ni} \right) + \tau \, n'_{Pb} \, \overline{S}'_{Pb} \qquad (7\text{-}26)$$

where $\Gamma_{Ni} = \tau \left(n'_{Ni} - n_{Ni} \right)$ and $\Gamma_{Pb} = \tau \, n'_{Pb}$; τ is the thickness of the boundary; n'_{Ni} and n'_{Pb} the number of moles of nickel and lead, respectively, per unit volume of boundary; n_{Ni} the number of moles of nickel per unit volume of solid nickel; $\overline{S}'_{Ni}$ and $\overline{S}'_{Pb}$ the partial molar entropies of nickel and lead, respectively, in the grain boundary; and $\underline{S}_{Ni}$ the molar entropy of solid nickel.

The value for $\underline{S}_{Ni}$ is known.[101] Assume that $\overline{S}'_{Ni}$ is larger than $\underline{S}_{Ni}$ by the entropy of melting of nickel, and assume that $\overline{S}'_{Pb}$ is the same as the molar entropy of liquid lead. Thus,

$$\underline{S}_{Ni} = 5.30 \cdot 10^8 \text{ ergs/mol-°C}$$

$$\overline{S}'_{Ni} = 6.30 \cdot 10^8 \text{ ergs/mol-°C}$$

$$\overline{S}'_{Pb} = 9.44 \cdot 10^8 \text{ ergs/mol-°C}$$

From lattice parameter measurements at room temperature,[66] the ratio of atomic volumes of lead and nickel is 2.74. The ratio of molar densities of nickel and lead at 371°C gives a value of 2.91.[96,98] For purposes of calculation, assume

$$\frac{\text{Volume of Pb atom}}{\text{Volume of Ni atom}} = 2.8 \, .$$

If the only factor which influences the number of atoms present in the grain boundary is the displacement of nickel atoms by lead atoms, then,

$$n'_{Ni} + 2.8\, n'_{Pb} = n_{Ni}$$

If the mole fraction of lead atoms at the boundary is 0.5, then since $n_{Ni} = 0.149$ moles/cc, one has:

$$n'_{Ni} = n'_{Pb} = 0.03925 \text{ moles/cc}.$$

From these assumptions and Equation (7-26) one finds

$$S^{(s)}/\tau = -1.7 \cdot 10^7 \text{ ergs/cc-°C}$$

so if $\tau = 10^{-7}$ cm, then

$$S^{(s)} = -1.7 \text{ ergs/cm}^2\text{-°C} . \tag{7-27}$$

While this calculation indicates how a negative excess entropy can arise, the value of (7-27) is about 4 - 6 times smaller than Equation (7-25) would suggest. In view of the assumptions made to perform the calculation, this is, perhaps, as good agreement as can be expected. $S^{(s)}$ would have a greater negative value if a larger fraction of lead atoms was assumed present in the boundary or if the boundary was assumed to have a significant fraction of vacancies. However, the most critical values in the calculation (and the least certain) are the magnitudes assumed for the partial molar entropies and volumes of atoms in the interface.

4. Analysis of Results - Tension and Compresssion

The experimental data presented in the previous chapter show that applied tensile and compressive stresses change the shape of liquid lead inclusions in nickel. The results indicate further that the orientation of the lead particles with respect to the axis of tension (or compression) influences the magnitude of the change.

If one could prove that the changes in the median angle observed were solely the result of changes in interfacial tensions with applied stress, the problem of obtaining a meaningful dihedral angle from this data would still be formidable. It would be necessary to calculate a mean difference in orientation with respect to the tension axis for each group of angles. It would also be necessary to compute a correction to the distribution function for observed angles; this would require an assumption as to how the dihedral angle changes as a function of orientation with respect to the axis of tension (or compression).

It is not at all certain, however, that the changes observed in particle shapes are due solely to changes in interfacial tensions. To see this, let us consider in more detail the criteria of stability of a state of equilibrium which was discussed in section (3) of Chapter II.

The sufficient stability condition of an equilibrium state of a system involving interfaces with respect to motion of the interfaces at constant total entropy and mass of the individual components is

$$\min \left[-\sum_i \int P_i \, dv_i + \sum_i \int \gamma_i \, dA_i \right] \qquad (7\text{-}28)$$

(See section (3), Chapter II)

That is, the sum of the products of the interfacial tensions and their areas, less the sum of the products of the pressures of the phases and their volumes must be a minimum.[29,43] For fluid phases, the pressure throughout the phase will be constant, hence

$$\int P_i \, dv_i \longrightarrow P_i V_i .$$

For solids the term p_i must stand for a strain energy density which may vary from point to point in the solid. The total amount of this energy in a solid phase is represented by $\int p_i dv_i$.

Let us consider the system of a solid containing an included liquid phase, both phases being subjected to some hydrostatic pressure (see Figure 21(a)). The system is enclosed in a rigid envelope E, and has equal temperatures and chemical potentials in all parts of the system. The volumes of both phases are held constant. Thus the preliminary conditions are satisfied for the application of (7-28) above.

Now any perturbation of the shape of the included liquid phase will change the amount of liquid/solid interfacial area, but will not produce any significant change in the pressures of the phases. (Herring[43] points out that the change in particle shape must change the distribution of stresses set up in the solid to compensate for the surface stress of the interface. He concludes that such changes will be negligible.) Since neither the pressures nor the volumes of the bulk phases are affected by movement of the interface, the stability condition (7-28) reduces to

$$\min \left[\int \gamma dA \right] \tag{7-29}$$

where γ is the liquid/solid interfacial tension. If the solid is crystalline, γ will in general vary over the interface, so the condition (7-29) would require a shape which would depend on the manner and magnitude of the variations in γ. If γ is assumed constant over the interface, then condition (7-29) requires that the liquid phase assume a shape which has the minimum surface area for the volume contained. Thus, liquid phase has the form of a sphere in its state of stable equilibrium.
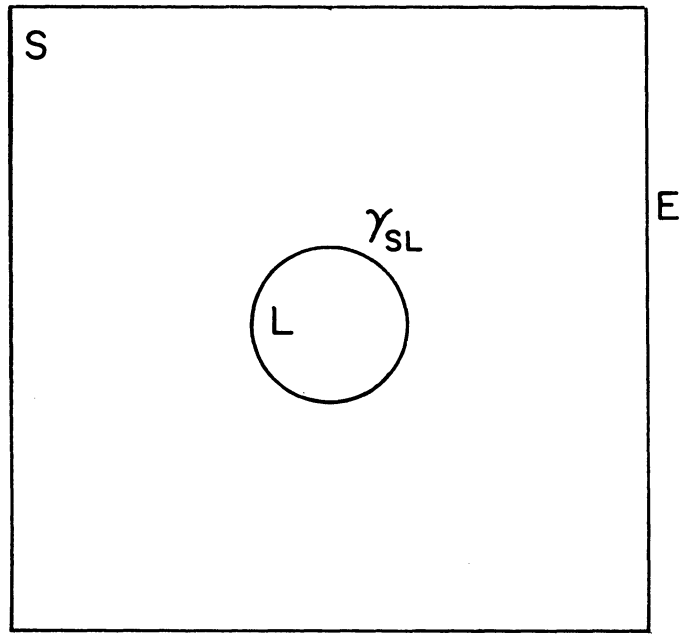
(a)
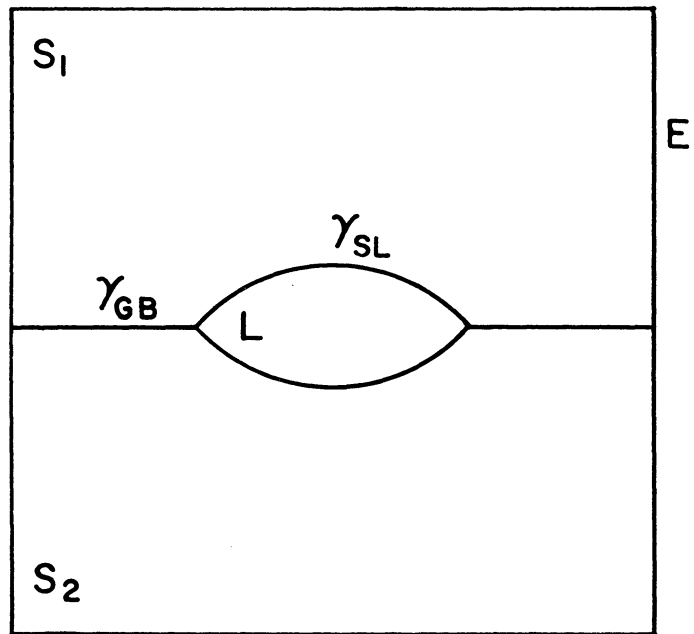
(b)

Figure 21. Sketches of Thermodynamic Systems

Now consider the more complex system of Figure 21(b), with two identical solid phases separated by a grain boundary and an included liquid phase lying in the grain boundary. The system is under a uniform hydrostatic pressure, and has equal temperature and chemical potentials in all phases.

Let us now consider the changes which occur in the system when the interfaces are allowed to move and the volumes of all the phases are held constant. As before, the pressures in each phase are virtually unaffected, so that the terms $\int p\,dv$ for each bulk phase are unchanged. Hence, as before, the stability condition (7-28) reduces to a simpler condition:

$$\min\left[\sum_i \int \gamma_i \, dA_i\right] . \tag{7-30}$$

Now the stability condition (7-30) may be applied to the line of intersection of the grain boundary and the solid/liquid interfaces, and produces a condition on the shape of the liquid phase which must be satisfied in a condition of stable equilibrium. If γ_{sl} and γ_{gb} are assumed constant everywhere on their interfaces and are not influenced by the crystallography of the solid phases, then the condition is simply[43]:

$$\gamma_{gb} = 2\gamma_{sl} \cos \theta/2 \tag{7-31}$$

where θ is the dihedral angle. The point to be emphasized here is that Equation (7-31) is only valid when the stability criterion (7-28) reduces to Equation (7-30).

Now let us consider the system of Figure 21(a) when the phases are not under uniform hydrostatic pressure. Let us suppose that a uniaxial tensile stress is applied to the solid so that in the region of the solid

surrounding the liquid particle stresses are set up which are not the same from point to point. In particular, the state of stress on elements of the solid adjacent to the liquid phase will vary along the solid/liquid interface, and, most important of all, the particular distribution of stresses in the solid will depend on the shape of the liquid particle. The liquid will be under some uniform hydrostatic pressure.

The temperature is constant throughout both phases. Let us assume that the chemical potentials of all components everywhere in the system have equilibrium values.

The chemical potential of a component in the solid is influenced by the state of stress and this varies within the solid. The only process which would produce a homogeneous state of stress, thus eliminating the gradients of chemical potential within the solid, is removal of the included liquid phase. Since this is not possible, the equilibrium conditions under the proposed constraints necessitate unequal chemical potentials in various parts of the solid. This situation may be compared to a column of liquid in a gravitational field. Gibbs[29, p. 146] shows that the chemical potentials of the components of the liquid vary from level to level in the liquid, when the whole system is in equilibrium.

It is true, however, that the chemical potentials of all components must be the same everywhere in the liquid phase, and that one must have these same values in the solid immediately adjacent to the liquid.

Now let the shape of the liquid phase be subjected to a perturbation. The area of the interface will change as before, thus the term $\int \gamma dA$ in Equation (7-28) will change. But as was pointed

out earlier, when the shape of the liquid phase is varied, the distribution
of stresses in the solid near the liquid must also vary in order to
preserve mechanical equilibrium. In general, the total energy of the
solid is a function of the shape of the liquid phase, so the term $\int pdv$
for the solid phase occurring in Equation (7-28) is not the same for all
positions of the interface. Since the pressure on the liquid must be
the same as the stress normal to the solid at the solid/liquid boundary,
it is conceivable that the pressure on the liquid may also vary slightly
with the position of the solid/liquid boundary. To summarize, the terms
$\int pdv$ in Equation (7-28) which have been shown to be independent of
the shape of the liquid particle under conditions of hydrostatic stress,
are not independent of the liquid particle shape under a system of
generalized stresses. Thus, the stability criterion (7-28) does not
reduce to the criterion (7-29).

It is apparent that a consideration of the more complex system
of Figure 21(b) results in the same conclusion, i.e., that the stable
shape of the liquid phase depends not on minimization of the total inter-
facial energy of the system, but on minimization of the sum of bulk and
interfacial energies. Since this is the case, Equation (7-31) is not a
condition on the shape of the liquid phase. Thus, the "dihedral angle"
under these conditions is not determined solely by the ratio of grain
boundary and solid/liquid tensions.

This result forces one to conclude that the dihedral angle
changes observed in tension and compression experiments are not
necessarily due only to changes in interfacial tensions. The sort of
changes which are observed are consistent with the analysis above.

For example, the stress concentration about a lead inclusion must depend on the orientation of the inclusion relative to the axis of tension (or compression). Hence, the observed dependence of the dihedral angle on this orientation is not surprising. Secondly, the fact that the magnitudes of the observed dihedral angle changes are so much larger for a given stress in these experiments than in hydrostatic compression, suggests that some other factors may be important.

To summarize, the foregoing discussion shows that the restricted condition for stability (7-30) is probably not applicable to solid-liquid systems in non-hydrostatic states of stress. Thus, because the energy contribution of the bulk phases depends on the particle shape, dihedral angles are not determined only by the relative magnitudes of solid/ liquid and solid/solid interfacial tensions. Without knowing the amount of extra strain energy arising from stress concentrations about a particle and how this energy varies with particle shape, it is not possible to isolate any possible effect of applied stress on interfacial tensions.

5. Summary

It is possible to relate the change in dihedral angles with pressure or temperature to changes in the interfacial tension at the solid/ solid and solid/liquid interfaces. The assumption required is that the surface tensions at each interface change linearly with temperature or pressure. The fact that the data can be correlated on this basis lends credibility to this assumption.

The properties of the solid/liquid interface can be obtained from the pressure and temperature coefficients of solid/liquid interfacial

tension. The surface excess concentration of nickel is determined using the assumption that the solid phase is pure nickel. The excess entropy of the interface is computed by either (a) assuming the solid is pure nickel, or (b) estimating the thermodynamic properties of the nickel/ lead liquid. Both methods yield approximately the same results. From the excess entropy and concentration, one can estimate a minimum thickness for the solid/liquid interface. This calculation suggests a rather diffuse interface.

The thermodynamic relations for the solid/solid boundary cannot be reduced to the formal simplicity that is obtained for the solid/liquid boundary. This arises because a dividing surface cannot be chosen in such a way as to make one of the surface excess concentrations vanish. Nevertheless, from the derived equations and the temperature and pressure coefficients of grain boundary tension, it is shown that the excess concentration of nickel at the interface is negative, the excess con- centration of lead is positive, and the excess entropy is negative.

Thermodynamic arguments lead to the conclusion that the dihedral angle in leaded nickel under general conditions of applied stress (not hydrostatic) cannot be interpreted as a ratio of interfacial tensions. This happens because the strain energy of the bulk phases depends on the position of the interfaces. Since energy contributions from the bulk phases as well as the total interfacial energy change when inter- faces move, the dihedral angle changes observed in tension and compression testing represent the combined tendency of the system to minimize its total interfacial energy and the strain energy of its phases. These conclusions, however, provide no simple basis for explaining the effects observed.

CHAPTER VIII

GENERAL SUMMARY

The dihedral angle of lead in nickel has been measured as a function of temperature and hydrostatic pressure. The dihedral angle changes from 52° at 371°C to 32° at 816°C. When pressure is applied at 371°C, the dihedral angle changes from 52° at zero pressure to 39° at a pressure of 50,000 psi. When pressure is applied at 593°C, the dihedral angle changes from 41° at zero pressure to 32° at a pressure of 52,600 psi.

Using the assumption that the interfacial tensions which determine the dihedral angle change linearly with temperature and pressure, one may obtain values for the temperature and pressure coefficients of interfacial tension from the observed dihedral angle changes. The results of these calculations, expressed in terms of the nickel grain boundary tension at 593°C (γ (593°)) are:

$$d\gamma_{sl}/dP \;=\; 1.60 \; (\pm 0.65) \cdot 10^{-10} \; \gamma(593°) \; cm \qquad \text{at } 371°C$$

$$d\gamma_{sl}/dP \;=\; 0.81 \; (\pm 0.63) \cdot 10^{-10} \; \gamma(593°) \; cm \qquad \text{at } 593°C$$

$$d\gamma_{sl}/dT \;=\; 4.07 \; (\pm 2.20) \cdot 10^{-4} \; \gamma(593°) \; \frac{dynes/cm}{°C} \quad \text{at 0 pressure}$$

$$d\gamma_{gb}/dP \;=\; 3.12 \; (\pm 1.22) \cdot 10^{-10} \gamma(593°) \; cm \qquad \text{at } 371°C$$

$$d\gamma_{gb}/dP \;=\; 1.63 \; (\pm 1.32) \cdot 10^{-10} \; \gamma(593°) \; cm \qquad \text{at } 593°C$$

$$d\gamma_{gb}/dT \;=\; 9.04 \; (\pm 4.05) \cdot 10^{-4} \; \gamma(593°) \; \frac{dynes/cm}{°C} \quad \text{at 0 pressure.}$$

From the above coefficients and the thermodynamic relations which express the dependence of these coefficients on the properties of the interface and the properties of the bulk phases, one can calculate

the excess concentration of nickel at the solid/liquid interface and
estimate the excess entropy of the interface. The properties of the
grain boundary cannot be directly calculated by the same method.
The data imply a deficiency of nickel and segregation of lead at
the grain boundary.

A decrease in the dihedral angle was observed in leaded nickel
subjected to uniaxial tension and compression. An explanation for these
changes is not proposed for two reasons: (1) the stress distribution
about the liquid lead particles is not known, hence there is no way to
determine the stresses at the particle in terms of the applied stresses,
and (2) it is unlikely that the thermodynamic conditions which permit
the dihedral angle to be expressed as a ratio of interfacial tensions
are satisfied. It has been established, however, that the changes
seen are not due to cracks beginning at liquid lead inclusions.

APPENDIX A

DERIVATION OF THEORETICAL DISTRIBUTION FUNCTION FOR OBSERVED ANGLES

The following derivation is due to Harker and Parker.[39]

If planes of all orientations are passed through the line of intersection of two surfaces in space meeting in an angle θ, the distribution of apparent angles ψ observed on the planes made by the traces of the intersecting surfaces, is dependent only upon θ.

In order to obtain the required distribution function, it is first necessary to relate ψ and θ geometrically, in terms of parameters expressing the inclination of the intersecting plane relative to the intersecting surfaces.

Let surfaces A and B intersect in space. At a point q on their line of intersection, let the angle between the normals to each surface be $\pi - \theta$, where θ is the dihedral angle. Then define the following vectors, shown in Figure 22:

A: Unit normal to surface A at q. A in the xy plane.

B: Unit normal to surface B at q. B in the xy plane.

N: Unit normal to intersecting plane P at q.

m: Unit tangent vector to the line of intersection of A and P, perpendicular to N and A.

n: Unit tangent vector to the line of intersection of B and P, perpendicular to N and B.

ψ: Angle between m and n (the "observed angle").

Then in terms of the dihedral angle θ and the spherical coordinates α, β we have:
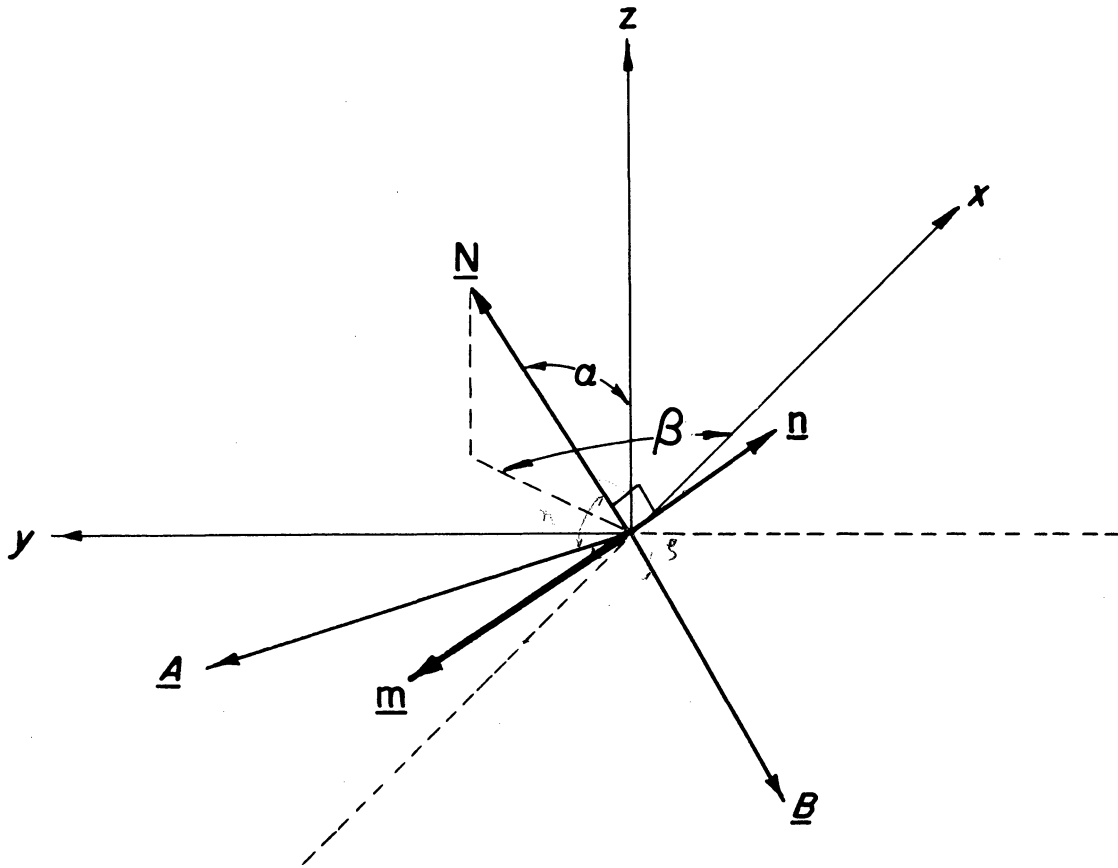
Figure 22. Vectors Used in Deriving Relation
Between the Observed Angle, the Dihedral
Angle and Orientation Parameters.

$$\underline{A} = \begin{bmatrix} -\sin \theta/2 \\ \cos \theta/2 \\ 0 \end{bmatrix} ; \quad \underline{B} = \begin{bmatrix} -\sin \theta/2 \\ -\cos \theta/2 \\ 0 \end{bmatrix} ; \quad \underline{N} = \begin{bmatrix} \sin \alpha \cos \beta \\ \sin \alpha \sin \beta \\ \cos \alpha \end{bmatrix} .$$

If η is the angle between $\underline{N}$ and $\underline{A}$ and ζ the angle between $\underline{N}$ and $\underline{B}$, the vectors $\underline{m}$ and $\underline{n}$ are given by

$$\underline{A} \times \underline{N} = \sin \eta \; \underline{m} ; \qquad \underline{N} \times \underline{B} = \sin \zeta \; \underline{n}$$

where η and ζ may be evaluated from the expressions $\underline{N} \cdot \underline{A} = \cos \eta$ and $\underline{N} \cdot \underline{B} = \cos \zeta$.

Then since $\underline{m} \cdot \underline{n} = \cos \psi$ and $\underline{n} \times \underline{m} = \underline{N} \sin \psi$, one can write the vector equation

$$\underline{N} \tan \psi = \frac{\underline{n} \times \underline{m}}{\underline{m} \cdot \underline{n}} .$$

Evaulation of the third component of this equation gives after simplification

$$\tan \psi = \frac{2 \sin \theta \cos \alpha}{\sin^2 \alpha (\cos 2\beta - \cos \theta) + 2 \cos \theta} \qquad (A-1)$$

which is the result given by Harker and Parker.

The probability of obtaining values ψ to $\psi + \Delta\psi$ may be obtained by considering all possible orientations of an element of grain edge of length $\Delta \ell$. The probability that $\Delta \ell$ will have a particular range of orientation parameters is given by the elemental area on the unit sphere, shown in Figure 23:

$$\delta A = \sin \alpha \; \delta\alpha \; \delta\beta .$$

But the probability of intersection is dependent on the projected length of $\Delta \ell$ on the normal to the intersecting plane. Taking this normal along the z axis, the projected length is $\Delta \ell \cos \alpha$. Thus, the net probability of seeing a particular orientation is
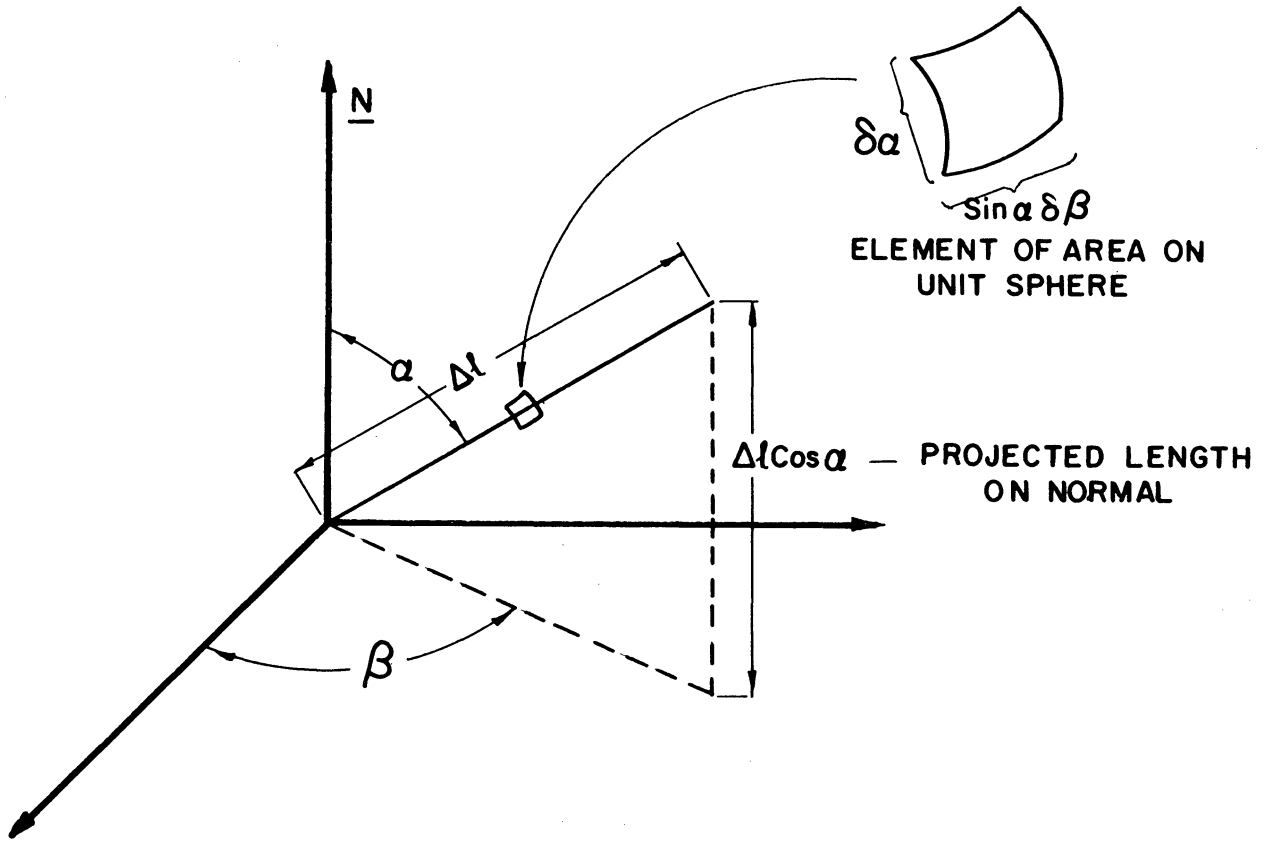
Figure 23. Sketch Showing Relationships Used to Obtain the Probability of Observing a Given Angle.
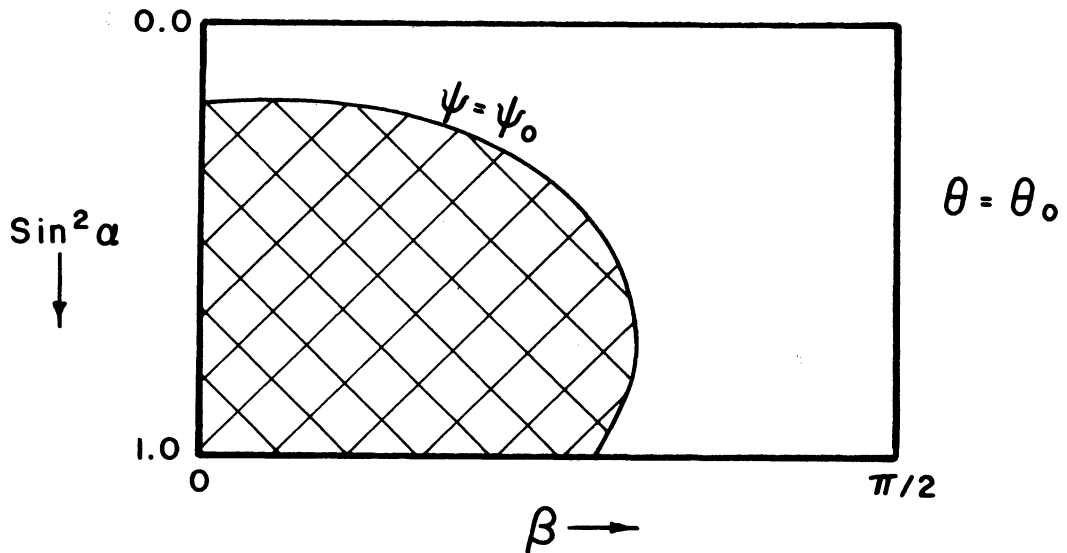

Figure 24. Probability Plot After Harker and Parker.[39] For a Given Dihedral Angle θ_0, the Ratio of the Crosshatched Area to the Total Area of the Diagram is the Fraction of Observed Angles Having a Magnitude Less Than or Equal to ψ_0. The Curved Line Bordering the Crosshatched Region is Obtained from Equation (A-1) With $\theta = \theta_0$ and $\psi = \psi_0$.

$$\Delta \ell \; \cos \alpha \; \sin \alpha \; \delta\beta \; \delta\alpha \qquad \propto \qquad \Delta \ell \; \delta \; \sin^2 \alpha \; \delta\beta \; . \quad (A\text{-}2)$$

The element of edge length, $\Delta \ell$, may be disregarded when integrating the above expression because the distribution of angles seen will not usually be influenced by the length of grain edge. (See error discussion for an amplification of this point.) From Equations (A-1) and (A-2) it follows that the relative chance of intersecting surfaces, meeting in an angle θ , producing an observed angle less than or equal to ψ , may be obtained from a plot of $\sin^2 \alpha$ vs β, as in Figure 24.

From Figure 24, the probability of observing an angle of magnitude ψ_0 or less is given by the ratio of the crosshatched area to the total area of the plot. Equation (A-1) for specified values of ψ and θ gives the curve $\psi = \psi_0$.

Analytically, the probability represented by the crosshatched area is given by the cumulative distribution function:

$$F(\psi \; ; \theta) \; = \; \frac{2}{\pi} \left[\int_K^{1.0} 1/2 \; \text{Arc} \; \cos \left(\frac{2}{Z} \left(\frac{\sin \theta \; \sqrt{1 - Z}}{\tan \psi} - \cos \theta \right) \right. \right.$$
$$\left. \left. + \; \cos \theta \right) \; dZ \; + \; C \right] \qquad (A\text{-}3)$$

where $Z = \sin^2 \alpha$, and when

$$\theta = \psi \; , \qquad K = 0, \qquad C = 0$$

$$\theta > \psi \; , \qquad K = \frac{2 \; (\cos \psi \; - \; \cos \theta \;)}{(1 \; - \; \cos \theta)(1 \; + \; \cos \psi)} \; , \qquad C = 0$$

$$\theta < \psi \; , \qquad K = \frac{2 \; (\cos \theta \; - \; \cos \psi \;)}{(1 \; + \; \cos \theta)(1 \; - \; \cos \psi)} \; , \qquad C = \frac{\pi K}{2} \; .$$

Equation (A-3) may be integrated numerically using Simpson's rule. The following properties of these curves are helpful for this integration:

(1) when $\sin^2 \alpha = 1.0$, $\beta = \dfrac{\pi - \theta}{2}$,   for all ψ

(2) when $\sin^2 \alpha = 0.0$, $\beta = 0$ for $\psi < \theta$

$\qquad\qquad\qquad\qquad\qquad = \pi/4$ for $\psi = \theta$

$\qquad\qquad\qquad\qquad\qquad = \pi/2$ for $\psi > \theta$.

Numerical integration of Equation (A-3) was carried out using an IBM 7090 computer, producing the family of cumulative distribution curves shown in Figure 25.
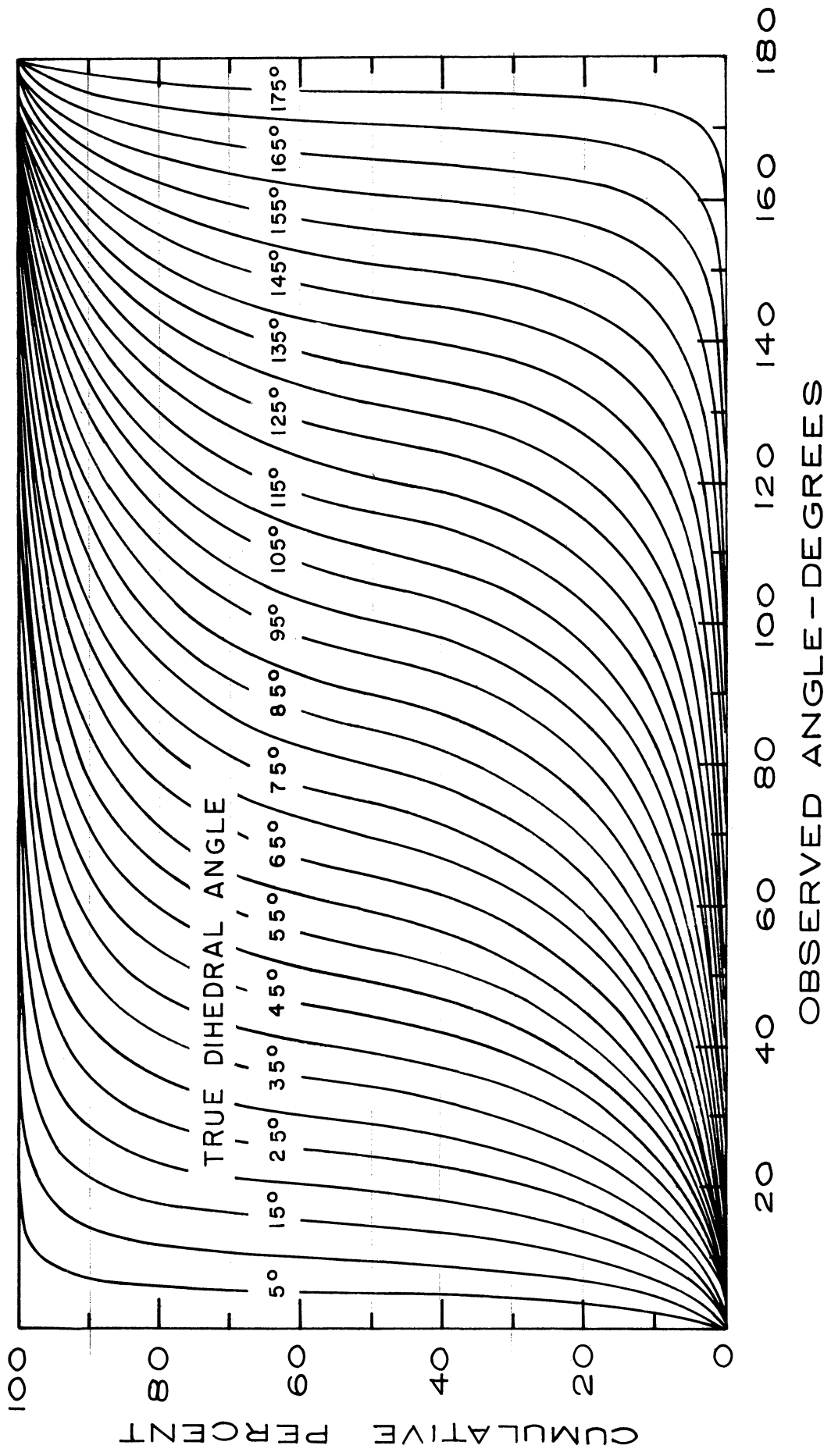
Figure 25. Theoretical Cumulative Frequency Curves for Various Dihedral Angles.

APPENDIX B

ESTIMATION OF THE NICKEL GRAIN BOUNDARY TENSION
IN THE PRESENCE OF LEAD

Hayward and Greenough[41] have determined the surface tension

of solid nickel, using the method of Udin, Shaler and Wulff.[104]

Since they determined the grain boundary groove angles in the course

of their experiments, their measurements also yield values for the

grain boundary tension of pure nickel.

Their measurements covered the range from 1250° to 1435°C

yielding a value for solid surface tension at the melting point of

1725 ergs/cm^2, a value for the change in surface tension with tempera-

ture in this range

$$\frac{d\gamma_s}{dT} = -0.6 \ \text{ergs/cm}^2\text{-°C}$$

and a grain boundary groove angle of 158°, constant over the temperature

range within the accuracy of its measurement. Their results imply that

the grain boundary tension increases with decreasing temperature.

The temperature coefficient of nickel grain boundary tension

in the presence of lead calculated in Chapter VII is positive (Equation

7-7). This is to be expected when a marked segregation of lead occurs

at the grain boundary. The nickel grain boundary tension with lead

adsorbed must be lower at all temperatures than the pure nickel grain

boundary tension measured by Hayward and Greenough.

It seems likely that the calculated positive temperature

coefficient holds up to the monotectic temperature (1340°C). From

the data of Hayward and Greenough the grain boundary tension of pure

nickel can be computed at this temperature. Using this for the value
of the grain boundary tension of leaded nickel, and using the calculated
temperature coefficient, one can find the grain boundary tension at any
other temperature (particularly at 593°C, the reference temperature used
in Chapter VII)by means of the relation:

$$\gamma_{gb}(1340°) = \gamma_{gb}(593°) + 9.04 \cdot 10^{-4} \gamma_{gb}(593°)(1340-593). \quad (B-1)$$

This procedure should produce estimates on the high side,
because the grain boundary tension of nickel with lead present will be
lower than the tension of pure nickel. It is difficult to estimate
the decrease to be expected, so this correction will not be made.
The data of Hilliard, Cohen and Averbach[46] on the Cu-Au system,
suggest a decrease on the order of 50-200 ergs/cm^2 might be anticipated.

Taking the surface tension of nickel at 1340°C to be 1794
ergs/cm^2, the groove angle to be 158°, the grain boundary tension at
1340°C is:

$$\gamma_{gb} = 2\gamma_s \cos 79° = 685 \text{ ergs/cm}^2 = \gamma_{gb}(1340°). \quad (B-2)$$

Inserting the value from (B-2) in Equation (B-1) one has:

$$\frac{\gamma_{gb}(1340°)}{\gamma_{gb}(593°)} = 1.68 .$$

So the grain boundary tension at 593°C is probably no higher than

$$\gamma_{gb}(593°) = 409 \text{ ergs/cm}^2. \quad (B-3)$$

APPENDIX C

CORRELATION OF DIHEDRAL ANGLE VS TEMPERATURE
DATA FROM THE LITERATURE

It has been proposed in Chapter VII that the change in dihedral

angle with temperature can be satisfactorily explained by assuming that

the interfacial tensions determining the dihedral angle are linear

functions of temperature. This implies that a plot of $(\cos \theta/2 -$

$\cos \theta°/2)^{-1}$ vs $(T - T°)^{-1}$ is a straight line, where $\theta°$ is the

dihedral angle at a reference temperature $T°$. For convenience a graph

of the latter functions will be referred to as an "R-plot."

Changes in the dihedral angle as a function of temperature

have been reported for only a few binary systems. Most of this data

is not sufficiently accurate (or is taken over too narrow a temperature

range) to provide a satisfactory test of the proposed correlation.

From the data that are available, the correlation seems valid

for systems where the liquid composition changes rather uniformly

(though not necessarily linearly) with temperature. When drastic

changes in liquid composition occur over a narrow temperature range,

the tensions seem to vary non-linearly with temperature.

The Cu-Pb System

Ikeuye and Smith[51] measured the change in dihedral angle with

temperature for this system. Their dihedral angles were determined

to the nearest 5°. Figure 26 is the phase diagram for the Cu-Pb system,

and Figure 27 shows how the dihedral angle changes with temperature.

From 350° to 800°C the dihedral angle is constant with temperature.

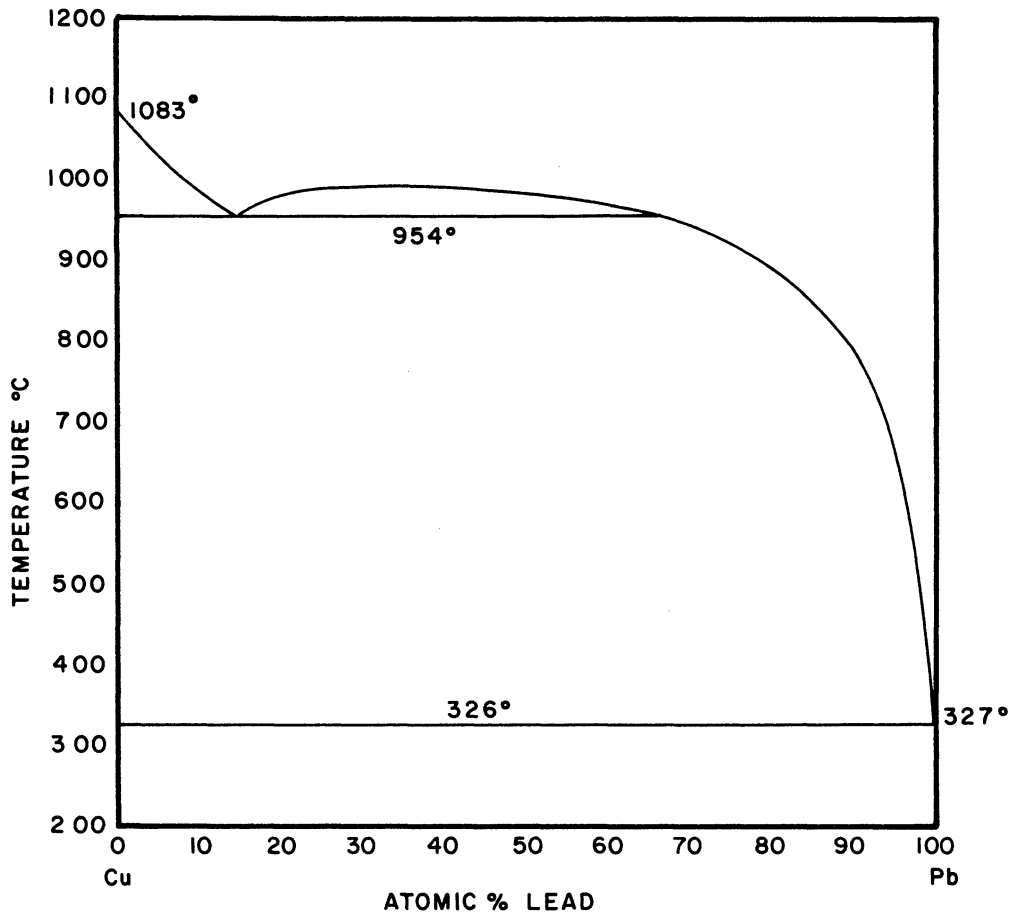This implies that either $d\gamma/dT$ is zero for each interface over this

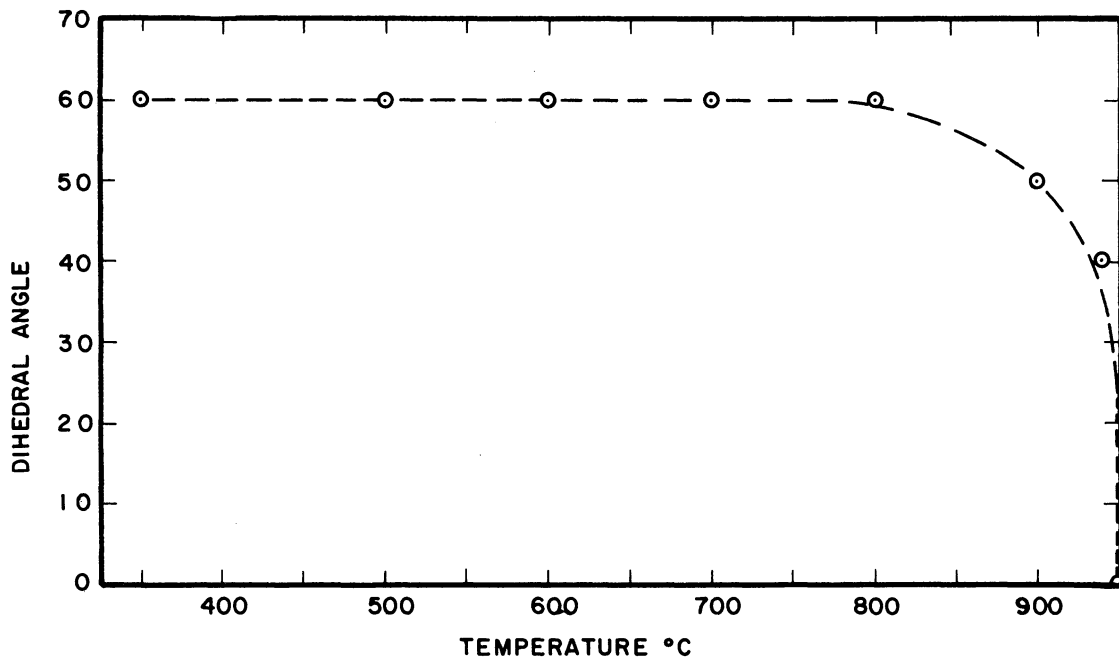Figure 26. The Copper-Lead Phase Diagram. Hansen.[37]

Figure 27. Dihedral Angle vs. Temperature. Copper-Lead System.
Ikeuye and Smith.[51]

range or that $(d\gamma_{gb}/dT) = K (d\gamma_{sl}/dT)$ where K is a constant

chosen so that the ratio γ_{gb}/γ_{sl} does not vary. Above 800°C, the

composition of the liquid is changing rapidly with temperature,

and the above relationship does not hold. These data indicate that

the surface tensions do not vary linearly with temperature from

350 - 950°C, although the linear dependence may be true from 350 -

800°C.

The Al-Sn System

Figures 28, 29, and 30 show the results for this system,

also from the data of Ikeuye and Smith.[51] The liquid here changes

composition rapidly between 550° and 660°C. The R-plot (Figure 30)

shows that the data points at 600° and 620°C do not fall on the

straight line which satisfactorily correlates the rest of the data.

The Zn-Sn System

The phase diagram for this system is given in Figure 31

and Miller and Williams' data[70] is shown in Figure 32. The R-plot

(Figure 33) shows that all this data fits a straight line. There

is a close similarity between the phase diagram for this system and

the Al-Sn system. Note that the dihedral angle in the Zn-Sn system

falls to zero at about 335°C, with a composition of 50 atomic % tin

in the liquid. The most rapid change in liquid solubility occurs

above this temperature. This is in contrast to the Al-Sn system

where the dihedral angle data cover the region of rapid composition

changes. This probably is the reason why all the data in the Zn-Sn

system are linear on an R-plot, while the data from the Al-Sn system
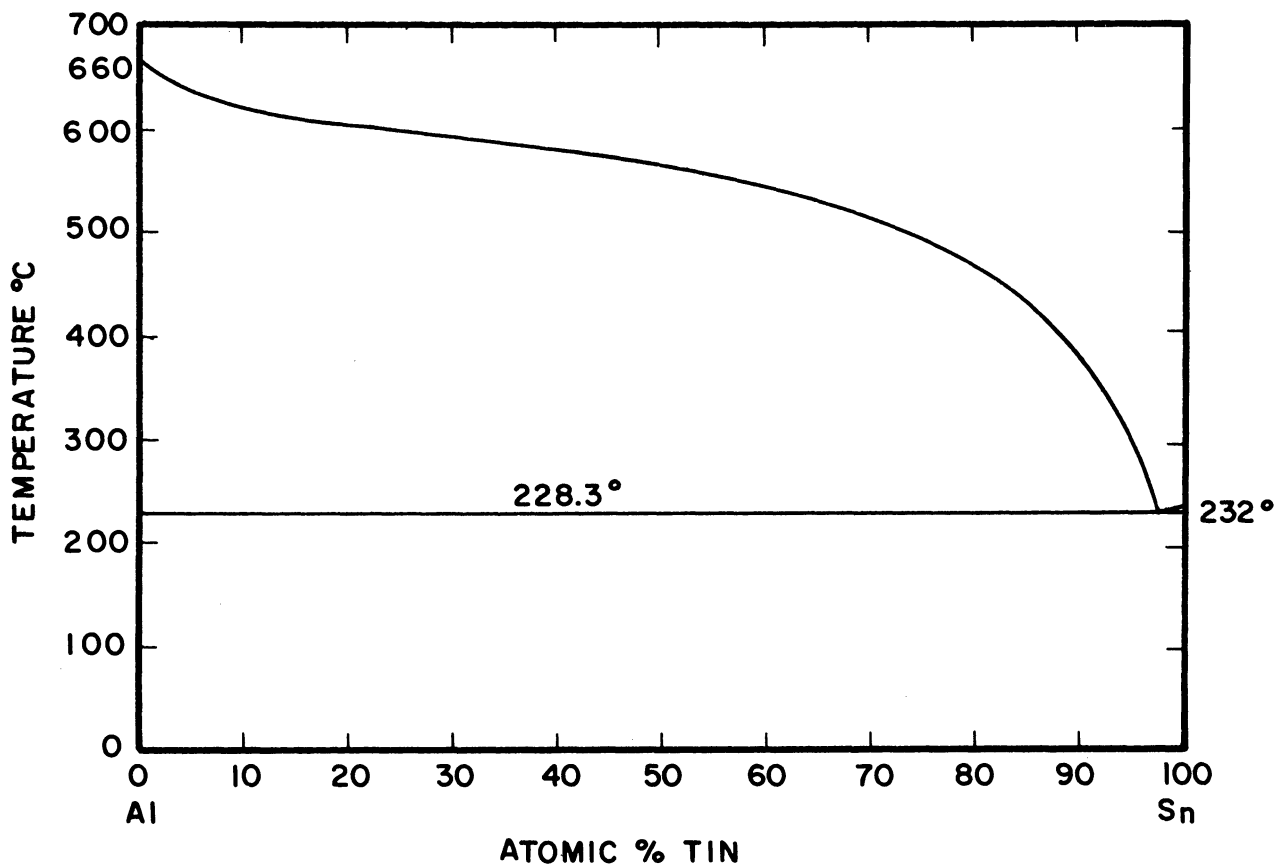
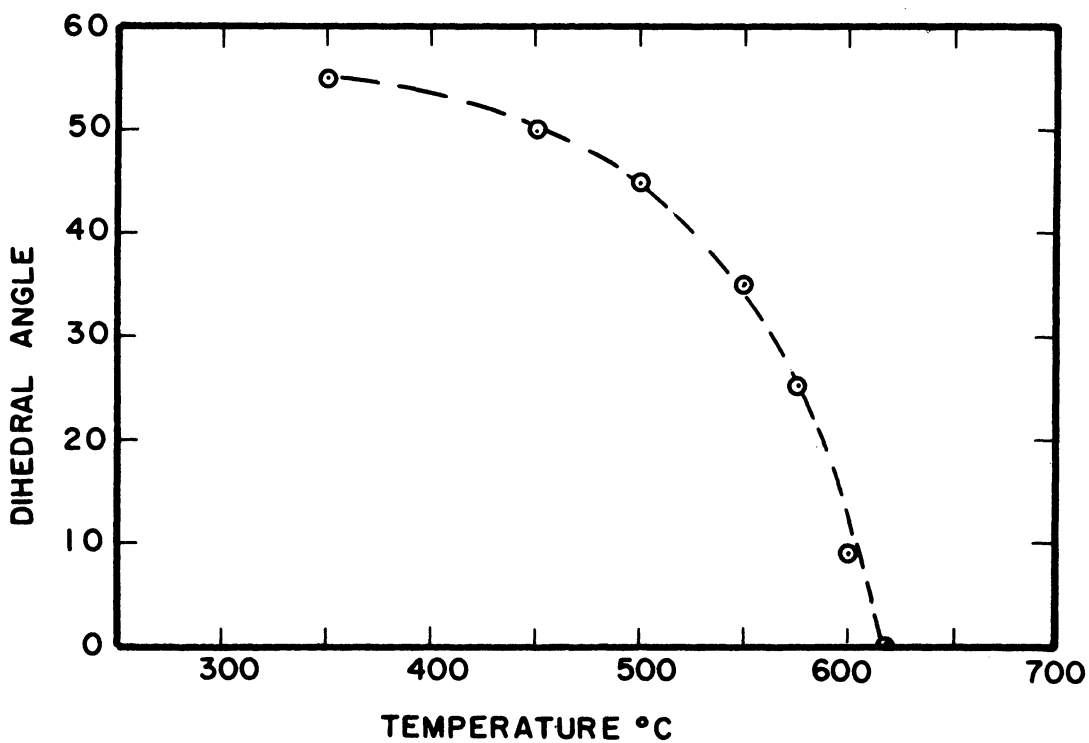are not.

Figure 28. Aluminum-Tin Phase Diagram. Hansen.[37]

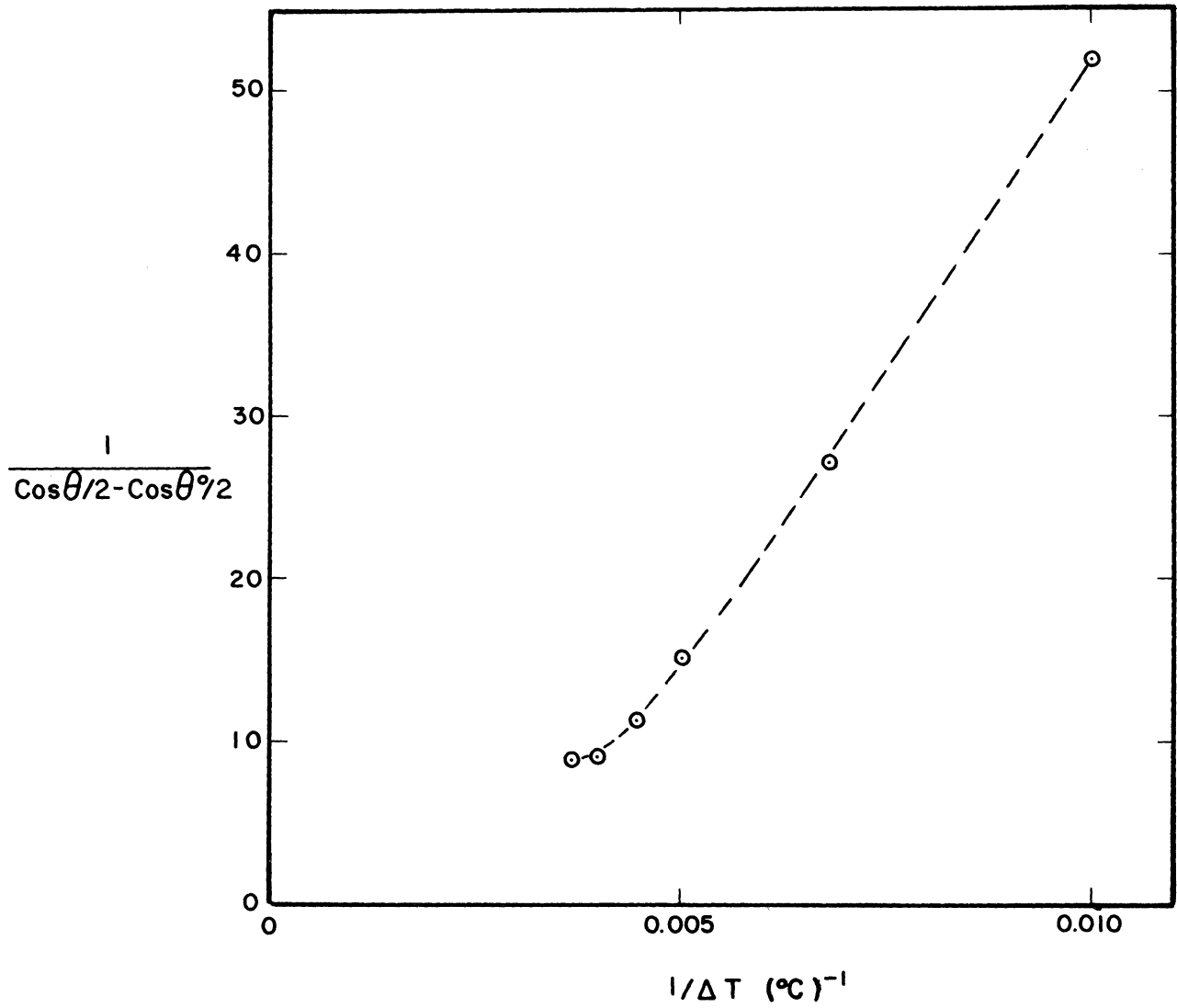Figure 29. Dihedral Angle vs. Temperature. Aluminum-Tin System. Ikeuye and Smith.[51]

Figure 30. R-plot for Aluminum-Tin System.
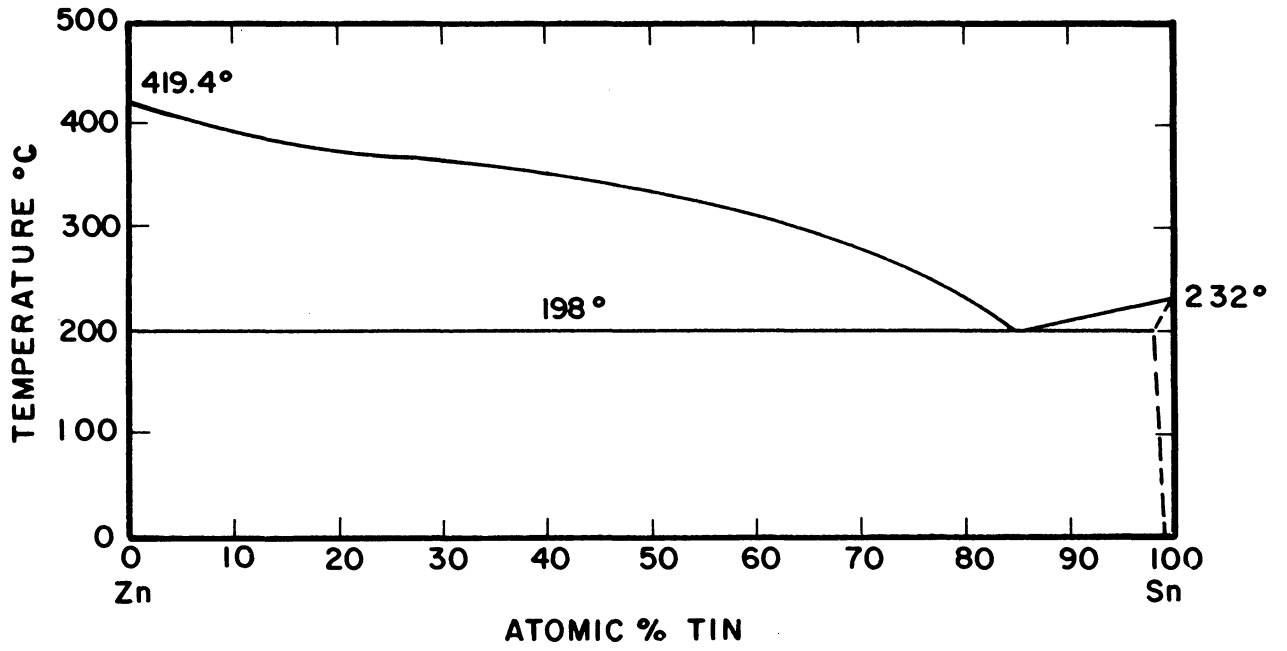Reference Point: 55° Dihedral Angle at 350°C.
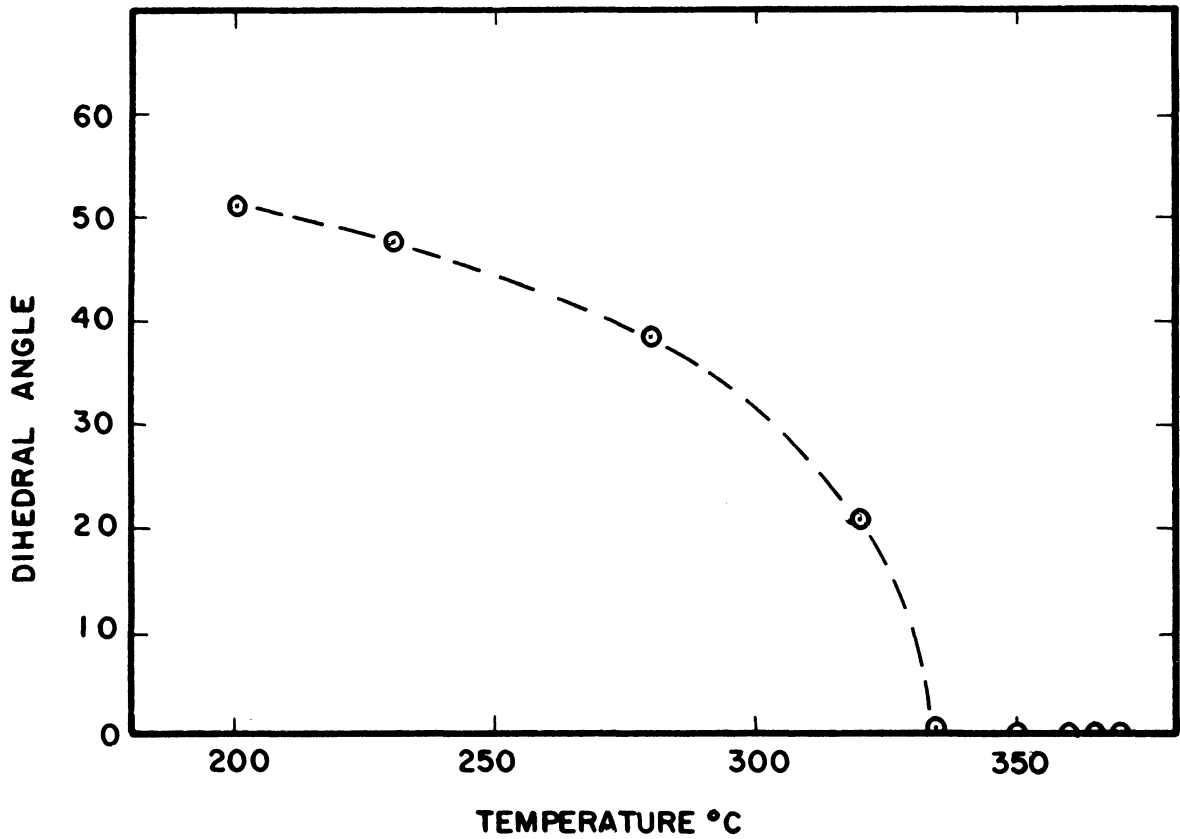
Figure 31.   Zinc-Tin Phase Diagram.   Hansen.[37]

Figure 32.   Dihedral Angle vs. Temperature.   Zinc-Tin System.
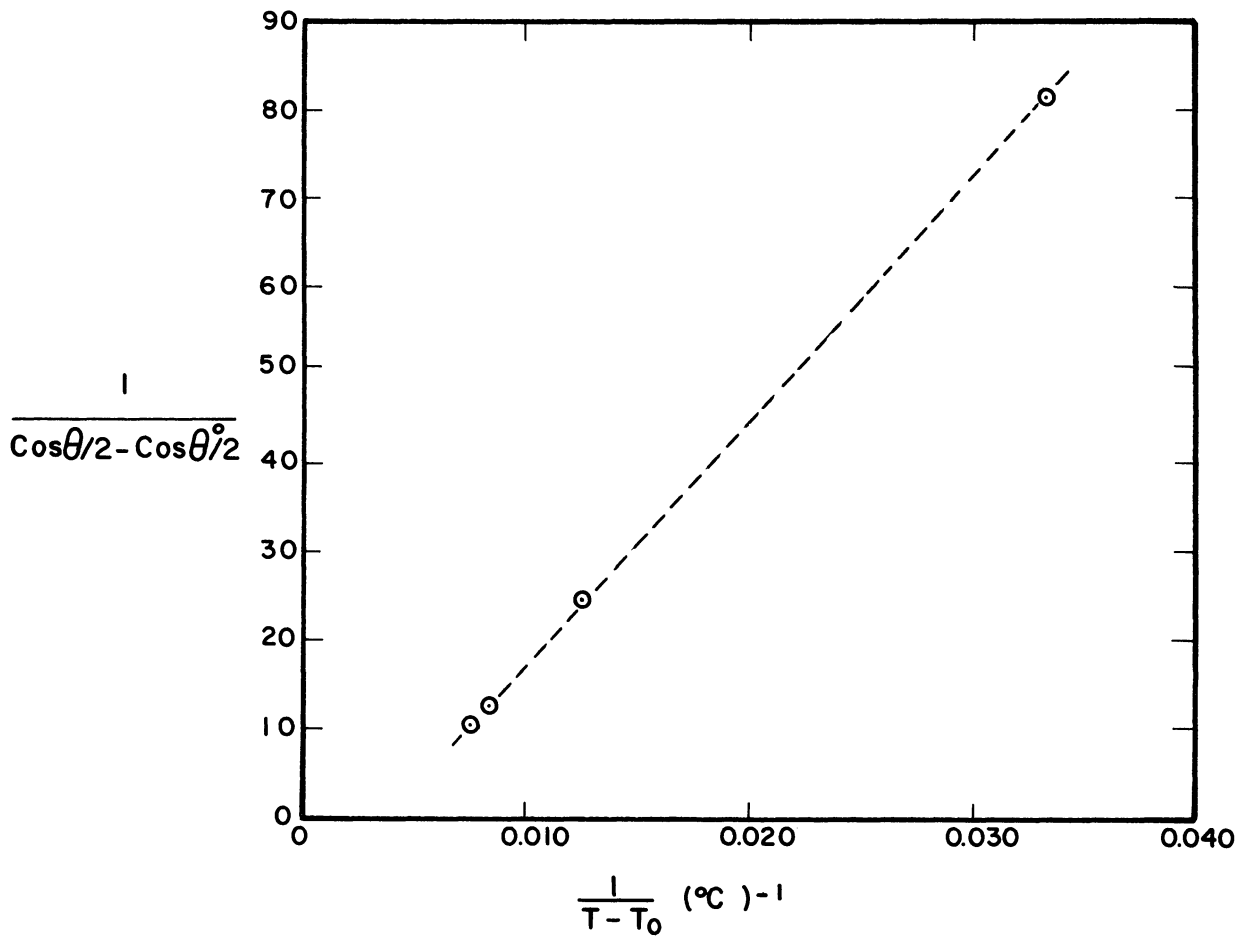Miller and Williams.[70]

Figure 33. R-Plot for Zinc-Tin System. Reference Point: 50.9° Dihedral Angle at 200°C.

The Sn-Te System

The phase diagram for this system is shown in Figure 34. Riegger[85] has measured the dihedral angle made by the Sn-rich liquid and the Te-rich liquid with the Sn-Te intermetallic compound. The scatter in these data (Figure 35) is too large for a good test of this correlation. However, from Figure 36 it appears that the data from the Te-rich liquid obey the proposed relation, and the data from the Sn-rich liquid do not. The phase diagram shows that the Sn-rich liquid undergoes a large change in composition between 650° and 790°C, while the Te-rich liquid changes composition uniformly from 405° to 790°C.

Both curves in the R-plot are drawn using a reference of 0° dihedral angle at 790°C. This fictitious datum is used because of the four data points for the Te-rich liquid, one appears to be bad. Use of one of the good data points as reference would leave only two good points for the R-plot.

The Al-Sb System

Riegger[85] has measured the dihedral angle of the Al-rich liquid and the Sb-rich liquid in equilibrium with the Al-Sb intermetallic compound (Figures 37 and 38). In this system too, the data from the solution which changes composition rather regularly with temperature (Sb-rich liquid) give a straight line on the R-plot (Figure 39). The Al-rich liquid, which changes composition less regularly, definitely does not obey the proposed linear relationship.
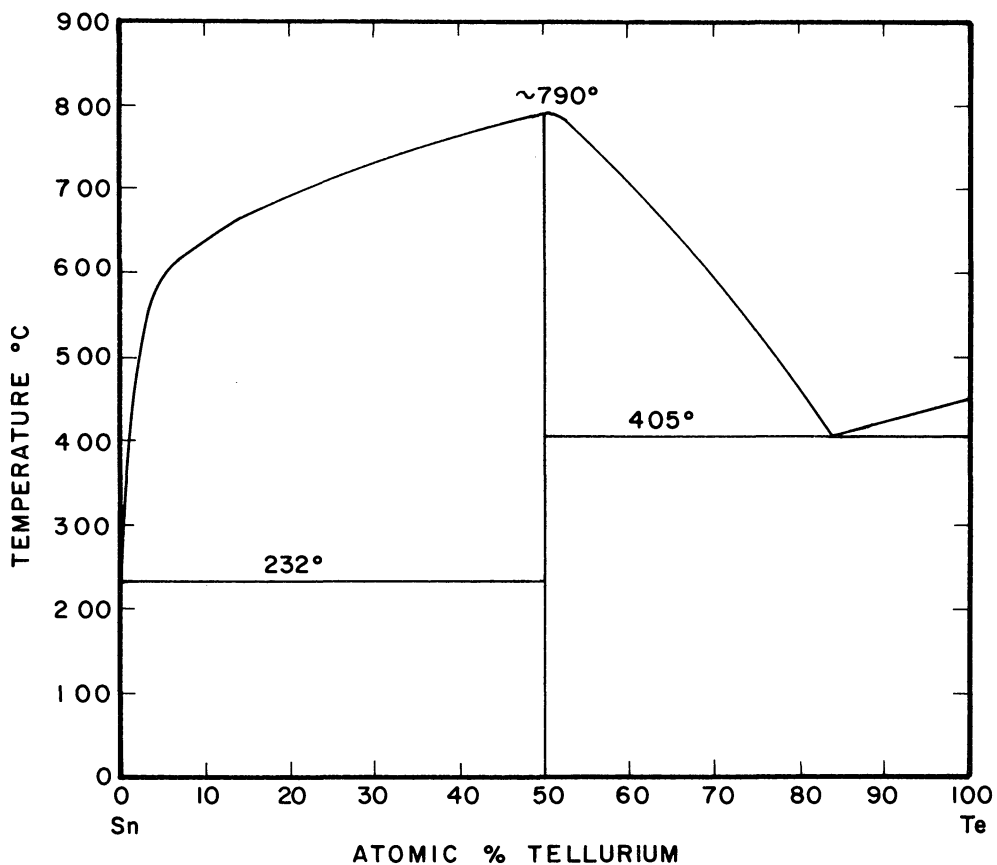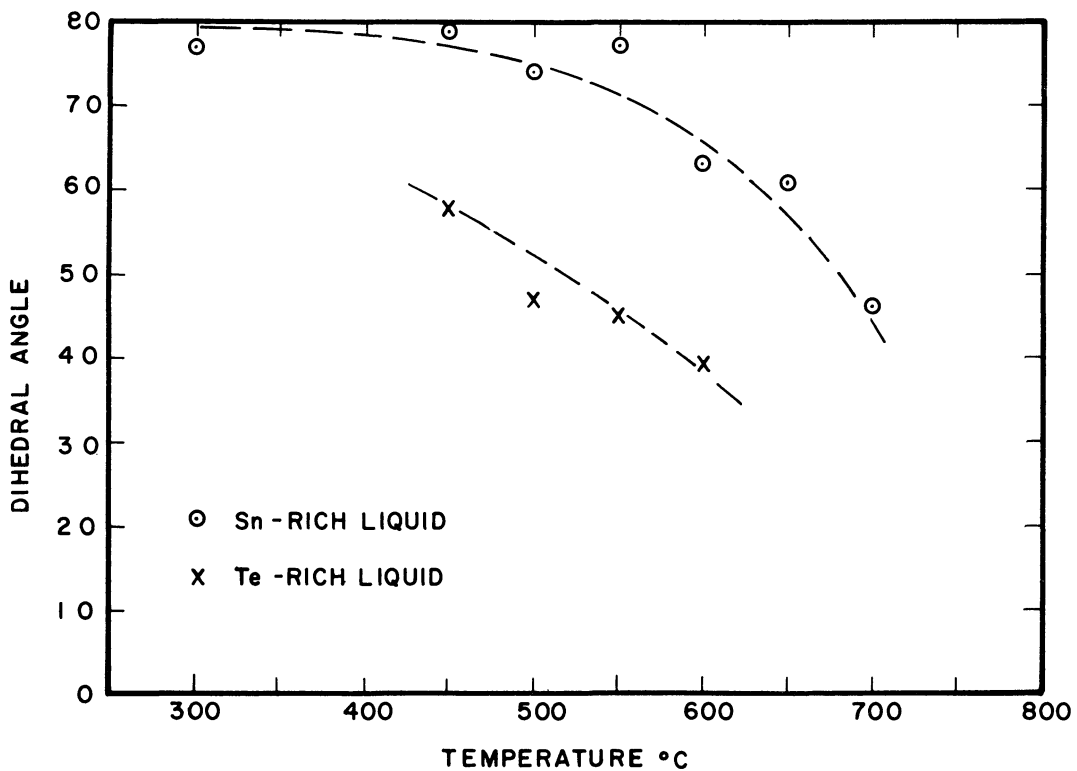
Figure 34. Tin-Tellurium Phase Diagram. Hansen.[37]

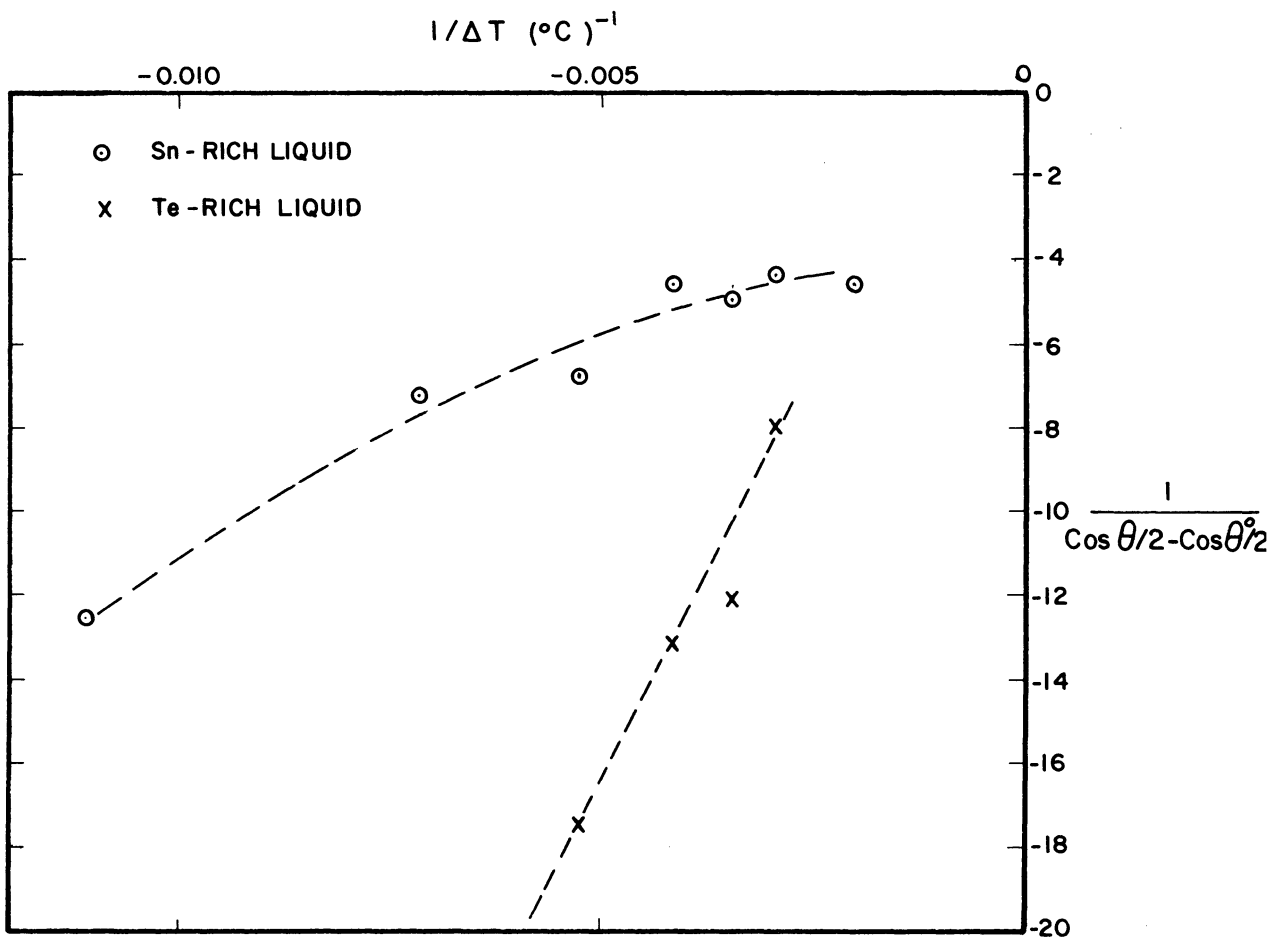Figure 35. Dihedral Angle vs. Temperature. Tin-Tellurium System.
Riegger.[85]

Figure 36. R-Plot for Tin-Tellurium System. Reference Point for Both Liquids:
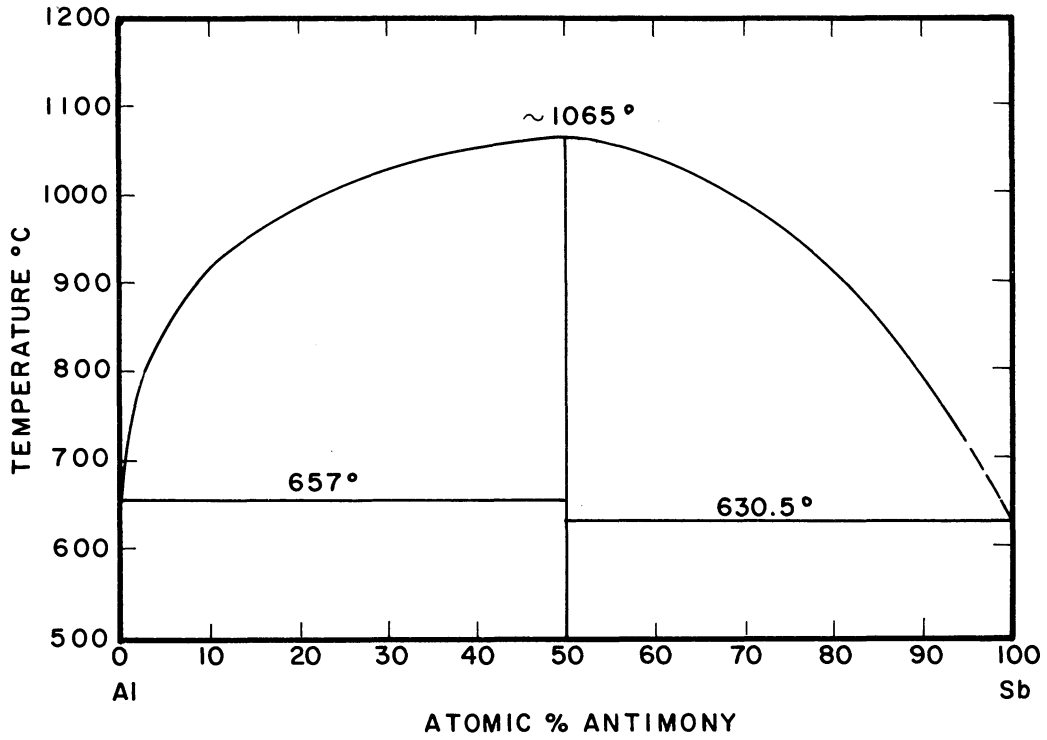0° Dihedral Angle at 790°C.

Figure 37. Aluminum-Antimony Phase Diagram. Hansen.[37]
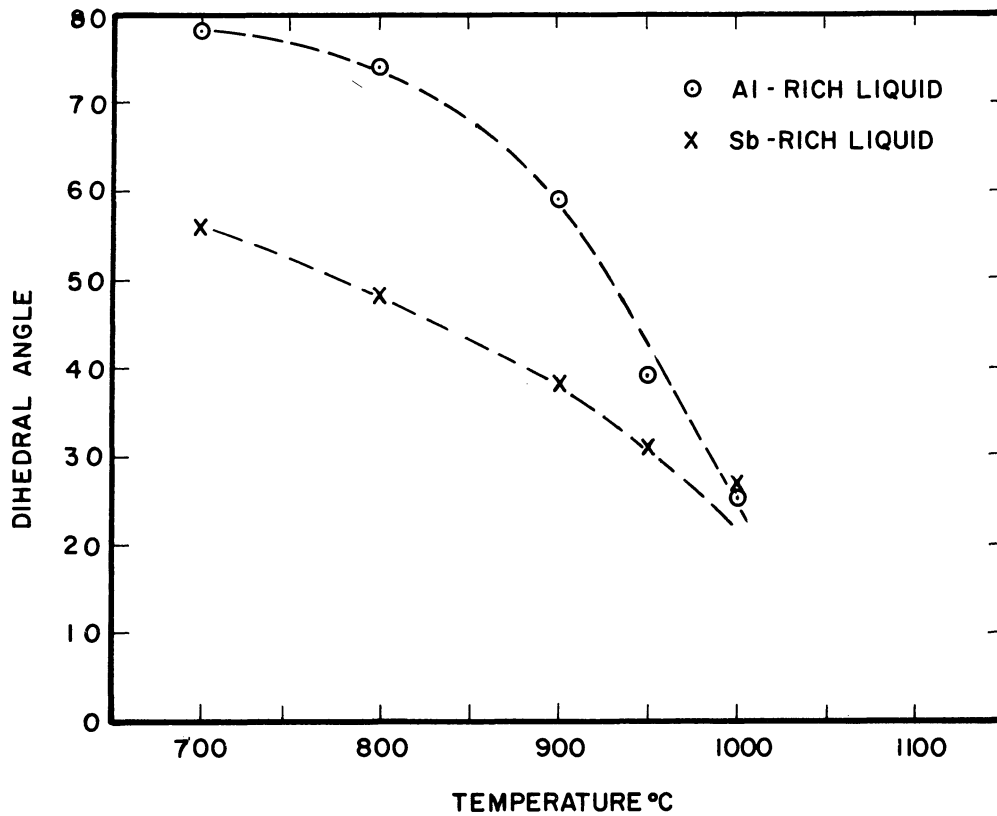
Figure 38. Dihedral Angle vs. Temperature. Aluminum-Antimony System. Riegger.[85]

$$\frac{1}{Cos\theta/2 - Cos\theta^{\circ}/2}$$

⊙   AL - RICH LIQUID

X   Sb - RICH LIQUID

1/ΔT (°C)⁻¹

Figure 39. R-Plot for Aluminum-Antimony System. Reference for Al-rich liquid: 78° Dihedral Angle at 700°C. Reference for Sb-rich liquid: 56° Dihedral Angle at 700°C. Starred Points Represent a 0° Dihedral Angle at 1065°C, the Critical Temperature for the Intermetallic Compound.

Comment

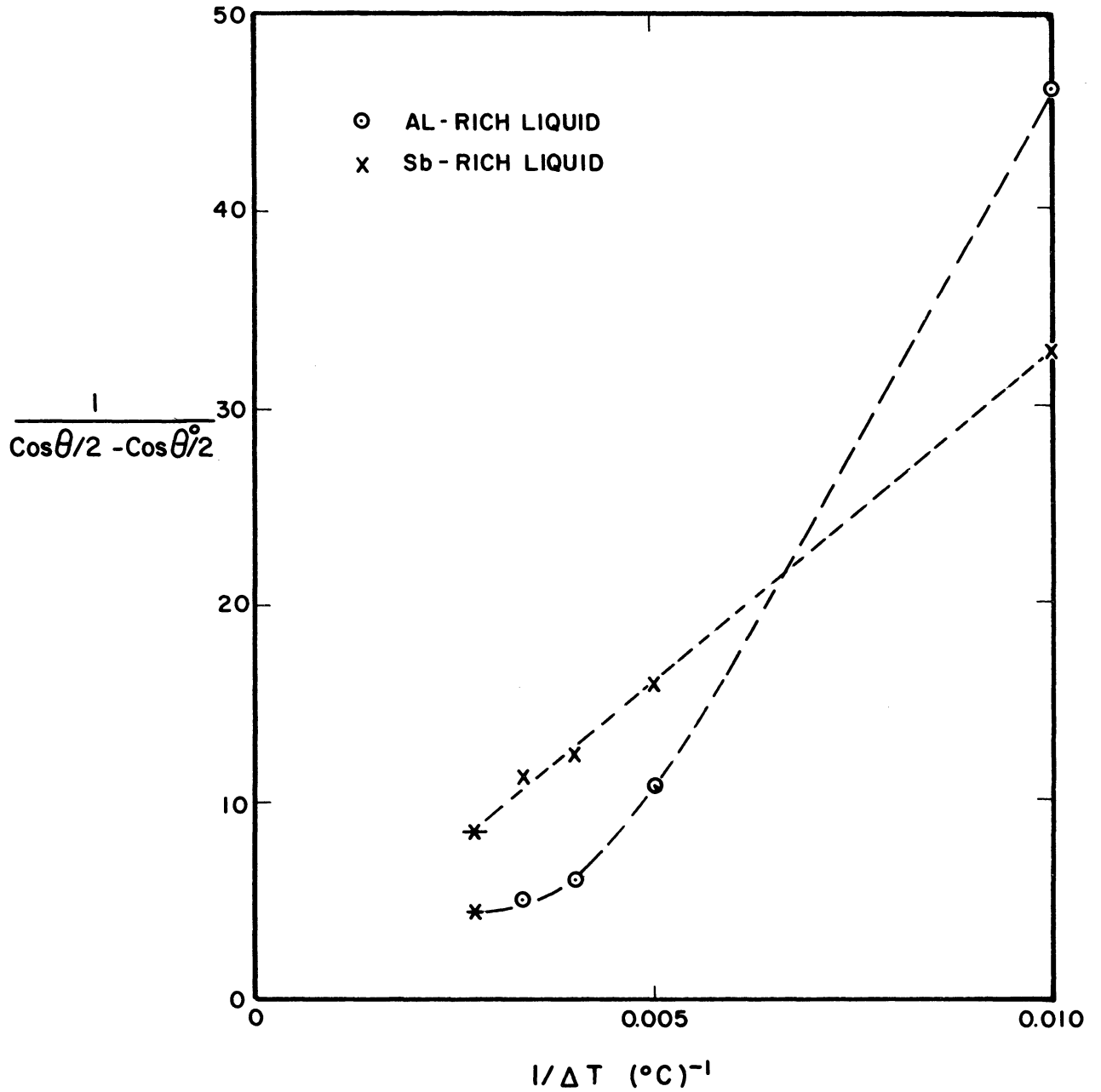All of these systems involve the equilibrium of an essentially pure solid with a liquid of varying composition. For this sort of system, equating the differentials of chemical potential for the solid component in both phases gives the relation:

$$\bar{S}_1^\ell - \underline{S}_1^s = \frac{\partial \mu_1}{\partial x} \frac{dx}{dT} \qquad (C-1)$$

where $\underline{S}_1^s$ is the molar entropy of the solid, $\bar{S}_1^\ell$ is the partial molal entropy of the solid component in the liquid, and x is the mole fraction of the solid component in the liquid. For a solution in which the activity coefficient is independent of composition

$$\frac{\partial \mu_1}{\partial x} = \frac{RT}{x} \qquad (C-2)$$

and Equation (C-1) becomes:

$$\bar{S}_1^\ell - \underline{S}_1^s = R \frac{d \ln x}{d \ln T} . \qquad (C-3)$$

Plots of $\ln x$ vs $\ln T$ are linear for most systems which show a regular change in liquid solubility with increasing temperature. The molar entropy of the solid, $\underline{S}_1^s$ changes quite uniformly up to the melting point of the solid. A radical change in liquid composition (which changes $\frac{d \ln x}{d \ln T}$) must then be due to a change in the partial molal entropy of the solid component in the solution.

A sudden increase in the solubility of the liquid with increasing temperature indicates a disproportionate increase in $\bar{S}_1^\ell$. This may be due to a "randomization" of a solution which was in some sense "ordered." For example, Strauss, et al.[97,98,99] suggested that dilute solutions of Cu and Ni in lead form an "interstitial-like" solution.

The sudden increase in liquid solubility below the monotectic temperature in these systems may indicate reversion to a "substitional-type" solution.

A change in liquid solubility will, to some extent, affect the excess concentrations and entropy at the solid/liquid interface, simply because these interfacial quantities are defined with respect to the properties of the bulk phases. But a very marked increase in solubility, may reflect some intrinsic change in the atoms making up the solution; such a change would also be expected to affect interfacial compositions.

In many cases, restricted liquid solubility is blamed on a large size difference between solute and solvent atoms. A large size difference probably promotes segregation at interfaces.[13,111] If a sudden increase in solubility with temperature is observed in such a system, it may be due to a decrease in the size difference between the atoms present. This will also cause a decrease in the segregation expected at the interfaces, and may explain why abnormal changes in the dihedral angle are associated with abnormal solubility changes.

In most of the systems for which dihedral angle data are presented, the size difference between solute and solvent atoms is more than 15% (based on Goldschmidt atomic diameters[19]). Only in the Sn-Te system are the atomic radii of solute and solvent nearly the same.

APPENDIX D

PROCEDURE FOR FITTING WEIGHTED
LEAST SQUARES LINE TO DATA

One can assume that the variance of the measured dihedral angle is independent of the magnitude of the angle. However, the variance of the function

$$Z = (\cos \theta/2 - \cos \theta°/2)^{-1}$$

which is plotted in Figures 18 - 20 depends on the magnitude of Z. One can calculate the variance of Z, $\sigma^2(Z)$, in terms of the variances of θ and $\theta°$ (which are equal) using the relation,

$$\sigma^2(Z) = \left(\frac{\partial Z}{\partial \theta}\right)^2 \sigma^2(\theta) + \left(\frac{\partial Z}{\partial \theta°}\right)^2 \sigma^2(\theta°).$$

Thus one has

$$\sigma^2(Z) = \frac{(\sin^2 \theta/2 + \sin^2 \theta°/2)}{(\cos \theta/2 - \cos \theta°/2)^4} \frac{\sigma^2(\theta)}{4}$$

which shows that the variance of Z is proportional to Z^4.

Weighted least square lines are fitted to the data using a weighting function W_i given by

$$W_i = 1/\sigma^2(Z_i).$$

The procedure used is given in reference (68). The variance of the dihedral angle was taken to be $1.713 \cdot 10^{-4}$ (radians)^2, which corresponds to a standard deviation of $0.75°$.

From this fitting procedure, one obtains the slope and intercept of a "best straight line" and the estimated variances of the slope and intercept. The slope and intercept are then used to calculate the quantities $d\gamma_{sl}/d\chi$ and $d\gamma_{gb}/d\chi$ using the Equations (7-6).

The variances of these quantities are given by the following equations:

$$\sigma^2\left[\gamma'_{sl}\right] = (\gamma'_{sl})^2 \left[\frac{\sigma^2(b)}{b^2} + \frac{\sigma^2(m)}{m^2} + \frac{\sigma^2(\theta°)}{4\cot^2\theta°/2}\right]$$

$$\sigma^2\left[\gamma'_{gb}\right] = \left(\frac{\gamma°_{gb}}{m}\right)^2 \left[\sigma^2(b) + (\sec\theta°/2 + b)^2\frac{\sigma^2(m)}{m^2}\right.$$

$$\left. + \frac{\sigma^2(\theta°)}{4\cos^2\theta°/2\cot^2\theta°/2}\right]$$

where $\sigma^2(b)$ is the variance of the intercept, $\sigma^2(m)$ is the variance of the slope, and the other quantities are defined by Equation (7-6). The square roots of $\sigma^2(\gamma'_{sl})$ and $\sigma^2(\gamma'_{gb})$ give the standard deviations of these coefficients.

The calculated standard deviations are 1/4 to 1/2 the magnitudes of the pressure and temperature coefficients, thus the latter are rather unreliable. The blame for this uncertainty lies not so much with the magnitude of the variance taken for the dihedral angle (which is a reasonable value), but rather with the high magnification of error brought about by the calculations.

Since the relative standard deviations of the data points in Figures 18 to 20 are roughly proportional to the square of the magnitude of the point on the Z-axis, deviations from the fitted straight line for points with high values of Z are relatively unimportant.

APPENDIX E

ESTIMATION OF THERMODYNAMIC PROPERTIES
OF NICKEL IN LIQUID LEAD

J. L. White[109] has fitted the solubility data for the Ni-Pb

system to a "sub-regular" solution model, proposed by Hardy.[38] Using

this model, one can obtain estimates for $\bar{S}_{Ni}$ and $\left.\dfrac{\partial \mu_{Ni}}{\partial x}\right)_{T,P} \dfrac{dx}{dT}$ to

use in calculating the excess entropy of the solid/liquid interface

(Chapter VII). The two parameters obtained from the solubility data

for the Ni-Pb system are:

$$\Delta \bar{H}_{Ni(\ell)}^{\infty} = 3050 \pm 600 \text{ cal/mol}$$

$$\Delta \bar{S}_{Ni(\ell)}^{xs,\infty} = -2.30 \pm 0.6 \text{ cal/mol-°C} . \tag{E-1}$$

The first of these terms is the difference in partial molal

enthalpy between Ni in solution and pure liquid Ni at the temperature

of interest, at infinite dilution. The second term is a similar entropy

term, except that it is an excess quantity determined relative to an

ideal solution.

These quantities serve as parameters for determining the

partial molal enthalpy and excess partial molal entropy at any solute

concentration, according to the relations:

$$\Delta \bar{H}_{Ni(\ell)} = \Delta \bar{H}_{Ni(\ell)}^{\infty} \left(1 - x_{Ni(\ell)}\right)^2$$

$$\Delta \bar{S}_{Ni(\ell)}^{xs} = \Delta \bar{S}_{Ni(\ell)}^{xs,\infty} \left(1 - x_{Ni(\ell)}\right)^2 \tag{E-2}$$

where $x_{Ni(\ell)}$ is the mole fraction of Ni in liquid lead.

The difference in partial molal Gibbs free energy between Ni

in solution and in the standard state is given by:

$$\Delta \overline{G}_{Ni(\ell)} = \overline{G}_{Ni(\ell)} - \underline{G}^{\circ}_{Ni} = \Delta \overline{H}_{Ni(\ell)} - T \Delta \overline{S}^{xs}_{Ni(\ell)}$$

$$+ RT \ln x_{Ni(\ell)}$$

Now since $\overline{G}_{Ni(\ell)} = \mu_{Ni}$, and $\underline{G}^{\circ}_{Ni}$ is independent of x, then

$$\frac{\partial \mu_{Ni}}{\partial x} = \frac{\partial \Delta \overline{G}_{Ni(\ell)}}{\partial x_{Ni(\ell)}} = -2 (1 - x_{Ni(\ell)})(\Delta \overline{H}^{\infty}_{Ni(\ell)} - T \Delta \overline{S}^{xs,\infty}_{Ni(\ell)})$$

$$+ \frac{RT}{x_{Ni(\ell)}} .$$

Dropping the subscripts on x, multiplying through by dx/dT and rearranging produces the relation:

$$(E-3) \qquad \frac{\partial \mu_{Ni}}{\partial x}\Bigg)_{T,P} \frac{dx}{dT} = \left[\Delta \overline{H}^{\infty}_{Ni(\ell)} - T \Delta \overline{S}^{xs,\infty}_{Ni(\ell)} \right] \frac{d(1-x)^2}{dT} + RT \frac{d \ln x}{dT} .$$

In order to evaluate this term for the saturated solution, plots of $(1-x)^2$ vs T and $\ln x$ vs T must be prepared, and slopes determined. The latter plot, using the available solubility data[2,79] produces a reasonably good straight line in the temperature range of interest. The former does not; however, in the region from 371°C to 593°C the slope does not change too much. The slopes to these plots and the calculated values of $\frac{\partial \mu_{Ni}}{\partial x} \frac{dx}{dT}$ at 371°C and 593°C are given below:

$$\frac{d(1-x)^2}{dT} = -7.96 \cdot 10^{-5} \ (°C)^{-1} \ \text{at } 371°C$$

$$\frac{d(1-x)^2}{dT} = -1.51 \cdot 10^{-4} \ (°C)^{-1} \ \text{at } 593°C$$

$$\frac{d \ln x}{dT} = 4.61 \cdot 10^{-3} \ (°C)^{-1}$$

$$\left.\frac{\partial \mu_{Ni}}{\partial x}\right)_{T,P} \frac{dx}{dT} = 5.54 \text{ cal/mol-}°C = 2.32 \cdot 10^8 \text{ ergs/mol-}°C$$
$$\text{at } 371°C$$
$$(E-4)$$

$$\left.\frac{\partial \mu_{Ni}}{\partial x}\right)_{T,P} \frac{dx}{dT} = 7.17 \text{ cal/mol-}°C = 3.00 \cdot 10^8 \text{ ergs/mol-}°C \, .$$
$$\text{at } 593°C$$

The difference between the partial molal entropy of Ni in solution in the standard state is given by:

$$\Delta \bar{S}_{Ni(\ell)} = \Delta \bar{S}^{xs}_{Ni(\ell)} - R \ln x_{Ni(\ell)} = \bar{S}_{Ni(\ell)} - \underline{S}°_{Ni} \, .$$

Thus,

$$\bar{S}_{Ni(\ell)} = \underline{S}°_{Ni} + \Delta \bar{S}^{xs}_{Ni(\ell)} - R \ln x_{Ni(\ell)} \, . \qquad (E-5)$$

The standard state is pure liquid nickel at the temperature of interest. The entropy in the standard state may be obtained by extrapolation from a given value of the entropy in the liquid above the melting point, using the heat capacity of liquid nickel. From reference (101), the entropy of liquid Ni at 1800°K is 23.37 cal/mol-°C, and the heat capacity is 9.2 cal/mol-°C. Thus,

$$\underline{S}°_{Ni} = 13.91 \text{ cal/mol-}°C \quad \text{at } 371°C$$
$$(E-6)$$
$$\underline{S}°_{Ni} = 16.64 \text{ cal/mol-}°C \quad \text{at } 593°C \, .$$

So from Equations (E-1), (E-2), (E-5), and (E-6) the partial molal entropy of Ni in liquid lead in the saturated solution is:

$$\bar{S}_{Ni} = 22.05 \text{ cal/mol-}°C \text{ at } 371°C$$
$$(E-7)$$
$$\bar{S}_{Ni} = 22.40 \text{ cal/mol-}°C \text{ at } 593°C \, .$$

The values obtained in Equations (E-4) and (E-7) above are used in Equation (7-15).

BIBLIOGRAPHY

1. N. K. Adam, <u>The Physics and Chemistry of Surfaces</u>, 3rd Ed., Oxford Univ. Press, London, (1941).

2. T. Alden, D. A. Stevenson, and J. Wulff, "Solubility of Nickel and Chromium in Molten Lead," <u>Trans AIME</u>, <u>212</u>, 15, (1958).

3. O. L. Anderson, "The Griffith Criterion for Glass Fracture," <u>Fracture</u>, Proceedings of an international conference on the atomic mechanisms of fracture held in Swampscott, Mass., April 12-16, 1959, The Technology Press of MIT and John Wiley and Sons, Inc., New York, (1959).

4. T. W. Anderson and D. A. Darling, "Asymptotic Theory of Certain 'Goodness-of-Fit' Criteria based on Stochastic Processes," <u>Ann. Math. Stat.</u>, <u>23</u>, 193, (1952).

5. K. T. Aust and B. Chalmers, "The Specific Energy of Crystal Boundaries in Tin," <u>Proc. Roy. Soc. (London)</u>, <u>A201</u>, 210, (1950).

6. K. T. Aust and B. Chalmers, "Surface Energy and Structure of Crystal Boundaries in Metals," <u>Proc. Roy. Soc. (London)</u>, <u>A204</u>, 359, (1950).

7. K. T. Aust and B. Chalmers, "Energies and Structure of Grain Boundaries," <u>Metal Interfaces</u>, ASM publication, Cleveland, Ohio, 153, (1952).

8. K. T. Aust, "Relative Interfacial Energies of Symmetrical Tilt Grain Boundaries in Silver," <u>Trans. AIME</u>, <u>206</u>, 1026, (1956).

9. B. L. Averbach, D. K. Felbeck, G. T. Hahn, and D. A. Thomas (Editors), <u>Fracture</u>, Proceedings of an international conference on the atomic mechanisms of fracture held in Swampscott, Mass., April 12-16, 1959, Technology Press of MIT and John Wiley and Sons, New York, (1959).

10. G. Bakker, "Capillarity and Surface Tension," <u>Handb. der Experimentalphysik</u>, <u>6</u>, Akademische Verlagsgesellschaft M.B.H., Leipzig, (1928).

11. P. W. Bridgman, <u>The Physics of High Pressure</u>, G. Bell and Sons, Ltd., London, (1931).

12. J. W. Cahn and J. E. Hilliard, "Free Energy of a Non-Uniform System: I. Interfacial Free Energy," <u>J. Chem. Phys.</u>, <u>28</u>, 258, (1958).

13. R. W. Cahn, "Grain Boundaries, Substructures, and Impurities," <u>Impurities and Imperfections</u>, ASM publication, Cleveland, Ohio, 41, (1959).

14. J. W. Cahn and J. E. Hilliard, "On the Equilibrium Segregation at a Grain Boundary," Acta Met., 7, 219, (1959).

15. B. Chalmers, "Some Crystal-Boundary Phenomena in Metals," Proc. Roy. Soc., A201, 210, (1950).

16. B. Chalmers, "Structure of Crystal Boundaries," Progress in Metal Physics, Vol. 3, Pergamon Press, London, 293, (1952).

17. E. G. Coleman, D. Weinstein and W. Rostoker, "On a Surface Energy Mechanism for Stress-Corrosion Cracking," Acta Met., 9, 491, (1961).

18. H. Cramér, Mathematical Methods of Statistics, Princeton Univ. Press, Princeton, New Jersey, 450, (1946).

19. L. S. Darken and R. W. Gurry, Physical Chemistry of Metals, McGraw-Hill Book Co., New York, (1953).

20. C. G. Dunn and F. Lionetti, "The Effect of Orientation Difference on Grain Boundary Energies," Trans. AIME, 185, 125, (1949).

21. C. G. Dunn, F. W. Daniels and M. J. Bolton, "Measurement of Relative Interfacial Energies of Twin Related Crystals," Trans. AIME, 188, 368, (1950).

22. C. G. Dunn, F. W. Daniels and M. J. Bolton, "Relative Energies of Grain Boundaries in Silicon Iron," Trans. AIME, 188, 1245, (1950).

23. R. Eborall and P. Gregory, "The Mechanism of Embrittlement by a Liquid Phase," Journ. Inst. of Metals, 84, 88, (1955-56).

24. J. F. Elliott and M. Gleiser, Thermochemistry for Steelmaking, Vol. I, Addison-Wesley Publ. Co., Reading, Mass., (1960).

25. D. K. Felbeck and E. Orowan, "Experiments on Brittle Fracture of Steel Plates," Welding Journal, 34, 570s, (1955).

26. B. Fleischer and J. F. Elliott, "The Solubility of Iron-Nickel Alloys in Lead, 700° - 1100°C," The Physical Chemistry of Metallic Solutions and Intermetallic Compounds, Symposium, Vol. 1, H.M. Stat. Office, London, (1959).

27. J. Friedel, B. D. Cullity, and C. Crussard, "Study of the Surface Tension of a Grain Boundary in a Metal as a Function of the Orientation of the Two Grains which the Boundary Separates," Acta Met., 1, 79, (1953).

28. R. L. Fullman, "Interfacial Free Energy of Coherent Twin Boundaries in Copper," J. Appl. Phys., 22, 448, (1951).

29. J. W. Gibbs, "On the Equilibrium of Heterogeneous Substances,"
     The Scientific Papers of J. Willard Gibbs, Vol. 1, Dover Publ.,
     Inc., New York, (1961).

30. J. Gielessen and W. Schmatz, "The Surface Tension of Liquids
     Under Foreign Gas Pressure up to 1000 kpds/cm^2," Z. Phys. Chemie,
     Neue Folge, 27, 157, (1961).

31. N. A. Gjostein and F. N. Rhines, "Absolute Interfacial Energies
     of [001] Tilt and Twist Grain Boundaries in Copper," Acta Met.,
     7, 319, (1959).

32. A. A. Griffith, "IV. The Phenomena of Rupture and Flow in Solids,"
     Phil. Trans. Roy. Soc. (London), A221, 163, (1921).

33. A. A. Griffith, "The Theory of Rupture," Proc. First Internat.
     Congr. for Appl. Mechanics--Delft, 55, (1924).

34. E. A. Guggenheim and N. K. Adam, "The Thermodynamics of Adsorption
     at the Surface of Solutions," Proc. Roy. Soc. (London), A139,
     218, (1933).

35. E. A. Guggenheim, Thermodynamics, North-Holland Publ. Co.,
     Amsterdam, (1957).

36. F. A. Halden and W. D. Kingery, "Surface Tension at Elevated
     Temperatures. II. Effect of Carbon, Nitrogen, Oxygen and Sulfur
     on Liquid Iron Surface Tension and Interfacial Energy with
     Al_2O_3," J. Phys. Chem., 59, 557, (1955).

37. M. Hansen, Constitution of Binary Alloys, McGraw-Hill Book Co.,
     Inc., New York, (1958).

38. H. K. Hardy, "A 'Sub-Regular' Solution Model and Its Application
     to Some Binary Alloy Systems," Acta Met., 1, 202, (1953).

39. D. Harker and E. Parker, "Grain Shape and Grain Growth," Trans. ASM,
     34, 156, (1945).

40. M. E. Hassen, R. F. Nielsen and J. C. Calhoun, "Effect of Pressure
     and Temperature on Oil-Water Interfacial Tensions for a Series of
     Hydrocarbons," Trans AIME, 198, 299, (1953).

41. E. R. Hayward and A. P. Greenough, "The Surface Energy of Solid
     Nickel," J. Inst. of Metals, 88, 217, (1960).

42. C. Herring, "Surface Tension as a Motivation for Sintering,"
     The Physics of Powder Metallurgy, A Symposium held at Bayside,
     Long Island, New York. August 24-26, 1949, McGraw-Hill Book Co.,
     New York, 143, (1951).

43. C. Herring, "The Use of Classical Macroscopic Concepts in Surface Energy Problems," Structure and Properties of Solid Surfaces, Gomer and Smith (Eds.), Univ. of Chicago Press, (1953).

44. J. B. Hess, "Measurement of Solid-Solid Interfacial Energies," Metal Interfaces, ASM Publication, Cleveland, Ohio, (1952).

45. J. E. Hilliard and J. W. Cahn, "On the Nature of the Interface Between a Solid Metal and Its Melt," Acta Met., 6, 772, (1958).

46. J. E. Hilliard, M. Cohen and B. L. Averback, "Grain Boundary Energies in Copper-Gold Alloys," Acta Met., 8, 26, (1960).

47. C. R. Hocott, "Interfacial Tension Between Water and Oil Under Reservoir Conditions," Trans. AIME, 132, 184, (1939).

48. E. W. Hough, M. J. Rzasa and B. B. Wood, Jr., "Interfacial Tensions at Reservoir Pressures and Temperatures; Apparatus and the H_2O-CH_4 System," Trans AIME, 192, 57, (1951).

49. E. W. Hough, B. B. Wood, Jr. and M. J. Rzasa, "Adsorption at H_2O-He, -CH_4, -N_2 Interfaces at Pressures to 15,000 psia," J. Phys. Chem., 56, 996, (1952).

50. E. W. Hough, G. J. Heuer and J. W. Walker, "An Improved Pendant Drop, Interfacial Tension Apparatus and Data for Carbon Dioxide and Water," Trans AIME, 216, 469, (1959).

51. K. K. Ikeuye and C. S. Smith, "Studies of Interfacial Energies in Some Aluminum and Copper Alloys," Trans AIME, 185, 762, (1949).

52. R. E. Johnson, "Conflicts between Gibbsian Thermodynamics and Recent Treatments of Interfacial Energies in Solid-Liquid-Vapor Systems," J. Phys. Chem., 63, 1655, (1959).

53. D. T. Jones, "Determination of Surface Tension and Specific Gravity of Crude Oil under Reservoir Conditions," Trans. AIME 118, 81, (1936).

54. G. L. Kehl, Principles of Metallographic Laboratory Practice, McGraw-Hill Book Co., New York, (1949).

55. W. D. Kingery and M. Humenik, Jr., "Surface Tension at Elevated Temperatures. I. Furnace and Method for Use of the Sessile Drop Method; Surface Tension of Silicon, Iron and Nickel," J. Phys. Chem., 57, 359, (1953).

56. W. D. Kingery, "Densification During Sintering in the Presence of a Liquid Phase. I. Theory," J. Appl. Phys., 30, 301, (1959).

57. W. D. Kingery, "Densification During Sintering in the Presence of a Liquid Phase. II. Experimental," J. Appl. Phys., 30, 307, (1959).

58. W. D. Kingery. "Sintering in the Presence of a Liquid Phase," Kinetics of High Temperature Processes, Conference on the Kinetics of High Temperature Processes, MIT, 1958, The Technology Press of MIT and John Wiley and Sons, Inc., New York, (1959).

59. D. A. Kraai, S. Floreen, C. A. Stickels, D. V. Ragone and E. E. Hucke, "The Effect of Surface Tension of a Liquid Metal Environment on the Fracture Strength of Solid Metals," AFOSR TR-60-116, Contract No. AF 49(638)-422, (July 1960).

60. A. Kundt, "Concerning the influence of pressure on the surface tension at the common surface of separation of liquids and gases, and on the relation of this influence to the Cagniard de la Tour State of the Liquid," Annalen der Physik und Chemie, 12, 538, (1881).

61. G. N. Lewis and M. Randall, Thermodynamics, McGraw-Hill Book Co., New York, (1923).

62. G. N. Lewis, M. Randall, K. S. Pitzer and L. Brewer, Thermodynamics, 2nd Ed., McGraw-Hill Book Co., New York, (1961).

63. C. J. Lynde, "The Effect of Pressure on Surface Tension," Phys. Rev., 22, 181, (1906).

64. K. A. McCarthy and B. Chalmers, "Energies of Grain Boundaries in Silver Chloride Crystals," Canad. J. Phys., 36, 1645, (1958).

65. D. McLean, Grain Boundaries in Metals, Oxford Univ. Press, London, (1957).

66. _____, Metals Handbook, Vol. 1, Properties and Selection of Metals, 8th Ed., ASM Publication, Metals Park, Novelty, Ohio, (1961).

67. A. S. Michaels and E. A. Hauser, "Interfacial Tension at Elevated Pressure and Temperature II. Interfacial Properties of Hydrocarbon-Water Systems," J. Phys. Colloid Chem., 55, 408, (1951).

68. H. S. Mickley, T. K. Sherwood and C. E. Reed, Applied Mathematics in Chemical Engineering, McGraw-Hill Book Co., New York, (1957).

69. K. O. Miller and J. F. Elliott, "Phase Relationships in the Systems Fe-Pb-Ni, Fe-Ni-C (sat.) and Fe-Pb-Ni-C; 1300° to 1500°C," Trans AIME, 218, 900, (1960).

70. W. A. Miller and W. M. Williams, "The Microstructure of Zinc-Tin Alloys," (to be published).

71. W. W. Mullins, "Theory of Thermal Grooving," J. Appl. Phys., 28, 333, (1957).

72. H. Mykura, "The Variation of the Surface Tension of Nickel with Crystallographic Orientation," Acta Met., 9, 570, (1961).

73. H. Nichols and W. Rostoker, "On the Effective Surface Energy Involved in the Brittle Fracture of 70/30 Brass," Acta Met., 8, 788, (1960).

74. H. Nichols and W. Rostoker, "Ductile-Brittle Transition in α-Brass," Acta Met., 8, 848, (1960).

75. H. Nichols and W. Rostoker, "On the Mechanism of Crack Initiation in Embrittlement by Liquid Metals," Acta Met., 9, 504, (1961).

76. K. M. Olsen, C. F. Larkin and P. H. Schmitt, Jr., "Embrittlement of High Purity Nickel," ASM Trans, 53, 349, (1961).

77. E. Orowan, "Energy Criteria of Fracture," Welding J., 34, 1575, (1955).

78. K. Pearson (Ed.), The Tables of the Incomplete Beta Function, Cambridge Univ. Press, London, (1934).

79. E. Pelzel, "Solubility of Copper, Nickel and Cobalt in Molten Lead," Metall, 9, 692, (1955).

80. N. J. Petch, "The Lowering of Fracture-Stress due to Surface Adsorption," London Phil. Mag., 1, 331, (1956).

81. W. T. Read and W. Shockley, "Dislocation Models of Crystal Grain Boundaries," Phys. Rev., 78, 275, (1950).

82. J. Rice, "The Influence of Surfaces of Discontinuity upon Equilibrium of Heterogeneous Masses. Theory of Capillarity," A Commentary on the Scientific Writings of J. Willard Gibbs, Vol. I, F. G. Donnan and A. Haas, (Eds.), Yale Univ. Press, New Haven, Conn., (1936).

83. O. K. Rice, "The Effect of Pressure on Surface Tension," J. Chem. Phys., 15, 333, (1947).

84. O. K. Riegger and L. H. VanVlack, "Dihedral Angle Measurement," Trans. AIME, 218, 933, (1960).

85. O. K. Riegger, "The Role of the Solid-Liquid Interphase Boundary in Microstructures," Ph.D. Thesis, University of Michigan, Ann Arbor, Michigan, (1962).

86. W. M. Robertson and P. G. Shewmon, "Variation of Surface Tension with Surface Orientation in Copper," Trans AIME, 224, 804, (1962).

87. W. Rostoker, J. N. McCaughey and H. Markus, Embrittlement by Liquid Metals, Reinhold Publ. Co., New York, (1960).

88. _____, Russian Papers on effect of pressure on surface tension:

M. M. Kusakov, P. A. Rehbinder, and K. E. Zinchenko, "Surface Phenomena in Petroleum-Filtration Processes," Compt rend. acad. sci. U.R.S.S., 28, 433, (1940).

M. M. Kusakov, N. M. Lubman and A. Yu. Koshevnik, "An Apparatus for the determination of interfacial tension of oils and of contact angles of wetting (of the rocks) under the conditions in beds," Neftyanoe Khoz., 32, (2), 27; (3), 20, (1954).

P. E. Bol'shakov, "Ability of Solid Substances to be wet by liquids in the presence of compressed gases," Trudy Gosudarst. Nauch.-- Issledovatel. Inst. Azot. Prom., 1952, (1), 43; Referat. Zhur. Fiz. 1955, (13720).

M. A. Geĭman, V. B. Schneerson and A. G. Mamikonov, "Effects of Pressure on the Wettability of Oil-Bearing Minerals (Basins)," Invest. Akad. Nauk. S.S.S.R., Otdel. Tekh. Nauk. 1955, 127.

P. E. Bol'shakov and G. T. Levchenko, "Surface Tension at High Pressures at the Liquid-Gas Boundary," Trudy Gosudarst. Nauch.-- Issledovatel. i Proekt. Inst. Azot. Prom. 1952, (1), 30; Referat. Zhur. Fiz. 1955, (13719).

M. M. Kusakov and N. D. Tairov, "The Wetting of Quartz by Liquid Hydrocarbons and Water at High Pressures and Temperatures," Doklady Akad. Nauk Azerbaĭdzhan. S.S.R., 15, 1019, (1959).

D. S. Tsiklis and Yu. N. Vasil'ev, "Surface Tension at the Interface Between Two Gaseous Phases at High Pressure," Doklady Akad. Nauk S.S.S.R., 136, 394, (1961).

Yu. V. Efremov and I. F. Golubev, "Surface Tension at the Liquid-Gas Interface Under High Pressure," Zh. Fiz. Khim., 36, 1222, (1962).

89. R. A. Sack, "Extension of Griffith's Theory of Rupture to Three Dimensions," Proc. Phys. Soc. (London), 58, 729, (1946).

90. R. Shuttleworth, "The Surface Tension of Solids," Proc. Phys. Soc., A63, 444, (1950).

91. S. Siegel, Nonparametric Statistics for the Behavioral Sciences, McGraw-Hill Book Co., New York, (1956).

92. E. J. Slowinski, Jr., E. E. Gates and C. E. Waring, "The Effect of Pressure on the Surface Tension of Liquids," J. Phys. Chem., 61, 808, (1957).

93. C. S. Smith, "Grains, Phases, and Interfaces: An Interpretation of Microstructure," Trans AIME, 175, 15, (1948).

94. C. S. Smith, "Interphase Interfaces," Imperfections in Nearly Perfect Crystals, John Wiley and Sons, Inc., New York, (1952).

95. C. S. Smith, "Microstructure," ASM Trans, 45, 533, (1953).

96. C. J. Smithells, Metals Reference Book, Vol. I and II, Butterworth Scientific Publ., London, (1955).

97. S. W. Strauss, J. L. White and B. F. Brown, "The Atomic Size Effect and Alloying Behavior in Liquid Metals," _Acta Met._, 6, 604, (1958).

98. S. W. Strauss, L. E. Richards and B. F. Brown, "The Density of Liquid Lead and of Dilute Solutions of Nickel in Lead," _Nuclear Sci. Eng._, 7, 442, (1960).

99. S. W. Strauss and L. E. Richards, "The Density of Dilute Solutions of Copper in Liquid Lead," _Nuclear Sci. Eng._, 9, 281, (1961).

100. A. N. Stroh, "A Theory of the Fracture of Metals," _Advances in Physics_, 6, 418, (1957).

101. D. R. Stull and G. C. Sinke, _Thermodynamic Properties of The Elements_, No. 18, _Advances in Chemistry Series_, Amer. Chem. Soc., Washington, D.C., (1956).

102. C. A. Swartz, "The Variation in the Surface Tension of Gas-Saturated Petroleum with Pressure of Saturation," _Physics_, 1, 245, (1931).

103. J. W. Taylor, "An Evaluation of Interface Energies in Metallic Systems," _J. Inst. of Metals_, 86, 456, (1958).

104. H. Udin, A. J. Shaler and J. Wulff, "The Surface Tension of Solid Copper," _Trans AIME_, 185, 186, (1949).

105. H. Udin, "Measurement of Solid-Gas and Solid-Liquid Interfacial Energies," _Metal Interfaces_, ASM Publication, Cleveland, Ohio, 114, (1952).

106. L. H. Van Vlack, "Intergranular Energy of Iron and Some Iron Alloys," _Trans. AIME_, 191, 251, (1951).

107. R. S. Wagner and B. Chalmers, "Grain Boundaries in Germanium," _J. Appl. Phys._, 31, 581, (1960).

108. F. Weinberg, "Grain Boundaries in Metals," _Progress in Metal Physics_, Vol. 8, Pergamon Press, 105, (1959).

109. J. L. White, "A Thermodynamic Analysis of Solubility in Liquid Metal Systems," U.S. Naval Research Lab., NRL Rept 5555, Office of Tech. Services, U.S. Dept. of Commerce, Washington, D.C.,(1960).

110. S. S. Wilks, _Mathematical Statistics_, John Wiley and Sons, New York, (1962).

111. J. Winter and S. Weinig, "The Grain Boundary Adsorption of Solutes," _Trans AIME_, 215, 74, (1959).

112. _____, "The Solid/Liquid Interface," _Second International Congress of Surface Activity_, Vol. III, Academic Press, New York, (1957).